

# Spiral Waves in Cartesian, Polar and Spherical Geometries

Kara B. Roberson

A Thesis Submitted to the  
University of North Carolina Wilmington in Partial Fulfillment  
Of the Requirements for the Degree of  
Master of Science

Department of Mathematics and Statistics

University of North Carolina Wilmington

2010

Approved by

Advisory Committee

---

Wei Feng

---

Susan Simmons

---

Russell Herman

Chair

Accepted by

---

Dean, Graduate School

This thesis has been prepared in the style and format

Consistent with the journal

American Mathematical Monthly.

## TABLE OF CONTENTS

ABSTRACT . . . . .	v
DEDICATION . . . . .	vii
ACKNOWLEDGMENTS . . . . .	viii
LIST OF TABLES . . . . .	x
LIST OF FIGURES . . . . .	xii
1 INTRODUCTION . . . . .	1
2 SPIRAL DYNAMICS . . . . .	5
2.1 Spirals . . . . .	5
2.2 Spiral Waves in Physical Systems . . . . .	8
2.3 Spiral Waves and Cardiac Electrophysiology . . . . .	9
3 REACTION DIFFUSION MODELS FOR CARDIAC DYNAMICS .	16
3.1 History and Background on the FitzHugh-Nagumo Equations	16
3.2 Cartesian and Other Forms of the Model . . . . .	19
4 NUMERICAL MODELING . . . . .	24
4.1 Finite Difference Methods in Cartesian Coordinates . . . . .	24
4.2 Finite Difference Methods in Other Geometries . . . . .	29
4.3 Stability . . . . .	32
4.4 Exact Solution . . . . .	36
5 RESULTS . . . . .	38
5.1 Nullclines . . . . .	39
5.2 Results in Rectangular Coordinates . . . . .	40
5.3 Results in Polar Coordinates . . . . .	51
5.4 Results in Spherical Coordinates . . . . .	58
6 CONCLUSIONS . . . . .	67
REFERENCES . . . . .	70

APPENDIX . . . . .	76
Peter Hammer's MATLAB Code . . . . .	76
Testing Leveque's Mapping Function . . . . .	79
Code for Solving the System in Cartesian Coordinates . . . . .	82
MATLAB Code for Polar Coordinates . . . . .	86
MATLAB Code for Solving the Modified FHN system in Spherical Coordinates . . . . .	95
Generating Phase Fields . . . . .	99
Interactive Website with Cardiac Spiral Waves . . . . .	101

## ABSTRACT

The purpose of this thesis is to numerically model the behavior of a reaction-diffusion system in differing geometries, namely a FitzHugh-Nagumo (FHN) type system,

$$\begin{aligned}\frac{\partial u}{\partial t} &= c_1 u(u - a)(1 - u) - c_2 uv + I_{ex} + G\nabla^2 u \\ \frac{\partial v}{\partial t} &= b(u - dv)\end{aligned}\tag{1}$$

and to seek out spiral behavior in solutions to this system. The system was solved computationally in Cartesian coordinates using finite difference methods through implementation of a MATLAB code, which was modified from a code written by Peter E. Hammer [22]. The model was also transformed from Cartesian to polar and spherical geometries and solved numerically using MATLAB. Spiral behavior did not result in every simulation but was dependent on choosing certain FHN parameter values, namely  $a = 0.13$ ,  $b = 0.013$ ,  $c_1 = 0.26$ ,  $c_2 = 0.1$ , and  $d = 1.0$ , sufficiently small diffusion constants and time step, sufficiently large duration, and appropriate mesh.

Such systems are used to model nerve conduction and cardiac wave propagation, because experimental methods are expensive and have physical limitations. Data for these two natural phenomena is collected by placing electrodes on samples of tissue [13, 11, 20]. Researchers are of course physically limited to fitting only a finite number of electrodes on a sample; and these electrodes burn the sample as they gather data, limiting the duration of experiments [43]. Thus, computational methods such as those used in this thesis provide more complete data since they do not have these limitations. Of course, mathematical models do have other limitations, and one has to be careful to choose proper boundary conditions and parameter values

so that the system remains stable and makes sense when compared to experimental data.

In the model used in this paper, spirals were seen in Cartesian coordinates with  $u_0 = v_0 = 0$  and an external stimulus applied to the system at two different time steps. This was consistent with the results of Agladze et alia and Pertsov et alia, who found that spirals can form in homogeneous media through collision of wavefronts [1, 40]. Spirals were also observed in polar and spherical coordinates with random initial conditions and no external stimulus applied, consistent with research in the field showing that spirals form in inhomogeneous media [9, 39, 44, 43].

## DEDICATION

This thesis is dedicated to all of the people who have been patient with me as I worked to complete my Master's degree: my husband Scott, my parents Harold and Sherry Blalock, my thesis advisor Dr. Russell Herman, my thesis committee Dr. Susan Simmons and Dr. Wei Feng, my advisor Dr. John Karlof, all of my professors, Nancy and David and Wanda in the Graduate School, Edwina Johnson, my extended family, and my friends. This group of people went to great lengths to help me succeed during this lengthy journey, despite numerous obstacles along the way.

I would also like to acknowledge Peggy Grigg, Gloria Barrett, Dr. Gregory Bell, and Dr. David Rowe, who were instrumental figures in my choice to pursue a career in Mathematics. It was their enthusiasm for the subject and their dedication as educators that influenced me to obtain a graduate degree in this area. I further dedicate this thesis to the memory of my grandmother, whose unwavering support made me feel I could accomplish anything, and to the memory of my Uncle Bill Kincaid, to whom I owe my ability to think abstractly.

## ACKNOWLEDGMENTS

I would like to thank Dr. Russell Herman, Dr. Wei Feng, and Dr. Susan Simmons for their help with this thesis.

It has been a great honor to work with Dr. Herman during this whole process, who can juggle more responsibilities at once than one would think humanly possible. There were numerous times during this process when life got in the way of my thesis, and I would not have thought any less of him if he had given up on me somewhere along the way. Dr. Herman, however, did not give up on me during this arduous journey, even when I was close to giving up on myself. I will be forever and endlessly grateful to him for this superhuman level of patience. Further, I would like to acknowledge Dr. Herman's contributions in getting the MATLAB codes up and running and for teaching me numerical analysis. This thesis would not have been even conceivable were it not for his guidance and support.

A warm thanks again to Dr. Feng and Dr. Simmons, for going out of their way to help me finish this thesis in time to graduate. Their insight and questions helped me to make my thesis a higher quality of work.

## LIST OF TABLES

1	Two-Dimensional Spirals. . . . .	6
2	Changing stimulus heights, with zero initial conditions. Images and values given are at 25000 time steps. . . . .	43
3	Images showing one run of the Cartesian code, spiralwu.m, with zero initial conditions at $a=0.13$ . . . . .	44
4	Changing activation threshold, with zero initial conditions, for $a = 0.1$ to 0.7. . . . .	47
5	Changing activation threshold, with zero initial conditions, for $a = 0.8$ to 0.14. . . . .	48
6	Changing activation threshold, with constant initial conditions. . . .	49
7	Changing activation threshold, with randomized initial conditions. . .	50
8	Solving the FHN system Analytically in Polar Coordinates. . . . .	52
9	Solving the FHN system Computationally in Polar Coordinates, with $u_0 = v_0 = 0$ and an External Stimulus Applied with Value $I_{ex} = 30$ . .	53
10	Solving the FHN system Computationally in Polar Coordinates, with Randomized Initial Conditions and No External Stimulus Applied. .	54
11	Solving the FHN system Computationally in Polar Coordinates, with Randomized Initial Conditions and an External Stimulus Applied with Value $I_{ex} = 30$ . . . . .	55
12	Solving the FHN system Computationally in Polar Coordinates, with Randomized Initial Conditions and No External Stimulus Applied. .	56
13	Solving the FHN system Computationally in Polar Coordinates, with Randomized Initial Conditions and No External Stimulus Applied, Showing Counterclockwise Rotation of Spiral. . . . .	57

14	Solving the FHN system Computationally in Spherical Coordinates, with $u_0 = v_0 = 0$ and an External Stimulus Applied with Value $I_{ex} = 30$ .	59
15	Solving the FHN system Computationally in Spherical Coordinates, with Randomized Initial Conditions and No External Stimulus Applied.	60
16	Solving the FHN system Computationally in Spherical Coordinates, with Randomized Initial Conditions and an External Stimulus Ap- plied with Value $I_{ex} = 30$ .	60
17	Solving the FHN system Computationally in Spherical Coordinates, with Randomized Initial Conditions and No External Stimulus Applied.	62
18	Solving the FHN system Computationally in Spherical Coordinates, with Randomized Initial Conditions and No External Stimulus Applied.	63
19	Solving the FHN system Computationally in Spherical Coordinates, with Randomized Initial Conditions and No External Stimulus Applied.	64
20	Solving the FHN system Computationally in Spherical Coordinates, with Randomized Initial Conditions and No External Stimulus Applied.	65
21	Solving the FHN system Computationally in Spherical Coordinates, with Randomized Initial Conditions and No External Stimulus Applied.	66

## LIST OF FIGURES

1	Mapping from a Rectangle to a Disk to a Sphere using Leveque's Mapping Scheme [6]. . . . .	3
2	Ionic Capital [15]. . . . .	5
3	The Milky Way Galaxy, an artist's updated rendition. Thanks to information from NASA's Spitzer Space Telescope, the galaxy is now believed to have two major spiral arms, rather than four [31]. . . . .	7
4	Spiral Jetty, created by artist Robert Smithson in 1970 on the north arm of Great Salt Lake, Utah. More information at [7]. Picture taken by Soren Hayward [24]. . . . .	7
5	Spiral Waves Appearing in the Belousov-Zhabotinsky Reaction [51]. .	9
6	Segmented spiral waves and target waves in the Belousov-Zhabotinsky Reaction [48]. . . . .	9
7	Anatomy of the Human Heart, Showing Direction of Blood Flow [16].	11
8	The Heart's Electrical System [8]. . . . .	12
9	Electrocardiogram with Normal Sinus Rhythm [2]. . . . .	13
10	Spiral Breakup in a modified FitzHugh-Nagumo Model [39]. . . . .	15
11	Phase plane for the FitzHugh's "BVP Model" [13]. . . . .	17
12	Microscopic view of Human Myocardial Tissue [17]. . . . .	19
13	Polar system blows up for $D = 1$ and $\Delta t = 0.00001$ . . . . .	34
14	Nullclines for the Modified FHN System, with $a = 0$ , $b = 0.013$ , $c_1 = 0.26$ , $c_2 = 0.1$ , and $d = 1.0$ . . . . .	40
15	Nullclines for the Modified FHN System, with $a = 0.1$ , $b = 0.013$ , $c_1 = 0.26$ , $c_2 = 0.1$ , and $d = 1.0$ . . . . .	41
16	Nullclines for the Modified FHN System, with $a = 0.13$ , $b = 0.013$ , $c_1 = 0.26$ , $c_2 = 0.1$ , and $d = 1.0$ . . . . .	41

17	Nullclines for the Modified FHN System, with $a = 0.15$ , $b = 0.013$ , $c_1 = 0.26$ , $c_2 = 0.1$ , and $d = 1.0$	42
18	Phase plane for modified FHN model with parameter values $a = 0.13$ , $b = 0.013$ , $c_1 = 0.26$ , $c_2 = 0.1$ , and $d = 1.0$ .	42
19	Close-up of phase plane for modified FHN model with same parameter values.	45
20	An archery target [3] and an image taken from solving the FHN sys- tem in Cartesian coordinates, with $t = 375.1$ , $a = 0.03$ , zero initial conditions, and $I_{ex} = 30$ .	46

## 1 INTRODUCTION

This thesis explores the dynamics of spiral waves in differing geometries. Although mathematics itself often precedes application and is riveting and beautiful of its own accord, it should be noted that spiral waves do form in some natural circumstances. Thus, the study of the dynamics of spiral waves does have practical application. Spiral waves have been noted to appear in Belousov-Zhabotinsky reactions, surface catalytic oxidation reactions, cAMP waves in dictyostelium discoideum,  $Ca^{+2}$  waves in pancreatic  $\beta$  cells and *Xenopus* oocytes, slime molds, chicken retina, Rayleigh-Bénard convection, and electric wave propagation in cardiac tissue [48, 1, 10]. In current research, there is evidence to support that spiral waves may be the cause for many cardiac arrhythmias [40, 11, 20]. Because of this connection, studying the dynamics of spiral waves may help in the development for treatments of such arrhythmias. It may also help to dissuade the use of some medications which are often developed using an oversimplified understanding of the dynamics of the electric current across the human heart and aid in the development of better treatments for cardiac arrhythmias.

Various factors influence the dynamics of spiral waves. Some of these factors are external fields, spatial inhomogeneities, the excitability of the medium, interactions with other spiral waves, boundaries, the size of the domain, and the geometry of the domain [44]. In a smaller domain, for instance, the spiral waves will have a greater chance for annihilation through collision with each other or boundaries.

Spiral wave dynamics have been studied on various 2-dimensional surfaces, including planar and nonplanar surfaces. With a rectangular surface, one has the benefit of working in a simple geometry but then will need to deal with the boundaries. On a rectangular surface, the spiral waves may collide with boundaries and annihilate or form multi-armed spirals [44]. In spherical coordinates, one has to

contend with a change of variables in exchange for having a chance to let the spiral waves roam free across the surface without worry of boundary collisions. Rohlf et alia remarked that in their studies, the curvature of the surface adds interest as it also affects the dynamics of the spiral waves; for instance, spirals rotate more rapidly on a sphere than on a flat surface [44]. That behavior, however, was not observed so far in the numerical simulations conducted for this thesis. When comparing to experimental data for the heart, a curved surface makes a more realistic model.

The model being studied in this paper is a FitzHugh-Nagumo (FHN) type system. After exploring various software programs, MATLAB was used to find numerical solutions. A code written by Peter Hammer for rectangular coordinates was adapted into cylindrical and spherical geometries [22]. Initially, mapping from the rectangular grid onto a sphere using a mapping function called mapctm from R.J. Leveque [6] was attempted, and then instead the more traditional approach of adapting the code to polar and spherical coordinates was taken. The various MATLAB codes used during this research can be found in the Appendix. The initial form of the system discussed in this paper, given in rectangular coordinates, is:

$$\begin{aligned}\frac{\partial u}{\partial t} &= c_1 u(u - a)(1 - u) - c_2 uv + I_{ex} + G_x \frac{\partial^2 u}{\partial x^2} + G_y \frac{\partial^2 u}{\partial y^2} \\ \frac{\partial v}{\partial t} &= b(u - dv).\end{aligned}\tag{2}$$

In this system,  $u$  represents potential for excitation and can be referred to as the “fast variable” [5].

The system was originally developed to model conduction across nerve cells but can also be used to model other excitable tissues such as cardiac tissue. The “slow,” or recovery, variable  $v$  was originally the sodium gating variable but more generally brings the system to a refractory state and prevents re-excitation for a given interval. An external current can be applied to the system by changing the value of  $I_{ex}$  or

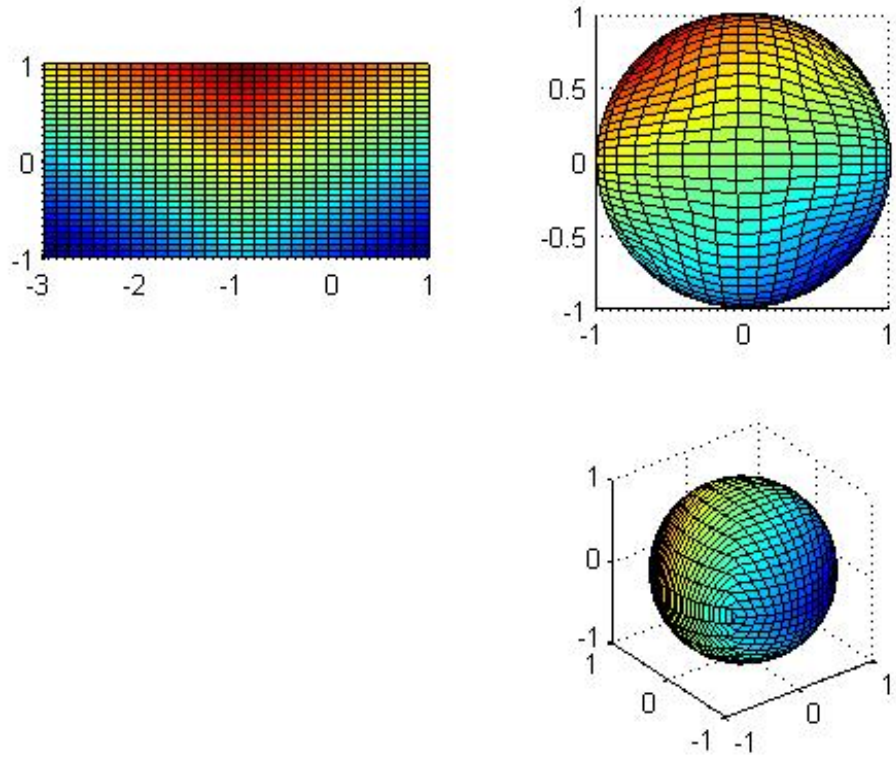


Figure 1: Mapping from a Rectangle to a Disk to a Sphere using Leveque's Mapping Scheme [6].

can be set to zero. The rate of diffusion can be adjusted by changing  $G_x$  and  $G_y$ . The other values,  $a$ ,  $b$ ,  $c_1$ ,  $c_2$ , and  $d$ , define the action potential and are constant in time but not necessarily in space [43].

Modified for cylindrical coordinates, the system becomes:

$$\begin{aligned} \frac{\partial u}{\partial t} &= c_1 u(u-a)(1-u) - c_2 u v + I_{ex} + G \left( \frac{1}{r} \frac{\partial}{\partial r} \left( r \frac{\partial u}{\partial r} \right) + \frac{1}{r^2} \frac{\partial^2 u}{\partial \theta^2} \right) \\ \frac{\partial v}{\partial t} &= b(u-dv). \end{aligned} \quad (3)$$

Only the diffusion term changes, as is also the case with the system in spherical

coordinates:

$$\begin{aligned}\frac{\partial u}{\partial t} &= c_1 u(u - a)(1 - u) - c_2 uv + I_{ex} + G \left( \frac{1}{r^2 \sin \theta} \frac{\partial}{\partial \theta} \left( \sin \theta \frac{\partial u}{\partial \theta} \right) + \frac{1}{r^2 \sin^2 \theta} \frac{\partial^2 u}{\partial \phi^2} \right) \\ \frac{\partial v}{\partial t} &= b(u - dv)\end{aligned}\tag{4}$$

Running through various simulations revealed that spiral waves do not always form for this system; modifying the parameters affects their formation.

In this thesis, background information on spirals will first be presented, detailing mankind's fascination with this hypnotic waveform. Further background will be given on current research with spirals in chemical and physical systems, followed by a discussion of the heart, which was what drew the author to research spirals. The FitzHugh-Nagumo model used to simulate the cardiac electric wave propagation will be presented in detail in section 3, with a history and background of earlier forms of the model. In section 4, the numerical scheme for approximating solutions to the model will be explained. The paper ends with a presentation of the results and findings of tweaking the model parameters in the quest to find spirals in a computer simulation of electrical current in cardiac tissue, followed by conclusions.

## 2 SPIRAL DYNAMICS

### 2.1 Spirals

According to Merriam-Webster, an object can be described as “spiral” if it is “winding around a center or pole and gradually receding from it or approaching it” [45]. Spirals can be observed in nature and are mimicked by man in art and machines [46]. One does not have to look far to see evidence of man’s fascination with the spiral. Spirals appear as designs in textiles and even adorning notebooks and cell phones. This is not a new phenomenon. Spirals were prevalent in the art of ancient Greece, primarily in architecture. Spirals can be seen in ionic capitals [see Figure 2], a capital being the ornate top to a column, which were originally built in ancient Greece and later revived during the medieval period [32]. The spring is another example of a spiral shape made by man which was utilized to power clocks as early as the sixteenth century [35].



Figure 2: Ionic Capital [15].

This fascination of mankind with the spiral has further led beyond art, architecture, and machines into mathematical studies. Archimedes used the spiral in his work *On Spirals* to square the circle around 250 BC, though he did not discover the spiral for which he is named [46]. The spiral studied by Archimedes, seen most commonly in decoration and in the edges of flat items which have been rolled up,

Name/Origin	Equation
Archimedean Spiral, “On Spirals”, 250 BC	$r = a\theta$
Logarithmic Spiral, (equiangular, Bernoulli), Descartes, 1638	$r = ke^{a\theta}$
Hyperbolic Spiral, (reciprocal spiral), Pierre Varignon, 1704	$r = \frac{a}{\theta}$
Littus, Cotes, 1722	$r^2\theta = a$
Cornu Spiral, (clothoid, Euler’s Spiral), Euler, 1744	$x = a\sqrt{\pi} \int_0^t \cos \frac{\pi t^2}{2} dt$ $y = a\sqrt{\pi} \int_0^t \sin \frac{\pi t^2}{2} dt$
Fermat’s Spiral, Fermat, 1636	$r^2 = a\theta$
Involute of a Circle, Huygens, 1673 [38]	$x = a(\cos \phi + \phi \sin \phi)$ $y = a(\sin \phi - \phi \cos \phi)$
Cochleoid, (snail form)	$r = a \frac{\sin \theta}{\theta}$

Table 1: Two-Dimensional Spirals.

has the equation

$$r = a\theta.$$

The spiral arms of galaxies are of the form of a logarithmic spiral, which is also referred to as an equiangular spiral or Bernoulli Spiral [46, 41]. This spiral was first examined by René Descartes in 1638 [46, 41] and has the equation

$$r = ke^{a \cot \theta},$$

where the angle between the straight line ( $\theta = \text{constant}$ ) and the tangent to the curve is constant. In Table 1 a summary is provided of the types of spirals in mathematics.

The intent of this thesis is to study spirals in nature, specifically spirals which occur in cardiac tissue and are believed to cause re-entrant tachycardia. Spirals occur elsewhere in nature in the shells of gastropods (snails) and nautili and also in the shape of galaxies such as our own Milky Way. See Figure 3. Horns and antlers of certain species like the African Kudu and the ram are spiral-shaped, along with the arrangement of seeds in a daisy or sunflower, and the shape of the web woven by the

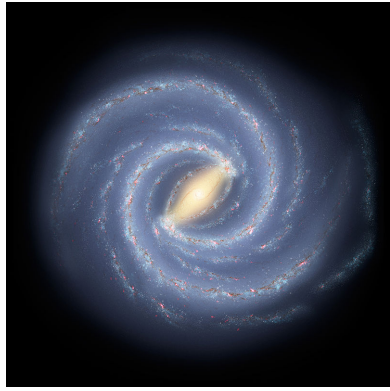


Figure 3: The Milky Way Galaxy, an artist’s updated rendition. Thanks to information from NASA’s Spitzer Space Telescope, the galaxy is now believed to have two major spiral arms, rather than four [31].

common *Eperia* spider [41]. To find spirals even closer to home, one’s fingerprints have spiral whorls; and, on the microscopic level, the DNA that defines us is in the form of a spiral double helix. According to physics theory, subatomic particles such as electrons may be composed of spiral structures known as “spiroons.” Pickover lists these other intriguing examples of spirals in nature: “the gentle curl of a fern tendril, the shape of an octopus’ retracted arm, the death form assumed by a centipede, the spiral intestine of a giraffe, the shape of a butterfly’s tongue, the spiral cross section of a scroll, the shape of the Yellow Brick Road in Munchkinland in the film classic *The Wizard of Oz* and even the characters in several written languages” [41].



Figure 4: Spiral Jetty, created by artist Robert Smithson in 1970 on the north arm of Great Salt Lake, Utah. More information at [7]. Picture taken by Soren Hayward [24].

## 2.2 Spiral Waves in Physical Systems

Spiral waves appear in chemical and biological systems, so that mathematical models which generate spiral wave solutions are relevant in the real world as ways to cheaply study these phenomena. Mathematical models also allow more rigorous study of phenomena where data collection is hindered or limited by the nature of the medium involved. For instance, measurement of electrical signals on the heart is physically limited by the number of electrodes that can be attached to the sample and limited in duration because the sample is burned and damaged in the process of measurement [43]. Some examples of chemical and biological systems where spirals occur are Belousov-Zhabotinsky (BZ) reactions [see Figure 5], surface catalytic oxidation reactions, cAMP waves in *dictyostelium discoideum*, and calcium waves in pancreatic beta cells [10].

Spiral waves in chemical and physical systems are generally smooth and continuous, with discontinuities more likely occurring in biological systems like lichens or flowers, but segmented spiral and target waves were observed by Vanag and Epstein in a BZ-type reaction. See Figure 6 [48]. In excitable media, difference in the ability to recover after a stimulus is known as heterogeneous (also inhomogeneous) refractoriness. This was from 1964 to 1994 the only logical reason that had been imagined for sudden formation of spiral waves until spirals were initiated in homogeneous excitable media by collision of wavefronts with inexcitable obstacles or sharp corners [1]. This was observed numerically and experimentally in the BZ reagent [1]. The Belousov-Zhabotinsky reaction consists of a “bromination of malonic acid by bromate ion in the presence of a ferrous phenanthroline (ferroin) catalyst,” and it transitions from an initial state of red solution to a spontaneous pattern of blue rings, which become spirals if broken mechanically or by changes in concentration and annihilate with collision with each other [10]. One can find excellent videos of

this reaction on the Internet.

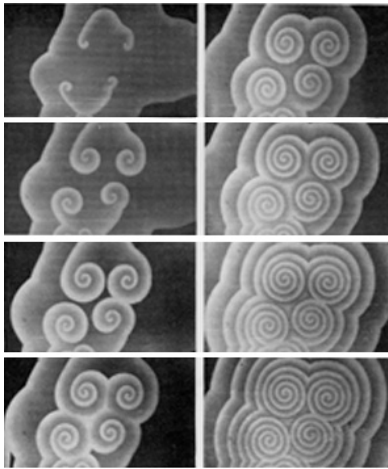


Figure 5: Spiral Waves Appearing in the Belousov-Zhabotinsky Reaction [51].

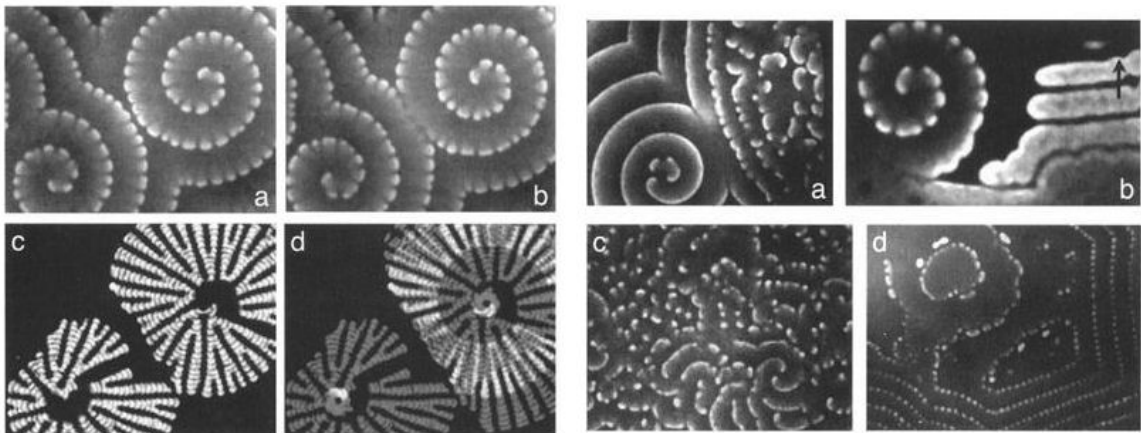


Figure 6: Segmented spiral waves and target waves in the Belousov-Zhabotinsky Reaction [48].

### 2.3 Spiral Waves and Cardiac Electrophysiology

Each heartbeat occurs largely unnoticed for most people but is a complex mechanism triggered and controlled by an intricate web of electrical activity through cardiac muscle tissue. A description of the anatomy and physiology of the heart could fill volumes, but a brief overview will be given here to facilitate understanding of the findings and the relevance of the mathematical model.

The heart is divided into four chambers: the left and right atria and the left and right ventricles. Each time the heart beats, oxygen-depleted blood from the body enters the right atrium via the superior and inferior vena cavae as the left atrium fills with oxygenated blood supplied from the lungs via the pulmonary vein. The next step in blood flow is atrial contraction. The right atrium contracts and pushes blood through the open tricuspid valve which separates the right atrium from the right ventricle. Simultaneously, the left atrium contracts and pushes the oxygen-rich blood into the left ventricle through the open valve separating the two chambers on the left side, which is called the bicuspid, or mitral, valve. When the ventricles are full, the valves snap shut to prevent a backflow of blood into the atria in the next step when the ventricles will squeeze to unload their precious cargo. In the last step of the cycle, the ventricles contract. Oxygen-depleted blood leaves the right ventricle via the pulmonic valve and goes onward through the pulmonary artery to the lungs, while oxygen-rich blood goes out to the body via the aorta after exiting the left ventricle via the aortic valve [19]. For most, this process happens unnoticed fifty to a hundred times every minute; but for some, there are abnormalities within this process.

Problems or abnormalities with the beat, or rhythm, of the heart are called arrhythmias. To better understand these arrhythmias, one needs to have a basic understanding of what triggers normal heart rhythm, also called normal sinus rhythm. Anyone who has ever watched a medical drama has probably seen a defibrillator being used to restart normal heart rhythm and noticed that an electric shock through two paddles is the mechanism used in this piece of equipment. Perhaps one might have even enjoyed Natalie Cole's hit, "Jump Start My Heart," back in the 1980's. Either way, this should supply the idea that electrical impulses control the contraction of cardiac muscle. The metronome of the heart's electrical system is the sinoatrial (SA) node, which is a specialized cell cluster located in the right

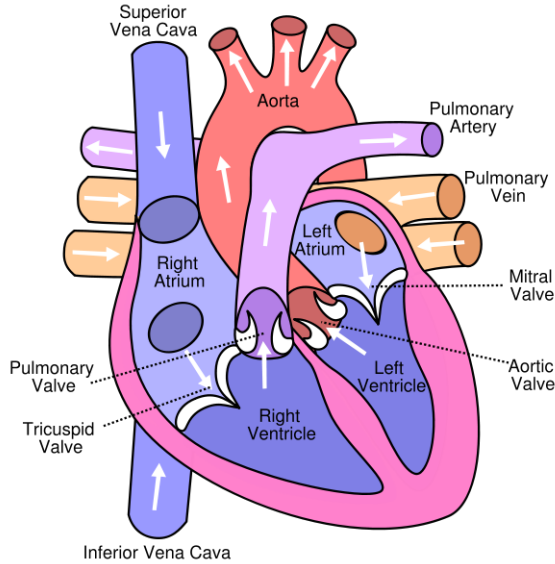


Figure 7: Anatomy of the Human Heart, Showing Direction of Blood Flow [16].

atrium. The electrical impulse for each beat begins here then travels through the walls of both atria, causing atrial contraction. The impulse then reaches another specialized cluster called the atrioventricular (AV) node, where there is a brief delay before the impulse is relayed to the ventricles through a network of fibers called the HIS-Purkinje system. As the impulse travels through the Purkinje fibers, ventricular contraction occurs, followed by the SA node firing another impulse and restarting the cycle [42].

Electrical activity of the heart can be measured using an electrocardiogram, or EKG/ECG. The P-wave represents atrial contraction, while the QRS-complex shows the electrical activity through the ventricles prior to ventricular contraction. The ST-interval is usually flat and represents the absence of electrical activity which occurs during ventricular contraction, while the T-wave shows the electrical reset of the ventricles as they prepare for their next contraction. The PR-interval indicates the time it takes an impulse to travel from the atria to the ventricles, which is usually 0.12 to 0.20 seconds. The QT-interval shows the length of time it takes the ventricles to depolarize as sodium enters and to repolarize as potassium leaves and is normally

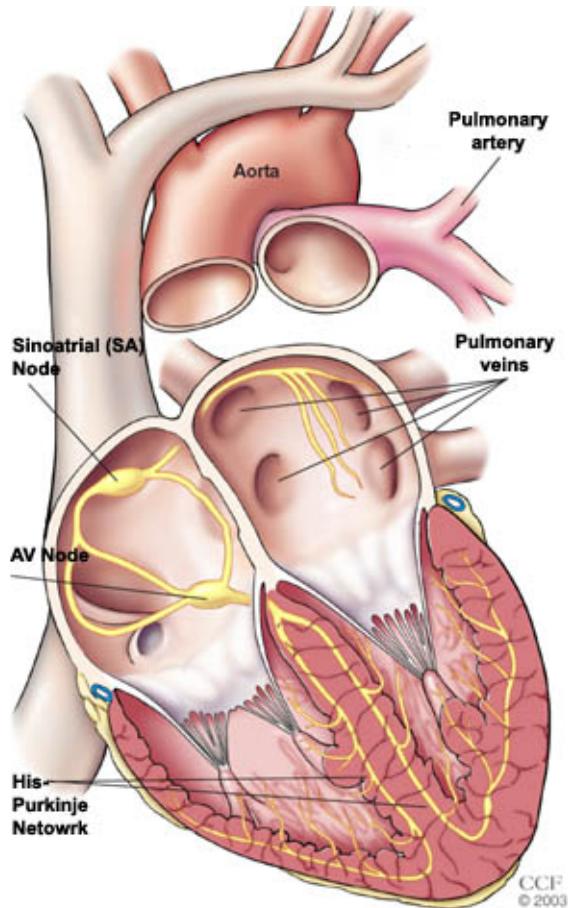


Figure 8: The Heart’s Electrical System [8].

less than half the R-R interval which varies based on the heart rate [42].

Arrhythmias are also referred to as irregular heart rhythms and dysrhythmias and can present as irregular patterns of electric current, rapid heart rate in excess of one hundred beats per minute (tachycardia), or slow heart rate below sixty beats per minute (bradycardia). A fast or slow heart rate does not always signify that one has an arrhythmia, however. Athletic activity, stress, and some medications can raise heart rate, while meditation, slow breathing, and other medications like sedatives can lower the heart rate. Arrhythmias are further classified by location, mechanism, and morphology. Supraventricular arrhythmias occur above the ventricles, as the name suggests, and ventricular arrhythmias occur within the ventricles [8].

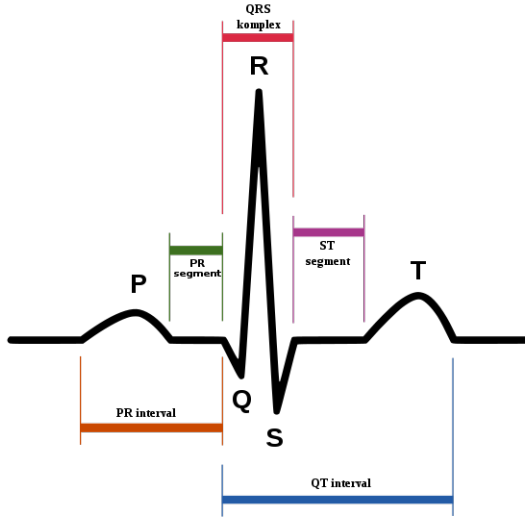


Figure 9: Electrocardiogram with Normal Sinus Rhythm [2].

The following are various types of supraventricular arrhythmias. Premature atrial contractions (PAC's) are early superfluous beats that originate in the atria. Paroxysmal supraventricular tachycardia (PVST) means a rapid but regular heart rhythm that comes from the atria, beginning and ending suddenly. Accessory pathway tachycardias, including Wolff-Parkinson-White Syndrome, are fast rhythms caused by the presence of an extraneous abnormal atrioventricular electrical connection [42]. This is like opening extra lanes on an expressway and allows electrical impulses to travel through the cardiac tissue very rapidly, leading to an accelerated heart rate. AV node re-entrant tachycardia (AVNRT) is a similar condition caused by having more than one pathway through the AV node [42]. Atrial tachycardia is any rapid heart rhythm in which the electrical impulses initiate in the atria and is sometimes called A-tach. Atrial fibrillation (A-fib) occurs when electrical impulses pop up all over the atria and compete for a chance to travel through the AV node, which causes a chaotic, rapid, and irregular heart rhythm. Because of the disorder among the electrical impulses, the muscles do not contract in a coordinated manner. Atrial flutter is caused by one or more rapid circuits of electrical activity in the atria.

but is usually more organized and regular than atrial fibrillation [8].

Ventricular arrhythmias originate in the two lower chambers of the heart. Premature ventricular contractions (PVC's) are early, extra beats just like PAC's except that they stem from the ventricles rather than the atria. PVC's are common, generally asymptomatic and do not usually require treatment, caused in some by stress, caffeine, nicotine, or exercise. On the other end of the spectrum is ventricular fibrillation (V-fib), which is a disorganized pattern of electrical activity in the ventricles. The ventricles cannot contract in an organized manner and instead quiver, making blood-flow to the body cease. Failure to quickly restore a normal sinus rhythm through electric shock (defibrillation) will result in sudden cardiac death, making it the most dangerous form of arrhythmia. The mechanism behind ventricular fibrillation remains debated, but there are several theories including Moe's multiple wavelet hypothesis, single source hypothesis, and spiral breakup and restitution hypothesis [39]. Spiral breakup and restitution hypothesis has gathered a following in the last three decades after computer models showed patterns similar to those seen experimentally in fibrillation. After the simulations begin, a single rotating spiral breaks off at the core, forming a second wavelet. This tries to form a second spiral, breaks, and eventually the broken spirals spread chaotic patterns to the entire medium [39].

Another type of ventricular arrhythmia is Long QT Syndrome (LQTS) in which there is a longer than normal time for the heart to contract and recover [8]. This leads to an increased risk for “torsades de pointes,” which is a form of polymorphic ventricular tachycardia. Polymorphic means that there are beat-to-beat differences in heart rhythm, which show up on an EKG, while monomorphic means there are no beat-to-beat variations. Ventricular tachycardias (V-tach) are rapid rhythms that begin in the lower heart and tend to be a more serious arrhythmia, because the rapid rate keeps the heart from adequately filling with blood and thus sending less blood to the body. This results both in less oxygenated blood reaching the tissues and in

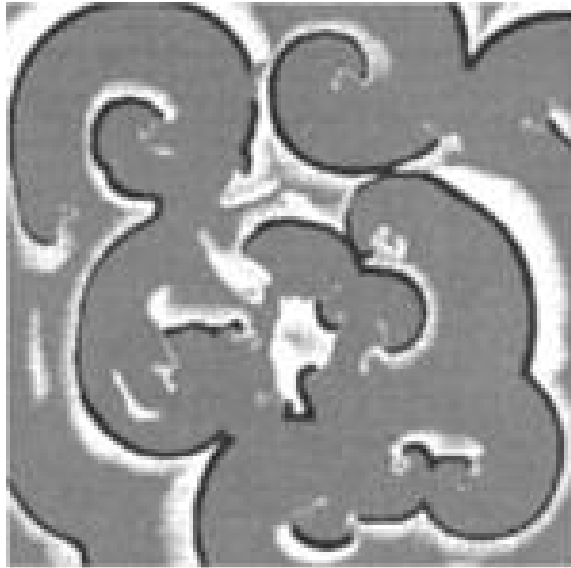


Figure 10: Spiral Breakup in a modified FitzHugh-Nagumo Model [39].

less efficiency in removing carbon dioxide and other waste and toxins from the body. Morphology of a tachycardia depends on its cause, which is why polymorphic tachycardias are more dangerous. When all beats look the same, it is because the impulse is generated from a single point or from a tight circle of electrical activity within the ventricle. One common example of this is when scarring of the heart occurs due to myocardial infarction (heart attack) [8]. This small area cannot conduct electrical current, so a circuit of potential around the scarred area causes the tachycardia. This is called a re-entrant circuit and can be modeled mathematically by creating a hole in the domain. Pertsov et alia determined through experimentation with dog and sheep ventricular epicardial muscle as well as computationally using a FHN type model similar to the one used in this thesis that spiral waves are a mechanism of tachycardia [40].

### 3 REACTION DIFFUSION MODELS FOR CARDIAC DYNAMICS

#### 3.1 History and Background on the FitzHugh-Nagumo Equations

Equations to model diffusion have long existed and have evolved to model diverse physical systems, from chemical reactions to nerve signals. The equations used in the code are adaptations of the FitzHugh-Nagumo system, which are a simplification of the Hodgkin Huxley (HH) equations, as described below.

Alan Lloyd Hodgkin and Andrew Fielding Huxley received the 1963 Nobel Prize in Physiology or Medicine for their work in studying nerve conduction [36]. They developed an ionic model through the study of electronic impulse propagation along the nerve axons of squid and cuttlefish [29, p. 177]. Their model was developed through the idea that a nerve fiber could be compared to an insulated metal wire that conducts electricity [23, p. 881]. This model is complex and so will only be briefly presented in this paper, so as not to add needless confusion, and will primarily be shown to emphasize the convenience and ease of the FitzHugh-Nagumo model.

In the HH model,  $V$  represents the transmembrane potential, while  $w$  represents the permeability to the different ions. The permeability of the membrane to sodium is determined by  $m$  and  $h$ , while  $n$  determines the permeability to potassium. The following are constants:  $R, V_K, V_{Na}$ , and  $V_L$ , though  $\tau_n, \tau_m, \tau_h, n_\infty, m_\infty$ , and  $h_\infty$  are functions. Precise definitions of these functions and constants can be found in [25], [26], [27], [28], and [29] but will not be given in this paper. The HH system is written:

$$\begin{aligned}\frac{\partial^2 V}{\partial x^2} &= R \left[ \frac{\partial V}{\partial t} + 36n^4(V - V_K) + 120m^3h(V - V_{Na}) + .3(V - V_L) \right] \\ \frac{\partial n}{\partial t} &= \frac{n_\infty(V) - n}{\tau_n(V)} \\ \frac{\partial m}{\partial t} &= \frac{m_\infty(V) - m}{\tau_m(V)}\end{aligned}$$

$$\frac{\partial h}{\partial t} = \frac{h_\infty(V) - h}{\tau_h(V)}. \quad (5)$$

This particular version of the system is borrowed from Hastings [23, p. 893].

Luckily, Richard FitzHugh constructed a simpler system which retains most of the same results of the Hodgkin-Huxley model, with greater ease in computation and analysis. FitzHugh's original model was dependent only on time and not position on the membrane's surface, so there was no diffusion term [14, p. 447]:

$$\begin{aligned} \frac{dx}{dt} &= c(y + x - \frac{x^3}{3} + z) \\ \frac{dy}{dt} &= -(x - a + by), \end{aligned} \quad (6)$$

where

$$1 - \frac{2b}{3} < a < 1, \quad 0 < b < 1, \quad b < c^2.$$

Here,  $x$  is the faster changing variable, and  $y$  changes slower than  $x$  except at the  $y$  nullcline.

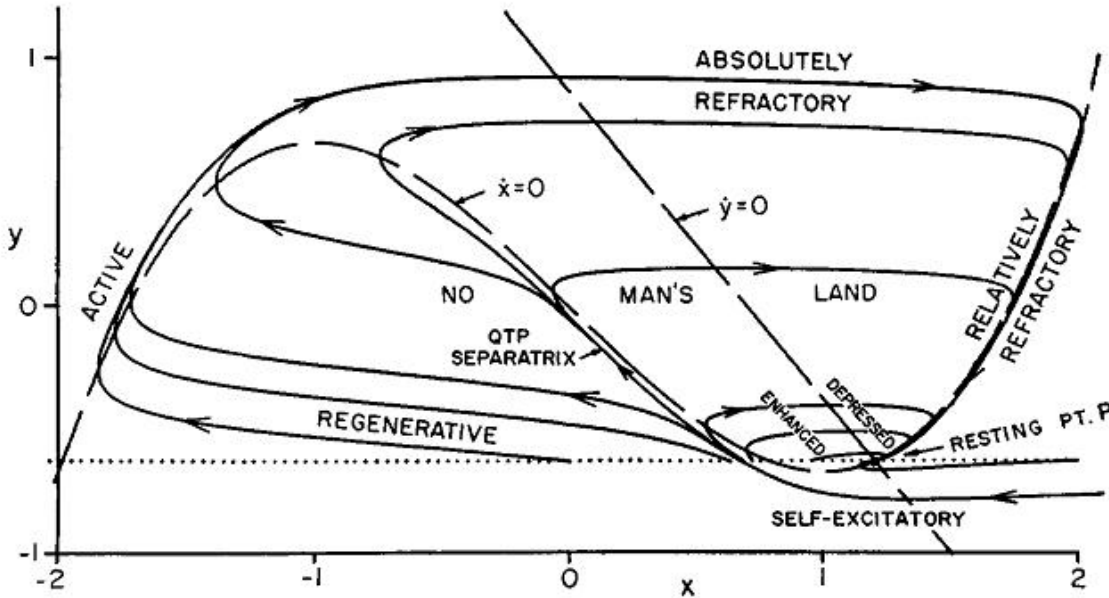


Figure 11: Phase plane for the FitzHugh's "BVP Model" [13].

Nullclines are found by setting  $\frac{dx}{dt}$  and  $\frac{dy}{dt}$  equal to zero, respectively, and solving for  $y$ . The phase plane for FitzHugh's system can be seen in Figure 11, where the equations for the nullclines are given by  $y = -x + \frac{x^3}{3} - z$  and  $y = \frac{a-x}{b}$ .

Stimulus intensity was represented by  $z$  in this system, where it is denoted  $I_{ex}$  in the model used in this thesis, and  $a$  and  $b$  were constants. Further, the model only contains ordinary differential equations. This reduction of the HH equations came from FitzHugh's observation that two gating variables  $n$  and  $h$  had slow kinetics relative to  $m$  [5]. FitzHugh stated that in his model, which he called the Bonhoeffer Van der Pol (BVP) model,  $x$  behaved as a combination of  $V$  and  $m$ , while  $y$  behaved like  $h$  and  $n$  in the HH equations [13]. Further, he noted that the  $V$ -nullcline was cubic in nature, while the  $n$ -nullcline could be linearly approximated, close enough to the physiological states of the variables [5]. It is this pairing of a cubic equation and linear equation that can be seen in Equation (6) and Equation (8), but simply with different variables used for the parameters.

The partial derivatives in the model used in this paper are due to Nagumo, Arimoto, and Yoshizawa [23, p.883]:

$$\begin{aligned}\frac{\partial^2 u}{\partial x^2} &= \frac{\partial u}{\partial t} - u(1-u)(u-a) + w \\ \frac{\partial w}{\partial t} &= bu,\end{aligned}\tag{7}$$

where  $a$  and  $b$  are positive constants with  $a < 1$  and  $b \ll 1$  due to  $w$  representing two slow-changing variables in the HH equations [23]. The variable  $u$  in the Nagumo system represents transmembrane potential, just as it does in the model used in this thesis. Various incarnations of the FitzHugh-Nagumo equations in different articles use different variable choices and slight modifications in arrangement, but the format remains the same: a cubic function for the first equation, which may or may not include a diffusion term or an external stimulus, and a linear function for the second

term.

### 3.2 Cartesian and Other Forms of the Model

The model examined in this thesis is from a paper by Jack Rogers and Andrew McCulloch, who used it to model cardiac electrical impulse propagation [43]. Such models attempt to give better insight into causes of cardiac arrhythmias by taking into account the complexities of the heart, such as fiber orientation as seen in Figure 12, and the heterogeneous curvature and topology of the organ as a whole.

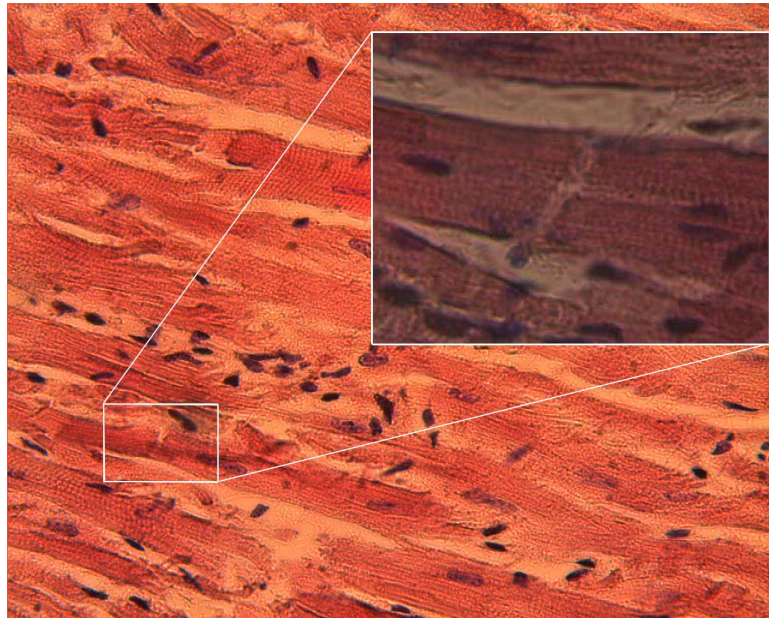


Figure 12: Microscopic view of Human Myocardial Tissue [17].

This paper uses the same model as Rogers and McCulloch, but with a different numerical scheme to find discretized solutions. The model can be written in Cartesian coordinates as:

$$\begin{aligned} \frac{\partial u}{\partial t} &= c_1 u(u - a)(1 - u) - c_2 uv + I_{ex} + G_x \frac{\partial^2 u}{\partial x^2} + G_y \frac{\partial^2 u}{\partial y^2} \\ \frac{\partial v}{\partial t} &= b(u - dv), \end{aligned} \quad (8)$$

where  $G_x$  and  $G_y$  are diffusion constants and  $a$ ,  $b$ ,  $c_1$ ,  $c_2$ , and  $d$  are membrane parameters that define the shape of the action potential. These are constant in time but not necessarily in space. The cubic term governs the activation, with three fixed points at  $u = 0$  (resting),  $u = 1$  (excited), and  $u = a$  (excitation threshold). The recovery variable is  $v$ , which brings the system to a refractory state, meaning it is at rest and briefly prevented from being re-excited for a certain period of time. This feature mirrors the recovery period the heart has between each electrical impulse, as discussed in the section on cardiac electrophysiology. In the second equation, the presence of  $u$  makes recovery dependent on the potential of neighboring regions. The final missing piece is  $I_{ex}$ , which is the amplitude of the external current, or stimulus being added to the system.

First, finite difference methods will be used to solve Equation (8), then Equation (8) will be extended to other geometries. To extend the scheme to polar coordinates, one must translate the Laplacian operator from Cartesian to polar coordinates.

Recall the derivation in polar coordinates,  $x = r \cos \theta$  and  $y = r \sin \theta$ . By the product rule and the chain rule,  $dx = \cos \theta dr - r \sin \theta d\theta$  and  $dy = \sin \theta dr + r \cos \theta d\theta$ .

This can be set up as a system of equations using matrices

$$\begin{bmatrix} dx \\ dy \end{bmatrix} = \begin{bmatrix} \cos \theta & -r \sin \theta \\ \sin \theta & r \cos \theta \end{bmatrix} \begin{bmatrix} dr \\ d\theta \end{bmatrix}. \quad (9)$$

Solve for  $dr$  and  $d\theta$  by multiplying both sides by the inverse matrix

$$\begin{aligned} \begin{bmatrix} \cos \theta & -r \sin \theta \\ \sin \theta & r \cos \theta \end{bmatrix}^{-1} &= \frac{1}{\cos \theta(r \cos \theta) - \sin \theta(-r \sin \theta)} \begin{bmatrix} r \cos \theta & r \sin \theta \\ -\sin \theta & \cos \theta \end{bmatrix} \\ &= \frac{1}{r} \begin{bmatrix} r \cos \theta & r \sin \theta \\ -\sin \theta & \cos \theta \end{bmatrix} = \begin{bmatrix} \cos \theta & \sin \theta \\ \frac{-\sin \theta}{r} & \frac{\cos \theta}{r} \end{bmatrix}. \end{aligned}$$

Thus,

$$\begin{bmatrix} dr \\ d\theta \end{bmatrix} = \begin{bmatrix} \cos \theta & \sin \theta \\ -\frac{\sin \theta}{r} & \frac{\cos \theta}{r} \end{bmatrix} \begin{bmatrix} dx \\ dy \end{bmatrix} = \begin{bmatrix} \frac{\partial r}{\partial x} & \frac{\partial r}{\partial y} \\ \frac{\partial \theta}{\partial x} & \frac{\partial \theta}{\partial y} \end{bmatrix} \begin{bmatrix} dx \\ dy \end{bmatrix} \quad (10)$$

$$\begin{bmatrix} u_x \\ u_y \end{bmatrix} = \begin{bmatrix} \frac{\partial r}{\partial x} & \frac{\partial \theta}{\partial x} \\ \frac{\partial r}{\partial y} & \frac{\partial \theta}{\partial y} \end{bmatrix} \begin{bmatrix} u_r \\ u_\theta \end{bmatrix} = \begin{bmatrix} \cos \theta & \frac{-\sin \theta}{r} \\ \sin \theta & \frac{\cos \theta}{r} \end{bmatrix} \begin{bmatrix} u_r \\ u_\theta \end{bmatrix}. \quad (11)$$

One can now write  $\frac{\partial}{\partial x}$  and  $\frac{\partial}{\partial y}$  in terms of  $\frac{\partial}{\partial r}$ ,  $\frac{\partial}{\partial \theta}$  as

$$\frac{\partial}{\partial x} = \cos \theta \frac{\partial}{\partial r} - \frac{\sin \theta}{r} \frac{\partial}{\partial \theta}$$

and

$$\frac{\partial}{\partial y} = \sin \theta \frac{\partial}{\partial r} + \frac{\cos \theta}{r} \frac{\partial}{\partial \theta}.$$

This allows one to compute the two dimensional Laplacian as

$$\begin{aligned} \frac{\partial^2}{\partial x^2} + \frac{\partial^2}{\partial y^2} &= \cos \theta \frac{\partial}{\partial r} (\cos \theta \frac{\partial}{\partial r}) - \cos \theta \frac{\partial}{\partial r} (\frac{\sin \theta}{r} \frac{\partial}{\partial \theta}) - \frac{\sin \theta}{r} \frac{\partial}{\partial \theta} (\cos \theta \frac{\partial}{\partial r}) + \frac{\sin \theta}{r} \frac{\partial}{\partial \theta} (\frac{\sin \theta}{r} \frac{\partial}{\partial \theta}) \\ &\quad + \sin \theta \frac{\partial}{\partial r} (\sin \theta \frac{\partial}{\partial r}) + \sin \theta \frac{\partial}{\partial r} (\frac{\cos \theta}{r} \frac{\partial}{\partial \theta}) + \frac{\cos \theta}{r} \frac{\partial}{\partial \theta} (\sin \theta \frac{\partial}{\partial r}) + \frac{\cos \theta}{r} \frac{\partial}{\partial \theta} (\frac{\cos \theta}{r} \frac{\partial}{\partial \theta}) = \\ &\quad \cos^2 \theta \frac{\partial^2}{\partial r^2} + \frac{1}{r^2} \sin \theta \cos \theta \frac{\partial}{\partial \theta} + \frac{1}{r} \sin^2 \theta \frac{\partial}{\partial r} + \frac{1}{r^2} \sin \theta \cos \theta \frac{\partial}{\partial \theta} + \frac{1}{r^2} \sin^2 \theta \frac{\partial^2}{\partial \theta^2} + \sin^2 \theta \frac{\partial^2}{\partial r^2} \\ &\quad - \frac{1}{r^2} \sin \theta \cos \theta \frac{\partial}{\partial \theta} + \frac{1}{r} \cos^2 \theta \frac{\partial}{\partial r} - \frac{1}{r^2} \sin \theta \cos \theta \frac{\partial}{\partial \theta} + \frac{1}{r^2} \cos^2 \theta \frac{\partial^2}{\partial \theta^2}. \end{aligned}$$

Note that the two pairs of  $\sin \theta \cos \theta$  terms have opposite signs and cancel each other.

Combine the remaining like terms:

$$\frac{\partial^2}{\partial x^2} + \frac{\partial^2}{\partial y^2} = (\cos^2 \theta + \sin^2 \theta) \frac{\partial^2}{\partial \theta^2} + (\sin^2 \theta + \cos^2 \theta) \frac{1}{r} \frac{\partial}{\partial r} + (\sin^2 \theta + \cos^2 \theta) \frac{1}{r^2} \frac{\partial^2}{\partial \theta^2}.$$

Since  $\cos^2 \theta + \sin^2 \theta = 1$ , this further simplifies to

$$\nabla^2 = \frac{\partial^2}{\partial r^2} + \frac{1}{r} \frac{\partial}{\partial r} + \frac{1}{r^2} \frac{\partial^2}{\partial \theta^2}. \quad (12)$$

Putting this in Sturm-Liouville form,

$$\nabla^2 = \frac{1}{r} \frac{\partial}{\partial r} \left( r \frac{\partial}{\partial r} \right) + \frac{1}{r^2} \frac{\partial}{\partial \theta^2}, \quad (13)$$

the system becomes

$$\begin{aligned} \frac{\partial u}{\partial t} &= c_1 u(u-a)(1-u) - c_2 uv + I_{ex} + G \left( \frac{1}{r} \frac{\partial}{\partial r} \left( r \frac{\partial u}{\partial r} \right) + \frac{1}{r^2} \frac{\partial^2 u}{\partial \theta^2} \right) \\ \frac{\partial v}{\partial t} &= b(u-dv). \end{aligned} \quad (14)$$

The following boundary conditions are imposed:

$$\begin{aligned} u(R, \theta, t) &= 0, \\ u(r, 0, t) &= u(r, 2\pi, t), \\ u_\theta(r, 0, t) &= u_\theta(r, 2\pi, t), \text{ and} \\ \lim_{r \rightarrow 0} u(r, \theta, t) &= \text{finite}, \end{aligned} \quad (15)$$

where,  $R$  is the radius of the disk. In a similar manner, one can rewrite the problem for a spherical geometry. In spherical coordinates, the diffusion term becomes:

$$\nabla^2 u = \frac{1}{r^2 \sin \theta} \frac{\partial}{\partial \theta} \left( \sin \theta \frac{\partial u}{\partial \theta} \right) + \frac{1}{r^2 \sin^2 \theta} \frac{\partial^2 u}{\partial \phi^2}. \quad (16)$$

So now the entire model in spherical coordinates is

$$\frac{\partial u}{\partial t} = c_1 u(u-a)(1-u) - c_2 uv + I_{ex} + G \left( \frac{1}{r^2 \sin \theta} \frac{\partial}{\partial \theta} \left( \sin \theta \frac{\partial u}{\partial \theta} \right) + \frac{1}{r^2 \sin^2 \theta} \frac{\partial^2 u}{\partial \phi^2} \right)$$

$$\frac{\partial v}{\partial t} = b(u - dv) \quad (17)$$

with periodic boundary conditions in  $\phi$ ,

$$\begin{aligned} u(R, \theta, 0, t) &= u(R, \theta, 2\pi, t) \\ u_\phi(R, \theta, 0, t) &= u_\phi(R, \theta, 2\pi, t), \end{aligned} \quad (18)$$

where R is the radius of the sphere, and singular at  $\theta = 0, \pi$  [18]. For the singular points, note that  $u(0, \phi_1, t) = u(0, \phi_2, t)$   $u(\pi, \phi_1, t) = u(\pi, \phi_2, t)$  for any  $\phi_1$  and  $\phi_2$ . So, any worry about the singular points can be removed by requiring that U is constant at the poles.

## 4 NUMERICAL MODELING

### 4.1 Finite Difference Methods in Cartesian Coordinates

Often, in cases where problems are of physical interest, it is desirable to find numerical solutions to partial differential equations. In this case, computational software (MATLAB) has been utilized to find numerical solutions for the diffusion term of our model using finite difference methods.

The creation of a finite difference method involves using a polynomial in  $\Delta x = x - x_0$  to approximate a function  $f(x)$  near a point  $x_0$ . Any order of polynomial can be used to approximate  $f(x)$ , beginning with a constant  $f(x) \approx f(x_0)$ . Each higher order polynomial gets increasingly more accurate, with the first order approximation being the line tangent to  $f(x)$  at  $x = x_0$ :

$$f(x) \approx f(x_0) + f'(x_0)\Delta x,$$

where  $\Delta x = x - x_0$ . A quadratic approximation of  $f(x)$  would be

$$f(x) \approx f(x_0) + f'(x_0)\Delta x + \frac{1}{2}f''(x_0)(\Delta x)^2.$$

A general form for this approximation can be written as

$$f(x) \approx f(x_0) + f'(x_0)\Delta x + \frac{1}{2}f''(x_0)(\Delta x)^2 + \dots + \frac{1}{n!}f^{(n)}(x_0)(\Delta x)^n + R_n$$

and is known as a Taylor Polynomial of degree  $n$  for  $\Delta x = x - x_0$ . The remainder  $R_n$  is the next term in the series evaluated at an intermediate point, typically unknown:

$$R_n = \frac{(\Delta x)^{n+1}}{(n+1)!}f^{(n+1)}(\xi_{n+1}), \quad \text{where } x_0 < \xi_{n+1} < x,$$

which is only valid if  $f$  has  $n + 1$  continuous derivatives.

This remainder is known as the truncation error and contributes to the accuracy of the approximation, and is described by the power on  $\Delta x$ . For example, the error in the linear approximation would be:

$$R_1 = \frac{(\Delta x)^2}{2} f''(\xi_2)$$

and has order  $(\Delta x)^2$ ,  $O((\Delta x)^2)$ . The linear approximation written with remainder is:

$$f(x) = f(x_0) + \Delta x f'(x_0) + \frac{(\Delta x)^2}{2} f''(\xi_2).$$

If  $\Delta x$  is small enough, then

$$R \approx \frac{(\Delta x)^2}{2} f''(x_0).$$

These polynomial approximations of  $f(x)$  can further be used to approximate derivatives for  $f(x)$ . One can find the first derivative by using the extended mean value theorem:

$$f(x_0 + \Delta x) = f(x_0) + \Delta x f'(x_0) + \frac{(\Delta x)^2}{2} f''(\xi_2)$$

Solving for  $f'(x_0)$  yields:

$$f'(x_0) = \frac{f(x_0 + \Delta x) - f(x_0)}{\Delta x} - \frac{\Delta x}{2} f''(\xi_2). \quad (19)$$

Thus, an approximation to  $f'(x)$  can be written as

$$f'(x_0) \approx \frac{f(x_0 + \Delta x) - f(x_0)}{\Delta x},$$

which is called the forward difference approximation. Equation (19) is valid for all

$x$ , so one can derive the backward difference approximation for  $f'(x)$  by substituting  $-\Delta x$  in place of  $\Delta x$  to yield:

$$f'(x_0) = \frac{f(x_0 - \Delta x) - f(x_0)}{-\Delta x} + \frac{\Delta x}{2} f''(\bar{\xi}_2)$$

or

$$f'(x_0) \approx \frac{f(x_0 - \Delta x) - f(x_0)}{-\Delta x}.$$

The truncation error for both schemes is  $O(\Delta x)$ , meaning  $|R| \leq C\Delta x$ , with  $C = \frac{M}{2}$  where M is an upper bound [21].

One can find a more accurate approximation for  $f'(x)$  by averaging the forward and backward difference schema to get a centered difference scheme:

$$\begin{aligned} 2f'(x) &= \frac{f(x_0 + \Delta x) - f(x_0)}{\Delta x} - \frac{\Delta x}{2} f''(\xi_2) + \frac{f(x_0 - \Delta x) - f(x_0)}{-\Delta x} + \frac{\Delta x}{2} f''(\bar{\xi}_2) \\ 2f'(x) &= \frac{f(x_0 + \Delta x) - f(x_0 - \Delta x)}{\Delta x} + \frac{\Delta x}{2} (f''(\bar{\xi}_2) - f''(\xi_2)). \end{aligned} \quad (20)$$

The error terms should nearly cancel since  $\xi_2$  and  $\bar{\xi}_2$  are very close, should be less than order  $\Delta x$ , and can be derived by using the Taylor Series for the forward and backward difference approximation,

$$\begin{aligned} f(x_0 + \Delta x) &= f(x_0) + \Delta x f'(x_0) + \frac{(\Delta x)^2}{2} f''(x_0) + \frac{(\Delta x)^3}{3!} f'''(x_0) + \dots \\ f(x_0 - \Delta x) &= f(x_0) - \Delta x f'(x_0) + \frac{(\Delta x)^2}{2} f''(x_0) - \frac{(\Delta x)^3}{3!} f'''(x_0) + \dots, \end{aligned} \quad (21)$$

subtracting

$$f(x_0 + \Delta x) - f(x_0 - \Delta x) = 2\Delta x f'(x_0) + \frac{2(\Delta x)^3}{3!} f'''(x_0) + \dots,$$

and solving for

$$f'(x_0) = \frac{f(x_0 + \Delta x) - f(x_0 - \Delta x)}{2\Delta x} - \frac{(\Delta x)^2}{6} f'''(\xi_3).$$

Thus, the centered difference approximation for  $f'(x_0)$  is:

$$f'(x_0) \approx \frac{f(x_0 + \Delta x) - f(x_0 - \Delta x)}{2\Delta x},$$

which has a truncation error  $O((\Delta x)^2)$ . This makes it more accurate and preferable to the forward or backward difference methods.

In the model used in this paper, second derivatives are needed. A central difference method will be utilized for finding the second derivative. In order to approximate the second derivative, one can add the forward and backward difference Taylor Series, so that odd terms vanish rather than the even ones:

$$f(x_0 + \Delta x) + f(x_0 - \Delta x) = 2f(x_0) + (\Delta x)^2 f''(x_0) + \frac{(\Delta x)^4}{12} f^{(4)}(\xi_4).$$

Solving for the second derivative

$$f''(x_0) = \frac{f(x_0 + \Delta x) + f(x_0 - \Delta x) - 2f(x_0)}{(\Delta x)^2} - \frac{(\Delta x)^2}{12} f^{(4)}(\xi_4).$$

So, the centered difference approximation for  $f''(x_0)$  is

$$f''(x_0) \approx \frac{f(x_0 + \Delta x) + f(x_0 - \Delta x) - 2f(x_0)}{(\Delta x)^2},$$

which has a truncation error  $O((\Delta x)^2)$ . This concept can be extended to partial derivatives as well; that is,

$$\frac{\partial^2 f}{\partial x^2} \approx \frac{f(x_0 + \Delta x, y_0) - 2f(x_0, y_0) + f(x_0 - \Delta x, y_0)}{\Delta x^2}.$$

Similarly,

$$\frac{\partial^2 f}{\partial y^2} \approx \frac{f(x_0, y_0 + \Delta y) - 2f(x_0, y_0) + f(x_0, y_0 - \Delta y)}{\Delta y^2}.$$

The next step is to set up the finite difference scheme for this system. Describe a Cartesian mesh with points  $(x_i, y_j), i = 2 \dots N - 1, j = 2 \dots M - 1$ . Then  $u_{i,j}$  is a numerical approximation of  $u(x_i, y_j)$ . Taking notation into account, the diffusion term in the system in rectangular coordinates becomes:

$$u_{yy} + u_{xx} \approx \frac{u_{i+1,j} - 2u_{i,j} + u_{i-1,j}}{\Delta x^2} + \frac{u_{i,j+1} - 2u_{i,j} + u_{i,j-1}}{\Delta y^2}.$$

This can be seen in these two lines of the code spiralwu.m, found in the Appendix:

```
uxx=(uu(2:end-1,1:end-2) + uu(2:end-1,3:end) -2*u)/h2;
uyy=(uu(1:end-2,2:end-1) + uu(3:end,2:end-1) -2*u)/h2;
```

In this code,  $h$  is the grid size, which is given to be the same in the  $x$  and  $y$  direction, so that “ $h2$ ” is  $h^2 = \Delta x^2 = \Delta y^2$ . Taking into account the padded matrix, the first term in the numerator of  $u_{xx}$  is always one row above  $u_0$  and thus is  $u_{i,j-1}$ , with the second term being  $u_{i,j+1}$ , and the third being  $-2u_{i,j}$ . Similarly for  $u_{yy}$ , the first is  $u_{i-1,j}$  the second  $u_{i+1,j}$ , and the third  $-2u_{i,j}$ . Matrices were used to optimize the code, in lieu of writing loops, because MATLAB computes very quickly using matrices. The matrices had to be padded in order to compute values along the boundaries, meaning extra rows and columns were added around the outer edges. The content of this “padding” can be changed according to various boundary conditions including Dirichlet and Neumann boundary conditions.

Using a forward difference in time and a centered difference in position, the scheme in Cartesian coordinates is

$$\mathbf{u}^{(n+1)} = \mathbf{u}^{(n)} + \Delta t \left( c_1 \mathbf{u}^{(n)} (\mathbf{u}^{(n)} - a)(1 - \mathbf{u}^{(n)}) - c_2 \mathbf{u}^{(n)} \mathbf{v}^{(n)} + I_{ex} + D \Delta_{ij}^{(n)} \right)$$

$$\begin{aligned}\mathbf{v}^{(n+1)} &= \mathbf{v}^{(n)} + \Delta tb \left( \mathbf{u}^{(n)} - d\mathbf{v}^{(n)} \right), \text{ where} \\ \Delta_{ij}^{(n)} &= \left( \frac{u_{i+1,j}^{(n)} - 2u_{i,j}^{(n)} + u_{i-1,j}^{(n)}}{\Delta x^2} \right) + \left( \frac{u_{i,j+1}^{(n)} - 2u_{i,j}^{(n)} + u_{i,j-1}^{(n)}}{\Delta y^2} \right).\end{aligned}\quad (22)$$

## 4.2 Finite Difference Methods in Other Geometries

This scheme had to be extended, then, to polar and spherical geometries in order to modify the code to simulate diffusion on a disk or a sphere.

Omitting for now the  $\frac{1}{r^2}$ , the second term in Equation (13) can be computed simply using the same finite difference method from before:

$$u_{\theta\theta} \cong \frac{1}{\Delta\theta^2} (u_{ij-1} - 2u_{ij} + u_{ij+1}) \quad (23)$$

where  $i = 2 \dots N - 1$  and  $j = 2 \dots M - 1$ . Again, the code was optimized by using matrices rather than loops. Equation (23) can be written as the matrix product

$$u_{\theta\theta} \cong u_t A_z,$$

where

$$u_t A_z = \frac{1}{\Delta\theta^2} \begin{bmatrix} u_{11} & u_{12} & u_{13} & u_{14} & \dots & u_{1M} \\ u_{21} & u_{22} & u_{23} & u_{24} & \dots & u_{2M} \\ u_{31} & u_{32} & u_{33} & u_{34} & \dots & u_{3M} \\ u_{41} & u_{42} & u_{43} & u_{44} & \dots & u_{4M} \\ \vdots & \vdots & \vdots & \vdots & & \vdots \\ u_{N1} & u_{N2} & u_{N3} & u_{N4} & \dots & u_{NM} \end{bmatrix} \begin{bmatrix} -2 & 1 & 0 & 0 & \dots & 1 \\ 1 & -2 & 1 & 0 & \dots & 0 \\ 0 & 1 & -2 & 1 & \dots & 0 \\ 0 & 0 & 1 & -2 & \dots & 0 \\ \vdots & \vdots & \vdots & \vdots & & \vdots \\ 1 & 0 & 0 & 0 & \dots & 0 \end{bmatrix}. \quad (24)$$

The first part of the diffusion term is a bit more complicated:

$$\frac{\partial}{\partial r} \left( r \frac{\partial u}{\partial r} \right)_{ij} = \frac{u_{i-1,j} (r_{i-1} + r_i)}{2\Delta r^2} - \frac{u_{ij} (r_{i-1} + 2r_i + r_{i+1})}{\Delta r^2} + \frac{u_{i+1,j} (r_i + r_{i+1})}{\Delta r^2}. \quad (25)$$

Letting  $s_{i-1} = r_{i-1} + r_i$ , this piece can also be set up in matrix form to run faster in MATLAB:

$$\frac{\partial}{\partial r} \left( r \frac{\partial u}{\partial r} \right)_{ij} = A_r u_t \quad (26)$$

where

$$A_r = \begin{bmatrix} \frac{-1}{\Delta r} & \frac{1}{\Delta r} & 0 & \dots & \dots & \dots & 0 \\ s_1 & -(s_1 + s_2) & s_2 & \dots & \dots & \dots & 0 \\ 0 & s_2 & -(s_2 + s_3) & \dots & \dots & \dots & 0 \\ 0 & 0 & s_3 & \dots & \dots & \dots & 0 \\ \vdots & \vdots & \vdots & \vdots & \vdots & \vdots & \vdots \\ 0 & 0 & 0 & \dots & s_{N-2} & -(s_{N-2} + s_{N-1}) & s_{N-1} \\ 0 & 0 & 0 & \dots & \dots & \dots & 0 \end{bmatrix} \quad (27)$$

and

$$u_t = \begin{bmatrix} u_{11} & u_{12} & u_{13} & u_{14} & \dots & u_{1M} \\ u_{21} & u_{22} & u_{23} & u_{24} & \dots & u_{2M} \\ u_{31} & u_{32} & u_{33} & u_{34} & \dots & u_{3M} \\ u_{41} & u_{42} & u_{43} & u_{44} & \dots & u_{4M} \\ \vdots & \vdots & \vdots & \vdots & & \vdots \\ \vdots & \vdots & \vdots & \vdots & & \vdots \\ u_{N1} & u_{N2} & u_{N3} & u_{N4} & \dots & u_{NM} \end{bmatrix}. \quad (28)$$

The first two elements in the  $A_r$  matrix are in place, because the center needs to be

finite. Rewriting

$$\frac{\partial}{\partial r} \left( r \frac{\partial u}{\partial r} \right) = r \frac{\partial^2 u}{\partial r^2} + \frac{\partial u}{\partial r},$$

one can see that at  $r = 0$ , the first term vanishes for  $u_{rr} = \text{finite}$ . Computing the product for the first row,

$$\begin{aligned} A_r u_0 &= \begin{bmatrix} \frac{u_{21}}{\Delta r} - \frac{u_{11}}{\Delta r} & \frac{u_{22}}{\Delta r} - \frac{u_{12}}{\Delta r} & \frac{u_{23}}{\Delta r} - \frac{u_{13}}{\Delta r} & \frac{u_{24}}{\Delta r} - \frac{u_{14}}{\Delta r} & \dots & \frac{u_{1M}}{\Delta r} - \frac{u_{1,M-1}}{\Delta r} \end{bmatrix} \\ &= \begin{bmatrix} 0 & 0 & 0 & 0 & \dots & 0 \end{bmatrix}, \end{aligned} \quad (29)$$

one can see having  $\frac{-1}{\Delta r}$  and  $\frac{1}{\Delta r}$  causes  $\frac{\partial u}{\partial r}$  to vanish at  $r = 0$  as well, meeting the condition that the center be finite. Putting this diffusion term in polar coordinates into the system, the finite difference scheme can be written:

$$\begin{aligned} \mathbf{u}^{(n+1)} &= \mathbf{u}^{(n)} + \Delta t \left( f(\mathbf{u}, \mathbf{v}) + I_{ex} + D \left( \frac{\mathbf{A}_r \mathbf{u}^{(n)}}{r} + \frac{\mathbf{u}^{(n)} \mathbf{A}_z}{r^2} \right) \right) \\ \mathbf{v}^{(n+1)} &= \mathbf{v}^{(n)} + \Delta t b \left( \mathbf{u}^{(n)} - d \mathbf{v}^{(n)} \right), \text{ for} \\ f(\mathbf{u}, \mathbf{v}) &= c_1 \mathbf{u}^{(n)} (\mathbf{u}^{(n)} - a) (1 - \mathbf{u}^{(n)}) - c_2 \mathbf{u}^{(n)} \mathbf{v}^{(n)} \end{aligned} \quad (30)$$

with Dirichlet boundary conditions in  $r$ ,  $\mathbf{u}_{N,j} = 0$ ,  $j = 1, \dots, M$ , and periodic boundary conditions in  $\theta$ ,  $\mathbf{u}_{N,1} = \mathbf{u}_{N,M+1}$ ,  $i = 1, \dots, N$ .

Comparing the diffusion term in polar coordinates (Equation (13)) and spherical coordinates (Equation (16)), one can see that some simple substitutions allow the forward difference scheme to easily be modified to work for spherical coordinates.

Letting

$$u_{\phi\phi} \cong u_t A_z,$$

for

$$u_t A_z = \frac{1}{\Delta\phi^2} \begin{bmatrix} u_{11} & u_{12} & u_{13} & u_{14} & \dots & u_{1M} \\ u_{21} & u_{22} & u_{23} & u_{24} & \dots & u_{2M} \\ u_{31} & u_{32} & u_{33} & u_{34} & \dots & u_{3M} \\ u_{41} & u_{42} & u_{43} & u_{44} & \dots & u_{4M} \\ \vdots & \vdots & \vdots & \vdots & & \vdots \\ u_{N1} & u_{N2} & u_{N3} & u_{N4} & \dots & u_{NM} \end{bmatrix} \begin{bmatrix} -2 & 1 & 0 & 0 & \dots & 1 \\ 1 & -2 & 1 & 0 & \dots & 0 \\ 0 & 1 & -2 & 1 & \dots & 0 \\ 0 & 0 & 1 & -2 & \dots & 0 \\ \vdots & \vdots & \vdots & \vdots & & \vdots \\ 1 & 0 & 0 & 0 & \dots & 0 \end{bmatrix}, \quad (31)$$

and the same matrices as above for  $A_r u_t$ , but with  $r = \sin \theta$  and the  $\frac{1}{r^2}$  from

$$\frac{1}{r^2 \sin \theta} \frac{\partial}{\partial \theta} \left( \sin \theta \frac{\partial u}{\partial \theta} \right) + \frac{1}{r^2 \sin^2 \theta} \frac{\partial^2 u}{\partial \phi^2}$$

pulled into the diffusion constant  $D$ , the forward difference scheme for spherical coordinates is

$$\begin{aligned} \mathbf{u}^{(n+1)} &= \mathbf{u}^{(n)} + \Delta t \left( f(\mathbf{u}, \mathbf{v}) + I_{ex} + D \left( \frac{\mathbf{A}_r \mathbf{u}^{(n)}}{r} + \frac{\mathbf{u}^{(n)} \mathbf{A}_z}{r^2} \right) \right) \\ \mathbf{v}^{(n+1)} &= \mathbf{v}^{(n)} + \Delta t b \left( \mathbf{u}^{(n)} - d \mathbf{v}^{(n)} \right), \text{ for} \\ f(\mathbf{u}, \mathbf{v}) &= c_1 \mathbf{u}^{(n)} (\mathbf{u}^{(n)} - a) (1 - \mathbf{u}^{(n)}) - c_2 \mathbf{u}^{(n)} \mathbf{v}^{(n)} \end{aligned} \quad (32)$$

with periodic boundary conditions in  $\phi$ ,  $\mathbf{u}_{N,1} = \mathbf{u}_{N,M+1}$ ,  $i = 1, \dots, N$ , and singular at the two poles,  $\theta = 0, \pi$ .

### 4.3 Stability

Haberman describes stability for the one dimensional heat equation in his section on Fourier-von Neumann Stability Analysis [21]. Define a finite difference scheme,

using a forward difference in time and centered difference in position as:

$$u_m^{(n+1)} = u_m^{(n)} + s \left( u_{m+1}^{(n)} - 2u_m^{(n)} + u_{m-1}^{(n)} \right), \quad (33)$$

with  $u_m^{(n)}$  is the numerical solution at time  $t = n\Delta t$ , position  $x = m\Delta x$ , and  $s \equiv \frac{D\Delta t}{\Delta x^2}$ .

One seeks a condition that the solution remains bounded as  $n$  gets large when finding solutions wave number  $k$  of the form

$$u_m^{(n)} = \lambda^n e^{ikm\Delta x}, \quad (34)$$

this condition being that  $|\lambda| < 1$ . Substituting Equation (34) into the finite difference scheme yields

$$\lambda = 1 - 2s [1 - \cos k\Delta x]. \quad (35)$$

Since  $|\lambda| < 1$ ,  $s \leq \frac{1}{2}$  [21].

This can be extended into a rectangular region as used in the Cartesian finite difference scheme in this thesis. Using a similar process as Haberman did for the one-dimensional heat equation, Neal shows that for  $\Delta x = \Delta y$ ,  $s \leq \frac{1}{4}$  [34, p. 16-18], and this same stability condition can also be seen on p. 254 of Haberman's book [21]. Requiring  $s < \frac{1}{4}$  allows the diffusion constant and time step to be larger than in the polar and spherical schema.

Estimates of the stability for polar and spherical allow one to choose appropriate choices of diffusion constant, time step, and mesh size. One can see what happens in Figure 13 when the system becomes unstable. Recalling the Laplacian operator,

$$\nabla^2 = D \left( \frac{1}{r} \frac{\partial}{\partial r} \left( r \frac{\partial u}{\partial r} \right) + \frac{1}{r^2} \frac{\partial^2 u}{\partial \theta^2} \right), \quad (36)$$

compare the last term to the 2-D Cartesian case above. It should contribute  $\frac{1}{r^2} \frac{D\Delta t}{\Delta \theta^2}$

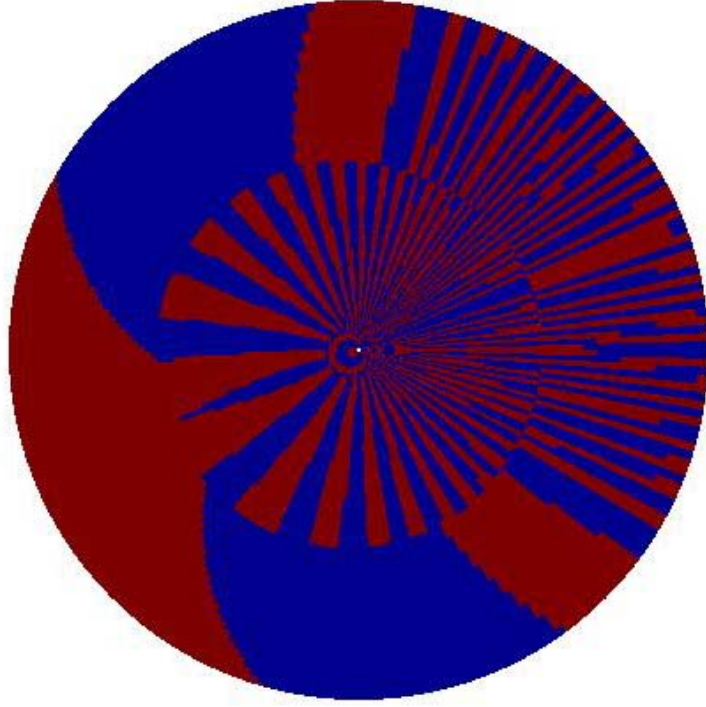


Figure 13: Polar system blows up for  $D = 1$  and  $\Delta t = 0.00001$

to the stability condition. Remembering that

$$\frac{\partial}{\partial r} \left( r \frac{\partial u}{\partial r} \right) = \frac{\partial^2 u}{\partial r^2} + \frac{1}{r} \frac{\partial u}{\partial r},$$

one finds a contribution of  $\frac{D\Delta t}{\Delta r^2}$  and  $\frac{1}{r} \frac{D\Delta t}{\Delta r}$  from each of the two radial terms. In addition to small values of  $\Delta t$ ,  $\Delta r$ , and  $\Delta\theta$  being of interest when looking at the behavior of the numerical solution,  $r$  can also be as small as  $\Delta r$  in the computations. Thus, terms containing  $r$  also contribute to system instability.

$$\frac{\partial}{\partial r} \left( r \frac{\partial u}{\partial r} \right)$$

then contributes  $\frac{D\Delta t}{\Delta r^2}$ , and

$$\frac{1}{r^2} \frac{\partial^2 u}{\partial \theta^2}$$

contributes  $\frac{1}{r^2} \frac{D\Delta t}{\Delta\theta^2}$  to the stability analysis, so that the entire system should reasonably require

$$\left| \frac{D\Delta t}{\Delta r^2 \Delta\theta^2} \right| << 1. \quad (37)$$

As seen in the appendix, the value in DiffusionFDcyl.m for  $\Delta r$  is  $\frac{1}{64}$  and  $\Delta\theta = \frac{2\pi}{101}$ .

Thus,

$$\Delta r^2 \Delta\theta^2 = \frac{4\pi^2}{41783296} \approx 9.45 \times 10^{-7}.$$

This means that  $D\Delta t$  must be even smaller to maintain stability. In DiffusionFDcyl.m,  $D\Delta t = (1 \times 10^{-6})0.1 = 1 \times 10^{-7}$ , so that

$$\frac{D\Delta t}{\Delta r^2 \Delta\theta^2} \approx \frac{1 \times 10^{-7}}{9.45 \times 10^{-7}} \approx 0.11. \quad (38)$$

For spherical coordinates, recall the Laplacian operator

$$\nabla^2 u = \frac{1}{r^2 \sin\theta} \frac{\partial}{\partial\theta} \left( \sin\theta \frac{\partial u}{\partial\theta} \right) + \frac{1}{r^2 \sin^2\theta} \frac{\partial^2 u}{\partial\phi^2}. \quad (39)$$

Similar to the Cartesian case, the second term logically contributes  $\frac{D\Delta t}{r^2 \sin^2\theta \Delta\theta^2}$ .

By product rule,

$$\frac{1}{r^2 \sin\theta} \frac{\partial}{\partial\theta} \left( \sin\theta \frac{\partial u}{\partial\theta} \right) = \sin\theta \frac{\partial^2 u}{\partial\theta^2} + \cos\theta \frac{\partial u}{\partial\theta}.$$

These two terms contribute  $\sin\theta \frac{D\Delta t}{\Delta\theta^2}$  and  $\cos\theta \frac{D\Delta t}{\Delta\theta}$ , producing for the stability condition

$$\left| \frac{D\Delta t}{\Delta\theta^2 \Delta\phi^2} \right| << 1. \quad (40)$$

Substituting the values  $D = 1 \times 10^{-6}$ ,  $\Delta t = 0.1$ ,  $\Delta\theta = \frac{\pi}{200}$ , and  $\Delta\phi = \frac{2\pi}{201}$  from

DiffusionFDsphere, as seen in the Appendix,

$$\frac{D\Delta t}{\Delta\theta^2\Delta\phi^2} \approx \frac{1 \times 10^{-7}}{2.41 \times 10^{-7}} \approx 0.42. \quad (41)$$

#### 4.4 Exact Solution

While developing the code and testing the diffusion part of the simulation, the analytical solution of the diffusion equation in polar coordinates,

$$u_t = \nabla^2 u, \quad (42)$$

satisfying Dirichlet boundary conditions,  $u(R, \theta, t) = 0$  and initial condition

$$u(r, \theta, 0) = \begin{cases} \beta, & r_1 < r < r_2, \quad \theta_1 < \theta < \theta_2 \\ 0 & \text{otherwise,} \end{cases} \quad (43)$$

was examined.

The solution of this problem can be obtained using the method of separation of variables. This results in the series solution

$$u(r, \theta, t) = \sum_{m=0}^{\infty} \sum_{n=1}^{\infty} [A_{mn} \cos m\theta + B_{mn} \sin m\theta] J_m \left( \sqrt{k_{mn}} r \right) e^{-k_{mn} t},$$

where

$$k_{mn} = \left( \frac{j_{mn}}{R} \right)^2$$

for  $j_{mn}$  the  $n$ th zero of the  $m$ th order Bessel function,  $J_m(j_{mn}) = 0$ . The initial condition thus satisfies

$$u(r, \theta, 0) = \sum_{m=0}^{\infty} \sum_{n=1}^{\infty} [A_{mn} \cos m\theta + B_{mn} \sin m\theta] J_m \left( \sqrt{k_{mn}} r \right).$$

This is a double Fourier-Bessel series, whose coefficient can be found through the insertion of the above piecewise constant function on the polar domain. For  $m > 0$ , one has

$$A_{mn} = \frac{2\beta}{\pi R^2 J_{m+1}^2(j_{mn})} \int_{\theta_1}^{\theta_2} \cos m\theta d\theta \int_{r_1}^{r_2} J_m(\sqrt{k_m n r}) r dr,$$

and

$$B_{mn} = \frac{2\beta}{\pi R^2 J_{m+1}^2(j_{mn})} \int_{\theta_1}^{\theta_2} \sin m\theta d\theta \int_{r_1}^{r_2} J_m(\sqrt{k_m n r}) r dr.$$

For  $m = 0$ ,

$$A_{0n} = \frac{2\beta}{\pi R^2 J_{m+1}^2(j_{mn})} \int_{\theta_1}^{\theta_2} d\theta \int_{r_1}^{r_2} J_m(\sqrt{k_m n r}) r dr,$$

The trigonometric integrals are easy to carry out. However, the Bessel function integrals are not, so in the code DiffusionPolar.m, these integrals are done numerically, using MATLAB's quadrature function, quadv.

## 5 RESULTS

Numerical models using a forward difference scheme were used to find approximate solutions to Fitz-Hugh Nagumo type systems in Cartesian,

$$\begin{aligned}\frac{\partial u}{\partial t} &= c_1 u(u - a)(1 - u) - c_2 uv + I_{ex} + G_x \frac{\partial^2 u}{\partial x^2} + G_y \frac{\partial^2 u}{\partial y^2} \\ \frac{\partial v}{\partial t} &= b(u - dv),\end{aligned}\tag{44}$$

cylindrical,

$$\begin{aligned}\frac{\partial u}{\partial t} &= c_1 u(u - a)(1 - u) - c_2 uv + I_{ex} + G \left( \frac{1}{r} \frac{\partial}{\partial r} \left( r \frac{\partial u}{\partial r} \right) + \frac{1}{r^2} \frac{\partial^2 u}{\partial \theta^2} \right) \\ \frac{\partial v}{\partial t} &= b(u - dv),\end{aligned}\tag{45}$$

and spherical,

$$\begin{aligned}\frac{\partial u}{\partial t} &= c_1 u(u - a)(1 - u) - c_2 uv + I_{ex} + G \left( \frac{1}{r^2 \sin \theta} \frac{\partial}{\partial \theta} \left( \sin \theta \frac{\partial u}{\partial \theta} \right) + \frac{1}{r^2 \sin^2 \theta} \frac{\partial^2 u}{\partial \phi^2} \right) \\ \frac{\partial v}{\partial t} &= b(u - dv),\end{aligned}\tag{46}$$

geometries. Parameters including the initial values of  $u$  and  $v$ , the positions and magnitude of the external stimuli ( $I_{ex}$ ), diffusion constants ( $G_x$  and  $G_y$ ), duration, size of time steps ( $\Delta t$ ), mesh size ( $h = \Delta x = \Delta y$ ), anisotropy (the ratio of the two diffusion constants  $G_x$  to  $G_y$ ), initial conditions, boundary conditions, and activation threshold ( $a$ ) were adjusted and then simulations run. For each simulation, data was collected in the form of images consistently captured at various time steps so that comparisons could be made between various simulations. Modifications were made to the code to optimize its performance and to make it simpler to modify given parameters.

### 5.1 Nullclines

In order to pick parameters in the system (Equations (44) - (46)) which lead to spiral waves, one needs to consider the nullclines in the non-diffusive system

$$\frac{du}{dt} = c_1 u(u - a)(1 - u) - c_2 uv \quad (47)$$

$$\frac{dv}{dt} = b(u - dv). \quad (48)$$

The nullclines occur for  $\frac{du}{dt} = 0$  or  $\frac{dv}{dt} = 0$ . Thus, one has

$$u [c_1(u - a)(1 - u) - c_2v] = 0 \quad (49)$$

$$b(u - dv) = 0. \quad (50)$$

So, the nullclines are given by two lines  $u = 0$ ,  $u = dv$ , and the parabola

$$v = \beta(1 - u)(u - a),$$

where  $\beta = \frac{c_1}{c_2}$ . There are three equilibrium points for this system, given by the intersections of the nullclines.

The idea, as discussed by Barkley [4], FitzHugh [13], Zykov [52], or Gomatam and Amdjadi [18], is that one of these fixed points is excitable and is stable to small perturbations. However, given a large enough perturbation, the system may be driven towards a new excitable region before returning to the stable fixed point. For the parameters used in this paper, one can plot the nullclines and note that the parabolic nullcline only intersects the slanted line for particular values of the parameters. This is shown in Figures 14, 15, 16, and 17. A further exploration of the first order system (48) in the phase plane (Figure 18) can quickly give the reader

an idea as to how solutions behave in the phase plane.

The points of intersection are easily found. Requiring  $\frac{du}{dt} = 0$  and  $\frac{dv}{dt} = 0$ , but for  $u \neq 0$ , we have

$$u = \beta'(1 - u)(u - a),$$

where  $\beta' = \beta d = \frac{c_1 d}{c_2}$ . This quadratic equation for  $u$  can only be solved when

$$(\beta'^{-1} - (1 + a))^2 \geq 4a.$$

The parameters are chosen  $b = 0.013$ ,  $c_1 = 0.26$ ,  $c_2 = 0.1$ , and  $d = 1.0$ . Varying  $a$ , one can see that the threshold is about  $a = 0.14$  as seen in Figures 14, 15, 16, and 17.

In exploration of the diffusive system (Equations (44) - (46)), a diffusive term for varying geometries (rectangular, polar, and spherical) will be added. The only differences in principle are the affects of the discretizations in space and time, and the diffusion constant. The expectations are that fixing the parameters at the above values with  $a = 0.13$  should lead to spiral waves.

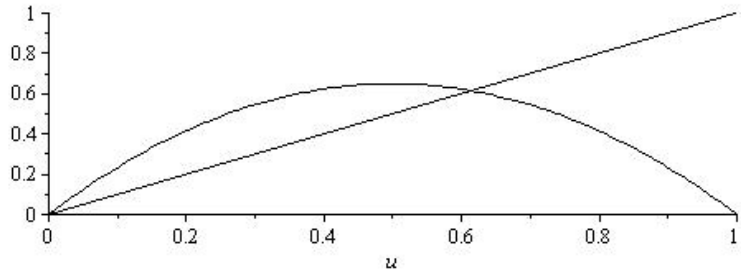


Figure 14: Nullclines for the Modified FHN System, with  $a = 0$ ,  $b = 0.013$ ,  $c_1 = 0.26$ ,  $c_2 = 0.1$ , and  $d = 1.0$

## 5.2 Results in Rectangular Coordinates

Results are given for two forms of the code in rectangular coordinates. The earlier form of the code only allowed for constant or zero values for the initial conditions,

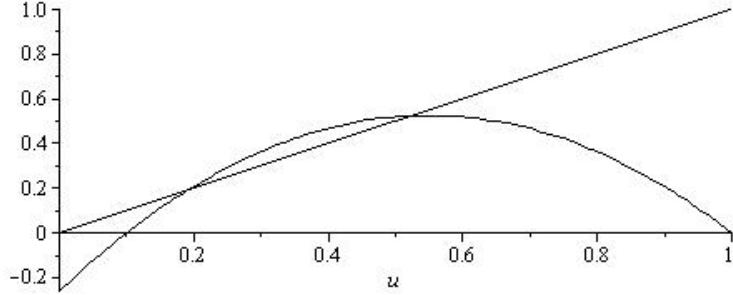


Figure 15: Nullclines for the Modified FHN System, with  $a = 0.1$ ,  $b = 0.013$ ,  $c_1 = 0.26$ ,  $c_2 = 0.1$ , and  $d = 1.0$

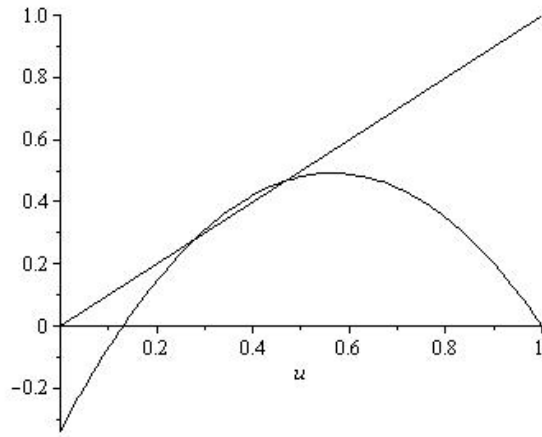


Figure 16: Nullclines for the Modified FHN System, with  $a = 0.13$ ,  $b = 0.013$ ,  $c_1 = 0.26$ ,  $c_2 = 0.1$ , and  $d = 1.0$

which would represent a homogeneous medium. The later code allows for random initial conditions, representing inhomogeneity of the medium, but can also be set to give results for constant or zero value initial conditions. The first and second stimulus were manipulated by trial and error to fit the mesh so that spirals would form. With no stimulus applied and constant initial conditions, of course, nothing would happen – the entire grid would simply remain at that constant value. Thus, in these cases external current was applied at heights ranging from 0.5 to 40. Letting the initial values for  $u$  and  $v$  be zero, for external stimulus values above 30, the wavefront rapidly extinguishes. Table 2 shows spiraling tips for stimulus values below 30, with FHN parameter values  $a = 0.13$ ,  $b = 0.013$ ,  $c_1 = 0.26$ ,  $c_2 = 0.1$ , and

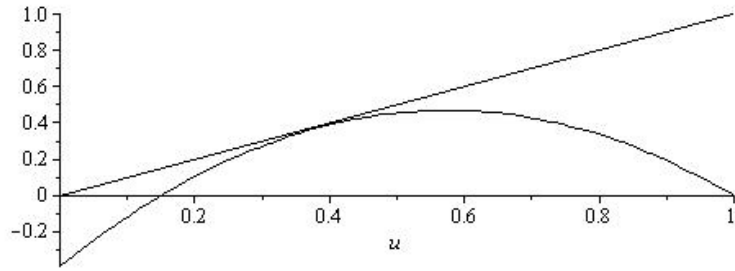


Figure 17: Nullclines for the Modified FHN System, with  $a = 0.15$ ,  $b = 0.013$ ,  $c_1 = 0.26$ ,  $c_2 = 0.1$ , and  $d = 1.0$

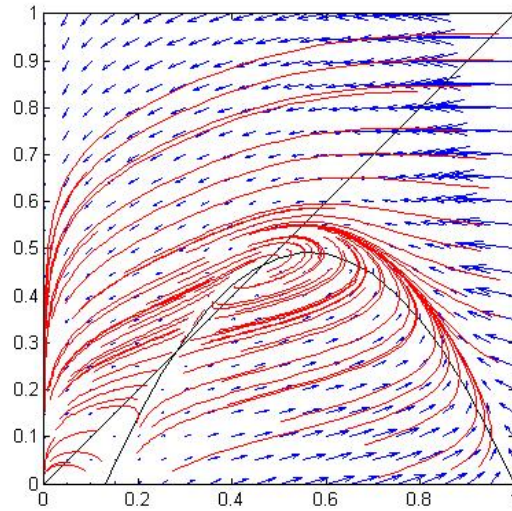


Figure 18: Phase plane for modified FHN model with parameter values  $a = 0.13$ ,  $b = 0.013$ ,  $c_1 = 0.26$ ,  $c_2 = 0.1$ , and  $d = 1.0$ .

$d = 1.0$ . Changing the amplitude of the external stimulus did not appear to affect the formation of spirals, except for values above 30, where the wavefront extinguishes so rapidly that the simulation ends abruptly shortly after it begins. In fact, the results at a given time,  $t = 25000$  in the table, are so similar that they appear identical, but one can see that the maximum values of  $u$  and  $v$  do indeed differ.

The initial choice for parameter values ( $a = 0.13$ ,  $b = 0.013$ ,  $c_1 = 0.26$ ,  $c_2 = 0.1$ , and  $d = 1.0$ ) comes from the work of Jack Rogers and Andrew McCulloch, who arrived at these values by “trial and error” [43]. Parameter values were tweaked after looking at the nullclines and phase planes for our system, as seen in Figures 16

Table 2: Changing stimulus heights, with zero initial conditions. Images and values given are at 25000 time steps.

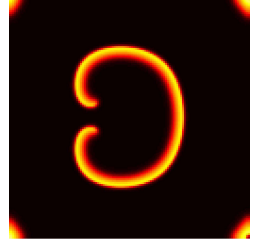
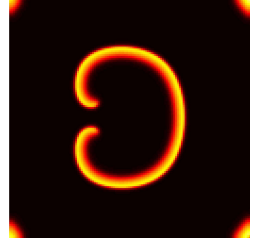
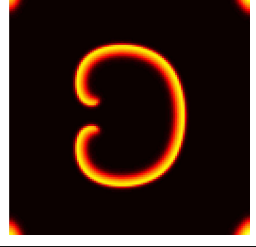
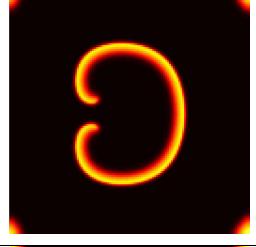
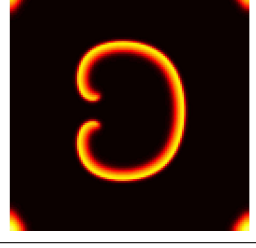
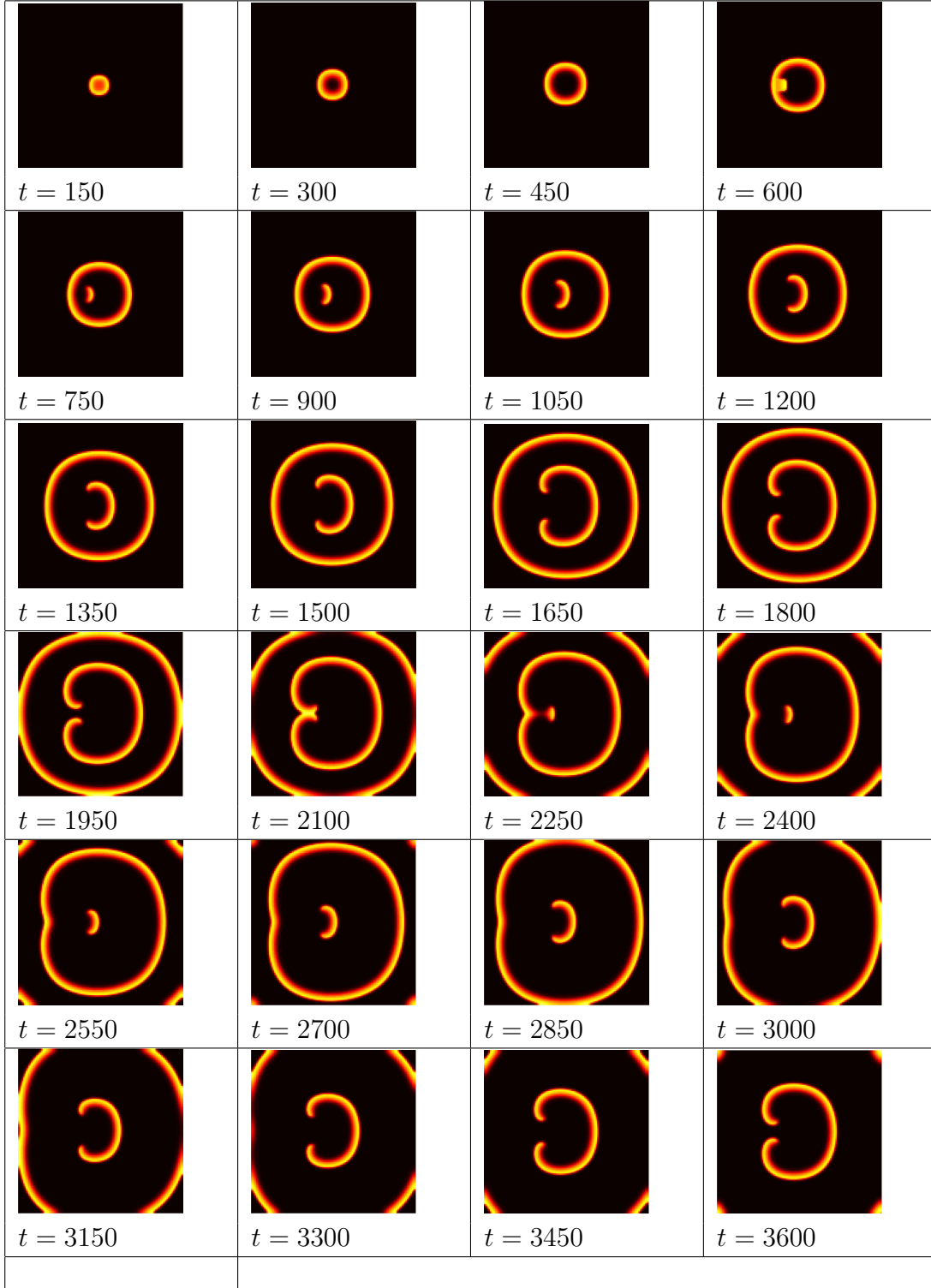
Stimulus Amplitude	$u_{max}$	$v_{max}$	Image
0.5	0.80	0.37	
1	0.73	0.45	
5	0.67	0.49	
10	0.66	0.50	
20	0.84	0.32	

Table 3: Images showing one run of the Cartesian code, spiralwu.m, with zero initial conditions at  $a=0.13$ .



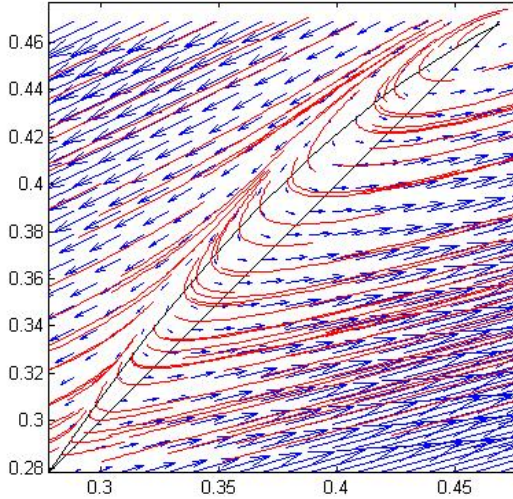


Figure 19: Close-up of phase plane for modified FHN model with same parameter values.

- 19. It was hypothesized that the most interesting behavior would take place in the area between the two intersection points of the nullclines, and one can see by looking at the nullclines for various values of  $a$  that the intersection is largest for  $a = 0$  and gets smaller until there is no intersection for  $a = 0.15$ . Thus, simulations were run for values of  $a$  from 0 to 0.15 for zero initial conditions, random initial conditions, and constant initial conditions.

For the tables and from here forward in the text, define  $u_0$  to be the initial values across the  $u$  matrix and similarly for  $v_0$ . Constant values for  $u$  and  $v$  were chosen to be values within the intersection,  $u_0 = v_0 = 0.4$ . Time steps are given under each image, and  $n$  can be calculated. In Tables 4-7,  $n = \frac{20}{3}t$ . Other variables were kept at the same constant values as before:  $b = 0.013$ ,  $c_1 = 0.26$ ,  $c_2 = 0.1$ , and  $d = 1.0$ .

Spiral behavior can be seen for zero initial conditions when the second stimulus target wave breaks through collision with another the first stimulus target wave. This collision is only initiated when the first stimulus does not disperse completely before the second stimulus begins and the two stimuli are placed carefully on the

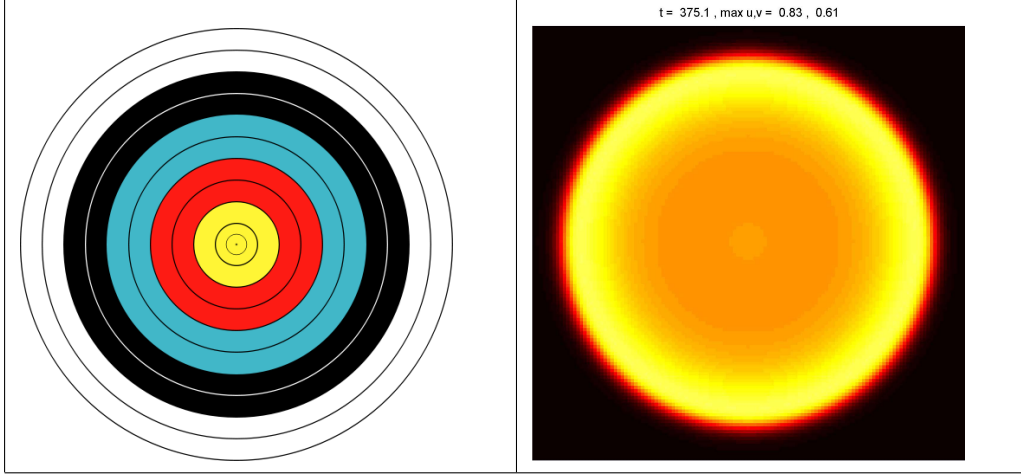


Figure 20: An archery target [3] and an image taken from solving the FHN system in Cartesian coordinates, with  $t = 375.1$ ,  $a = 0.03$ , zero initial conditions, and  $I_{ex} = 30$ .

mesh to facilitate collision. After the collision breaks apart the wave front, two tips spiral inward, collide, break apart, reform, and spiral inward again periodically, as seen in Table 3. The target wave is so named because of its resemblance to a target with concentric rings, such as an archery target (Figure 20).

Spiral behavior was not observed with constant initial conditions, the values for the constants being chosen based on the phase planes for the system to be  $u_0 = v_0 = 0.4$ , as seen in Table 6. Simulations were also run using values so that  $u_0 \neq v_0$ , but spirals were not observed in those cases either. Results from  $a = 0.02$  to  $a = 0.09$  were very similar to  $a = 0.01$ , and results from  $a = 0.14$  were very close to those of  $a = 0.12$ , so these results are not shown in Table 6.

For random initial conditions, target waves were seen for various values of the activation threshold, as seen in Table 7 for values of  $a$  from 0.12 to 0.14, with collision and breakup of wavefronts observed for  $a = 0.15$ , which was similar to the collision and breakup that lead to spirals for zero initial conditions.

Table 4: Changing activation threshold, with zero initial conditions, for  $a = 0.1$  to  $0.7$ .

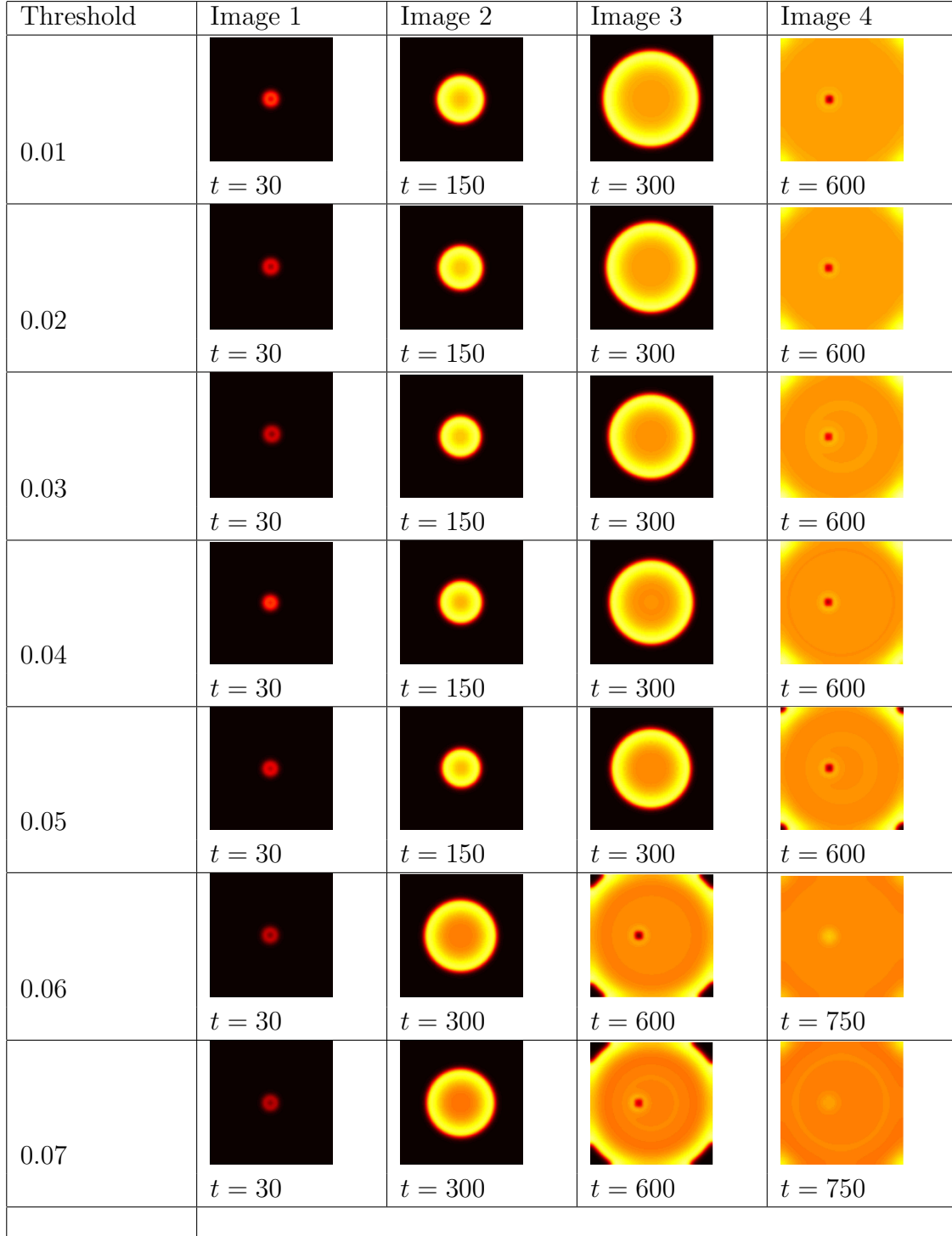


Table 5: Changing activation threshold, with zero initial conditions, for  $a = 0.8$  to  $0.14$ .

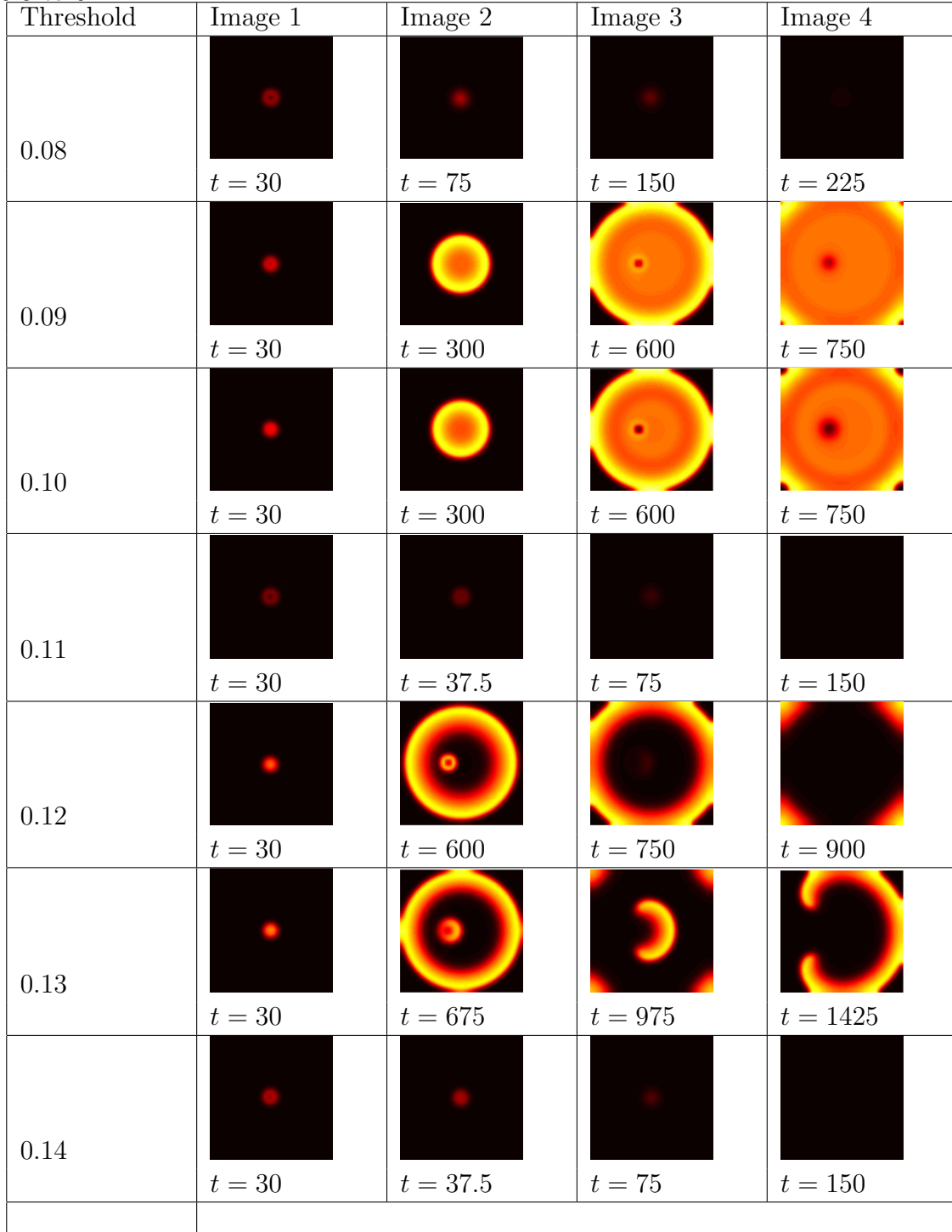


Table 6: Changing activation threshold, with constant initial conditions.

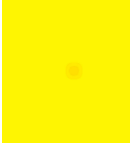
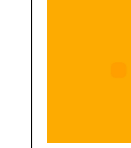
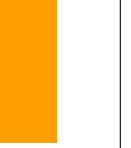
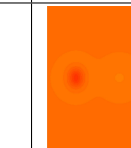
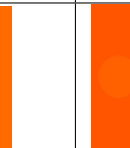
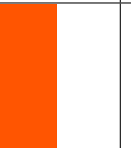
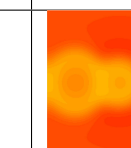
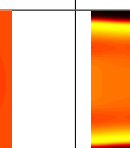
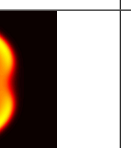
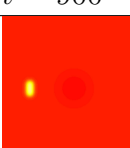
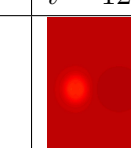
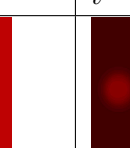
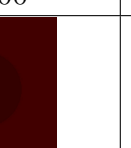
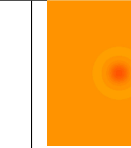
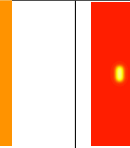
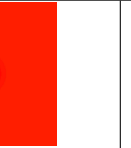
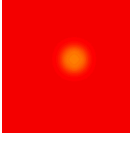
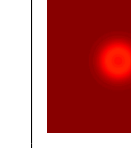
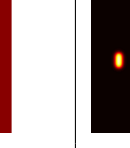
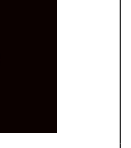
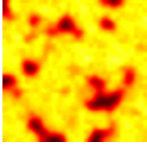
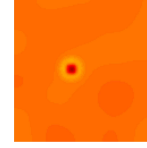
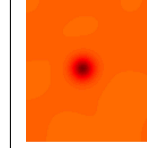
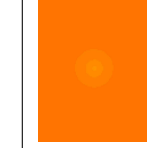
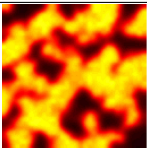
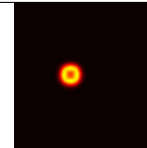
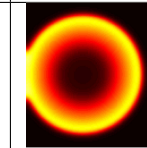
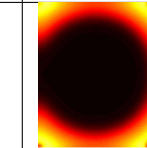
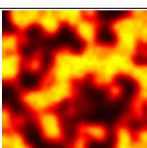
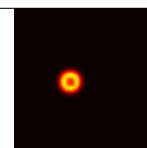
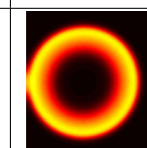
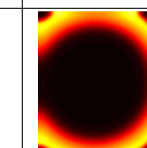
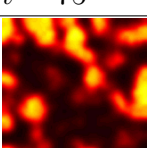
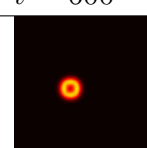
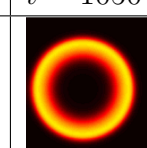
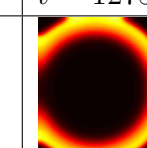
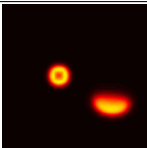
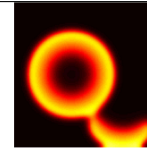
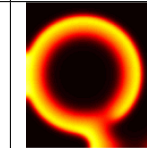
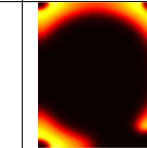
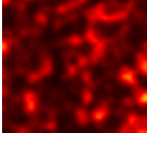
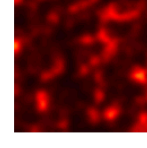
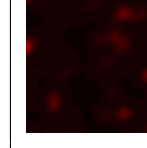
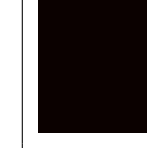
Threshold	Image 1	Image 2	Image 3	Image 4
0.01	 $t = 150$	 $t = 450$	 $t = 600$	 $t = 900$
0.10	 $t = 750$	 $t = 900$	 $t = 1500$	 $t = 2700$
0.11	 $t = 900$	 $t = 1200$	 $t = 3300$	 $t = 3450$
0.12	 $t = 600$	 $t = 750$	 $t = 900$	 $t = 1050$
0.13	 $t = 150$	 $t = 300$	 $t = 600$	 $t = 750$
0.15	 $t = 150$	 $t = 300$	 $t = 600$	 $t = 750$

Table 7: Changing activation threshold, with randomized initial conditions.

Threshold	Image 1	Image 2	Image 3	Image 4
0.10	 $t = 75$	 $t = 600$	 $t = 750$	 $t = 900$
0.12	 $t = 75$	 $t = 600$	 $t = 1050$	 $t = 1275$
0.13	 $t = 75$	 $t = 600$	 $t = 1050$	 $t = 1275$
0.14	 $t = 75$	 $t = 600$	 $t = 1050$	 $t = 1275$
0.15	 $nt = 600$	 $t = 975$	 $t = 1125$	 $t = 1350$
0.2	 $t = 30$	 $t = 37.5$	 $t = 75$	 $t = 600$

### 5.3 Results in Polar Coordinates

After narrowing down the proper FHN parameters in Cartesian coordinates where the run time was vastly shorter, these same parameters were utilized to run the code in polar and spherical coordinates. The system in polar coordinates was also solved analytically using the method of separation of variables and solutions plotted using MATLAB, seen in Table 8. Briefly, a pattern forms during the analytical solution because of the zeros of the Bessel functions, but by  $t = 0.3$ , the solution displays the same diffusion pattern as the finite difference scheme.

With the earlier simulations using the original DiffusionFDcyl4.m code, solutions were plotted with homogeneous initial conditions and with random, heterogeneous initial conditions with stimulus added, and then with random initial conditions and no stimulus applied, as seen in Tables 9 - 11.

These earlier results were a bit disheartening. One can see there are no spirals in those images. Further investigation led to finally seeing spiral behavior with random initial conditions by changing the diffusion constant from  $D = 0.1$  to  $D = 1 \times 10^{-6}$ , deactivating the external stimulus, changing grid size, and modifying the size of the time step from  $\Delta t = 1 \times 10^{-6}$  to  $\Delta t = 0.1$ , as seen in Tables 12 and 13 and in the DiffusionFDcyl.m code in the Appendix. The product of the diffusion constant and the time step had to be small to maintain stability, as was discussed previously. By reversing the two values, the code ran much faster and diffused slow enough to observe spirals. One can see the random initial conditions at  $t = 0.1$  and the spiral beginning to form at  $t = 3095$ . At  $t = 4135.7$ , the excited regions have intensified. The images for  $t = 5368.35$  to  $t = 6225.2$  show these curves of excitation drifting into the boundaries; and they have disappeared by  $t = 6934.9$ , leaving only the counterclockwise rotating spiral for the duration of the simulation.

Table 8: Solving the FHN system Analytically in Polar Coordinates.

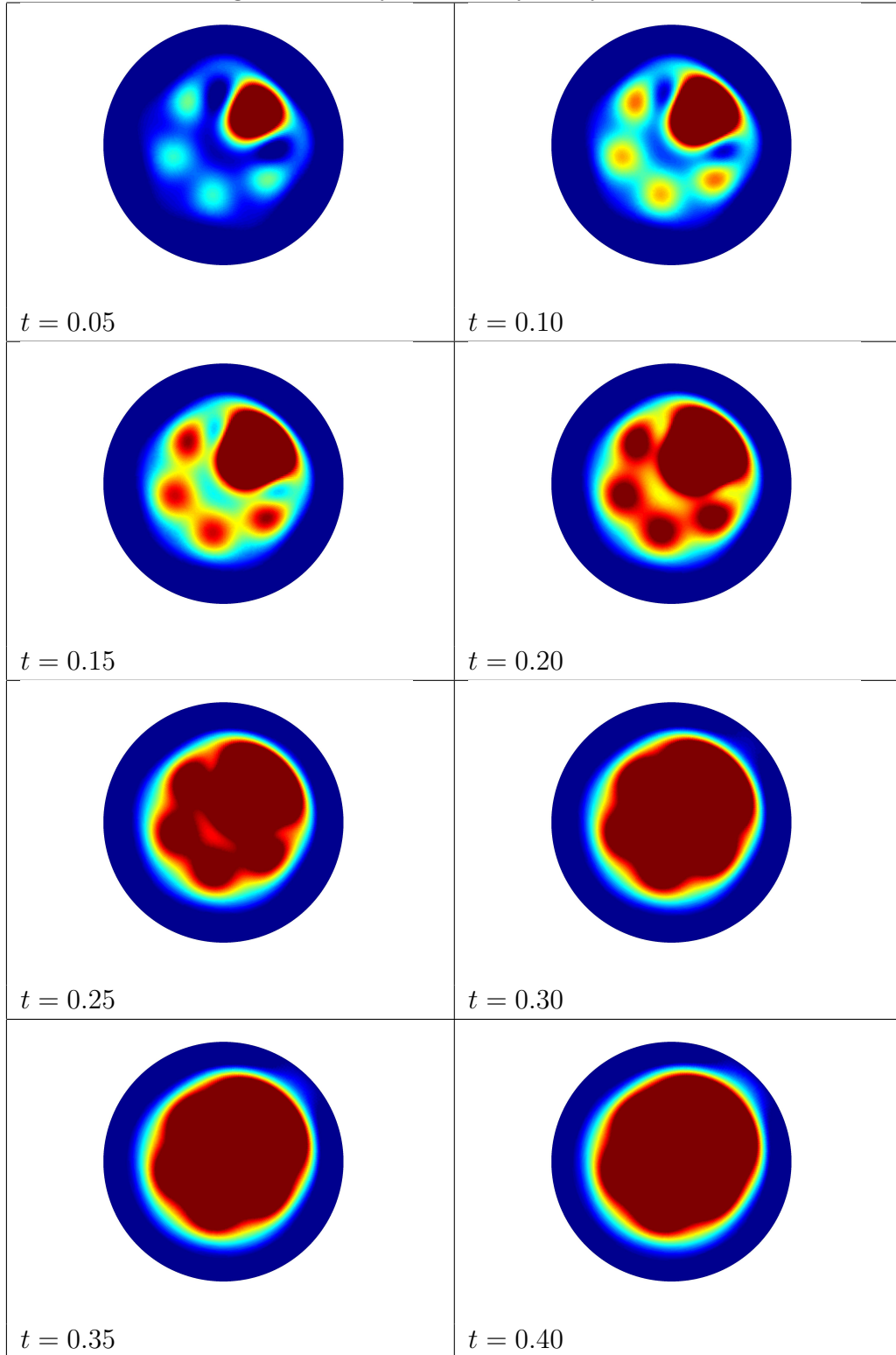


Table 9: Solving the FHN system Computationally in Polar Coordinates, with  $u_0 = v_0 = 0$  and an External Stimulus Applied with Value  $I_{ex} = 30$ .

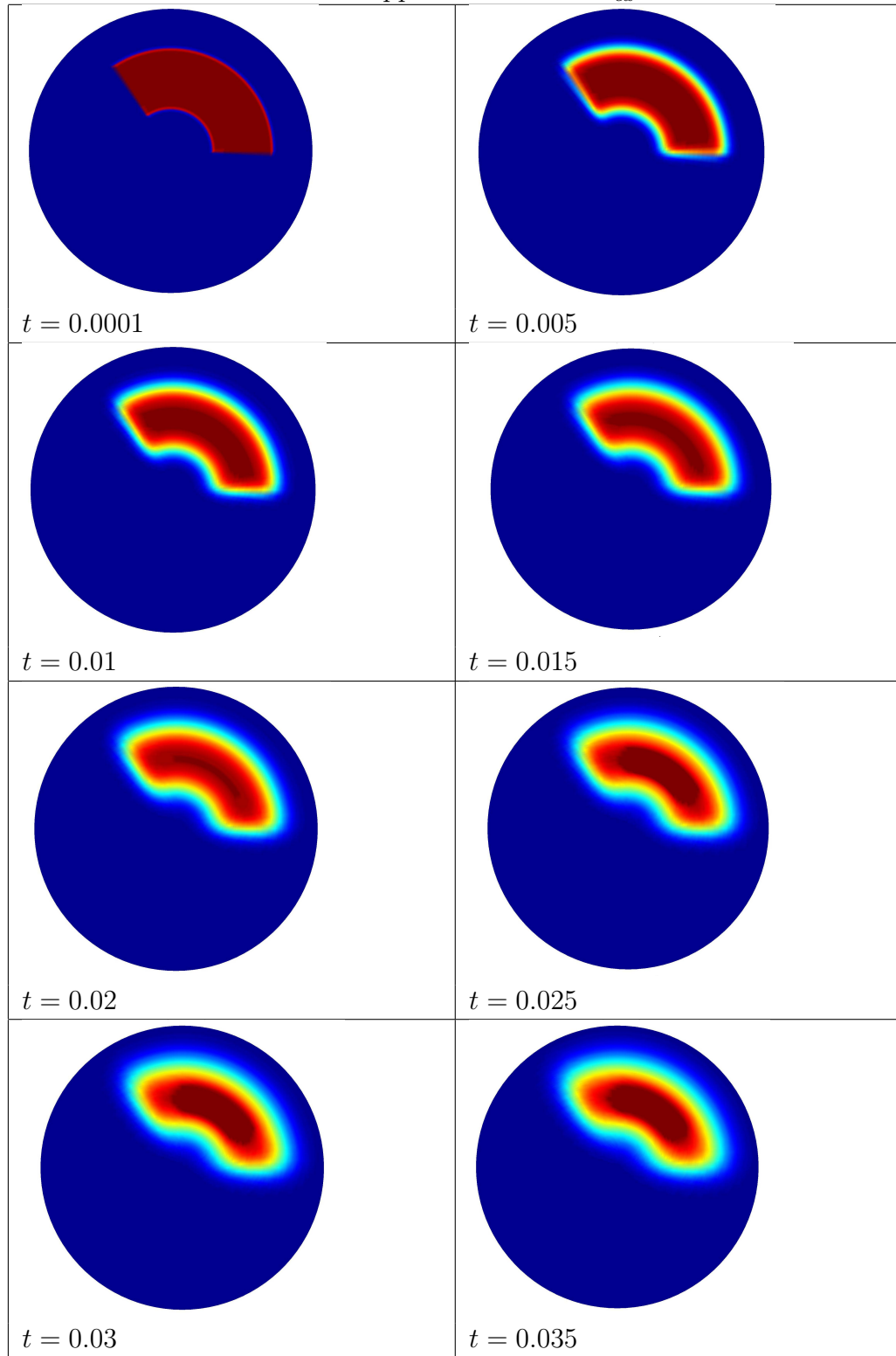


Table 10: Solving the FHN system Computationally in Polar Coordinates, with Randomized Initial Conditions and No External Stimulus Applied.

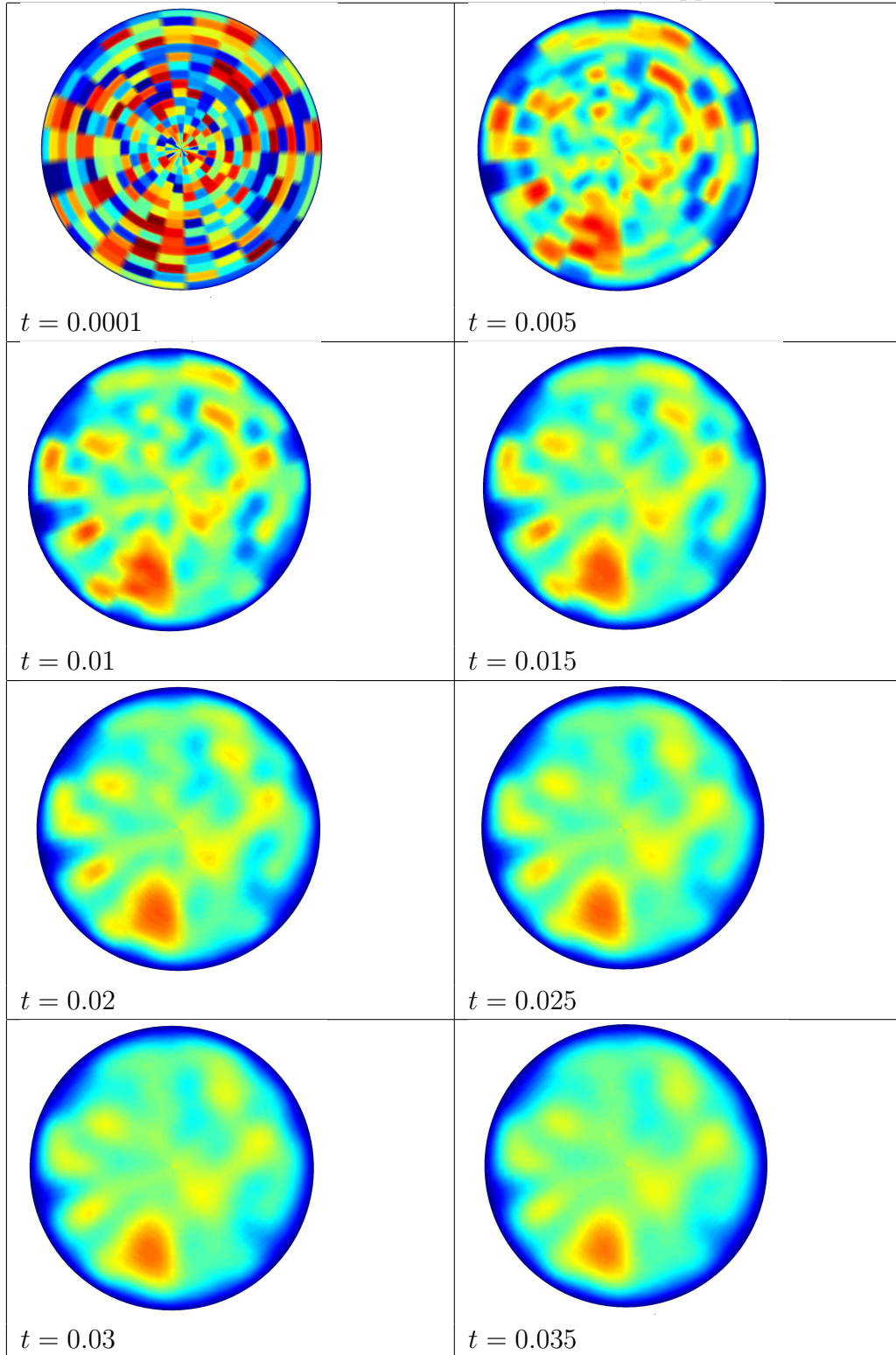


Table 11: Solving the FHN system Computationally in Polar Coordinates, with Randomized Initial Conditions and an External Stimulus Applied with Value  $I_{ex} = 30$ .

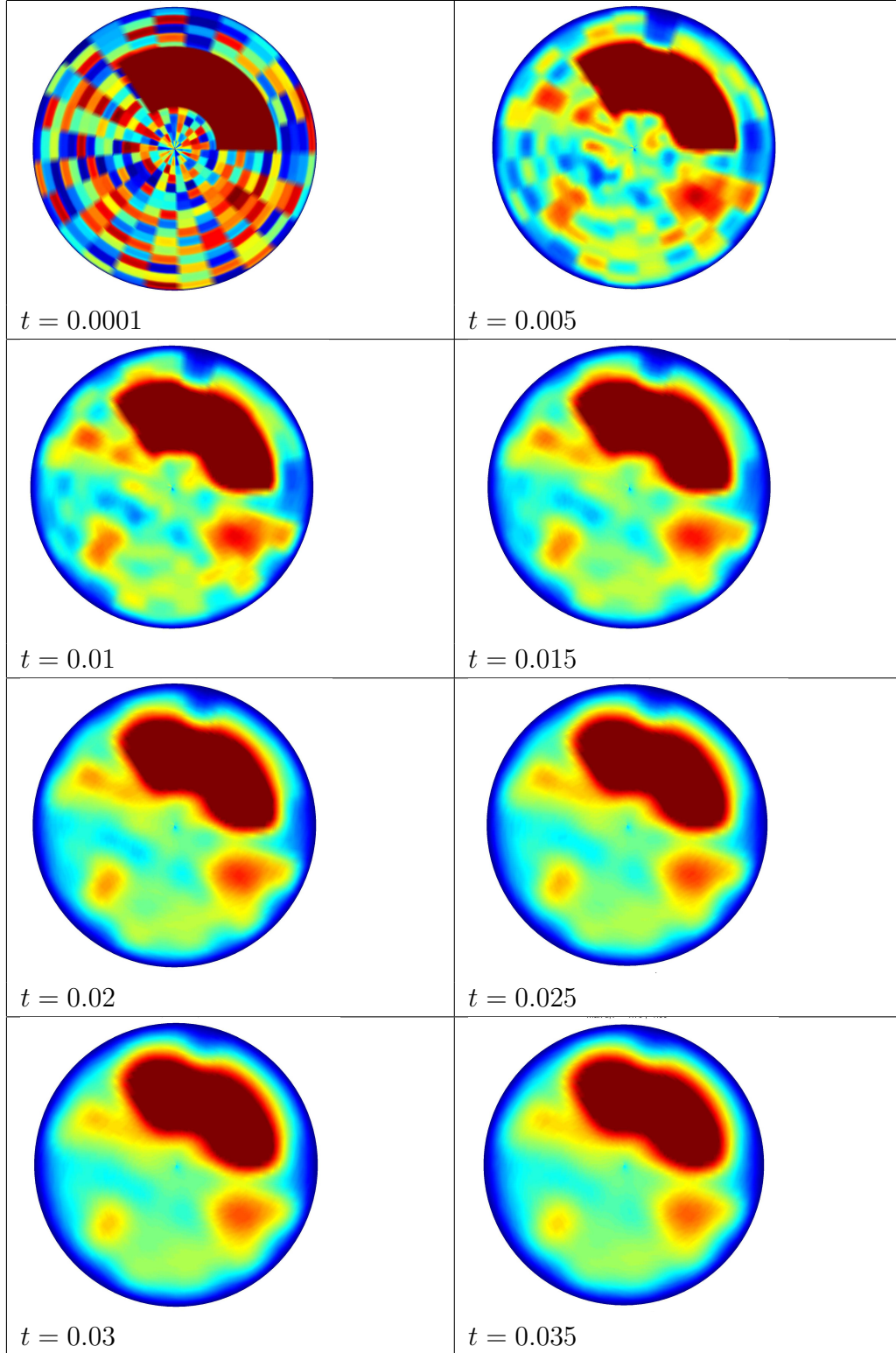


Table 12: Solving the FHN system Computationally in Polar Coordinates, with Randomized Initial Conditions and No External Stimulus Applied.

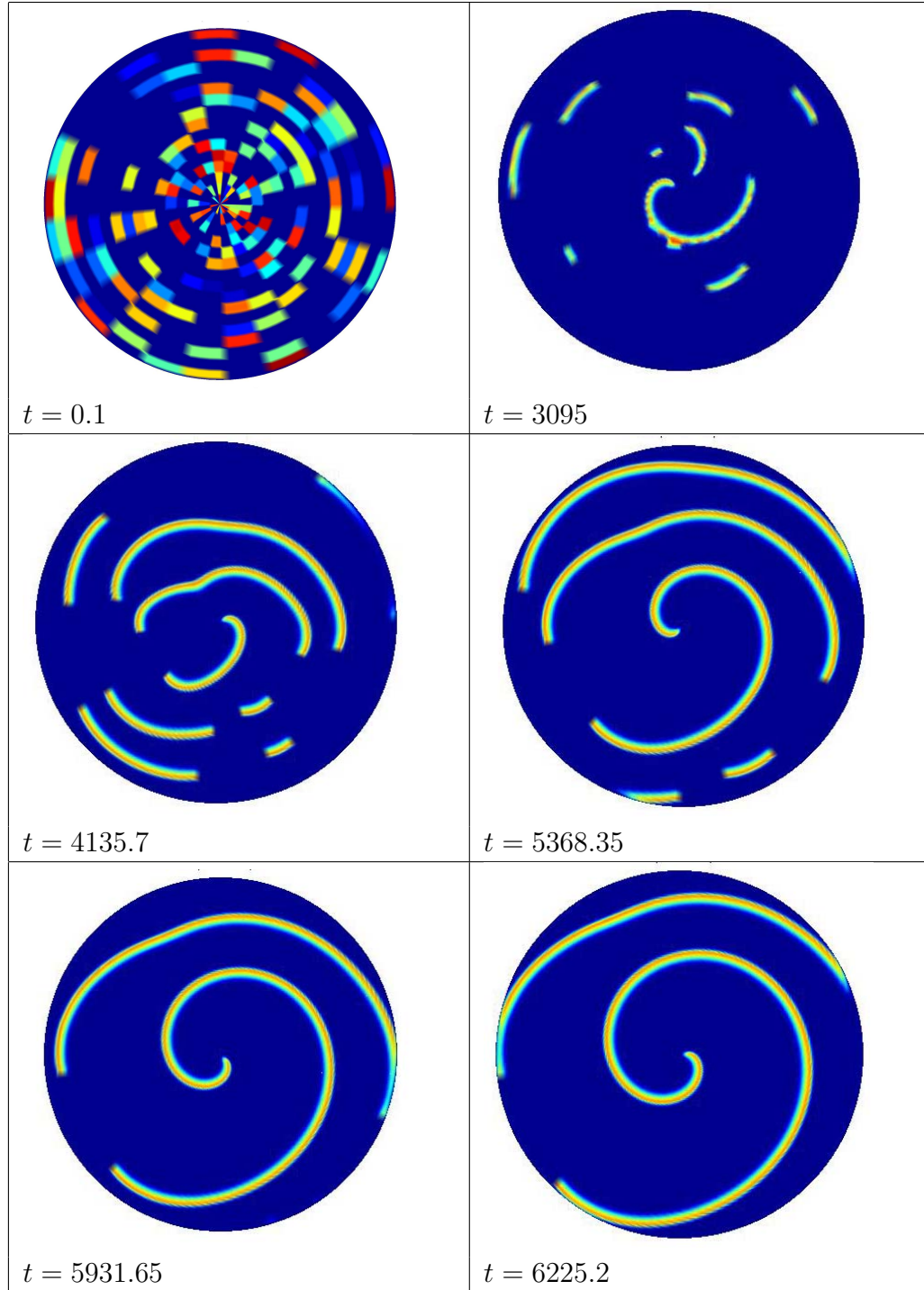
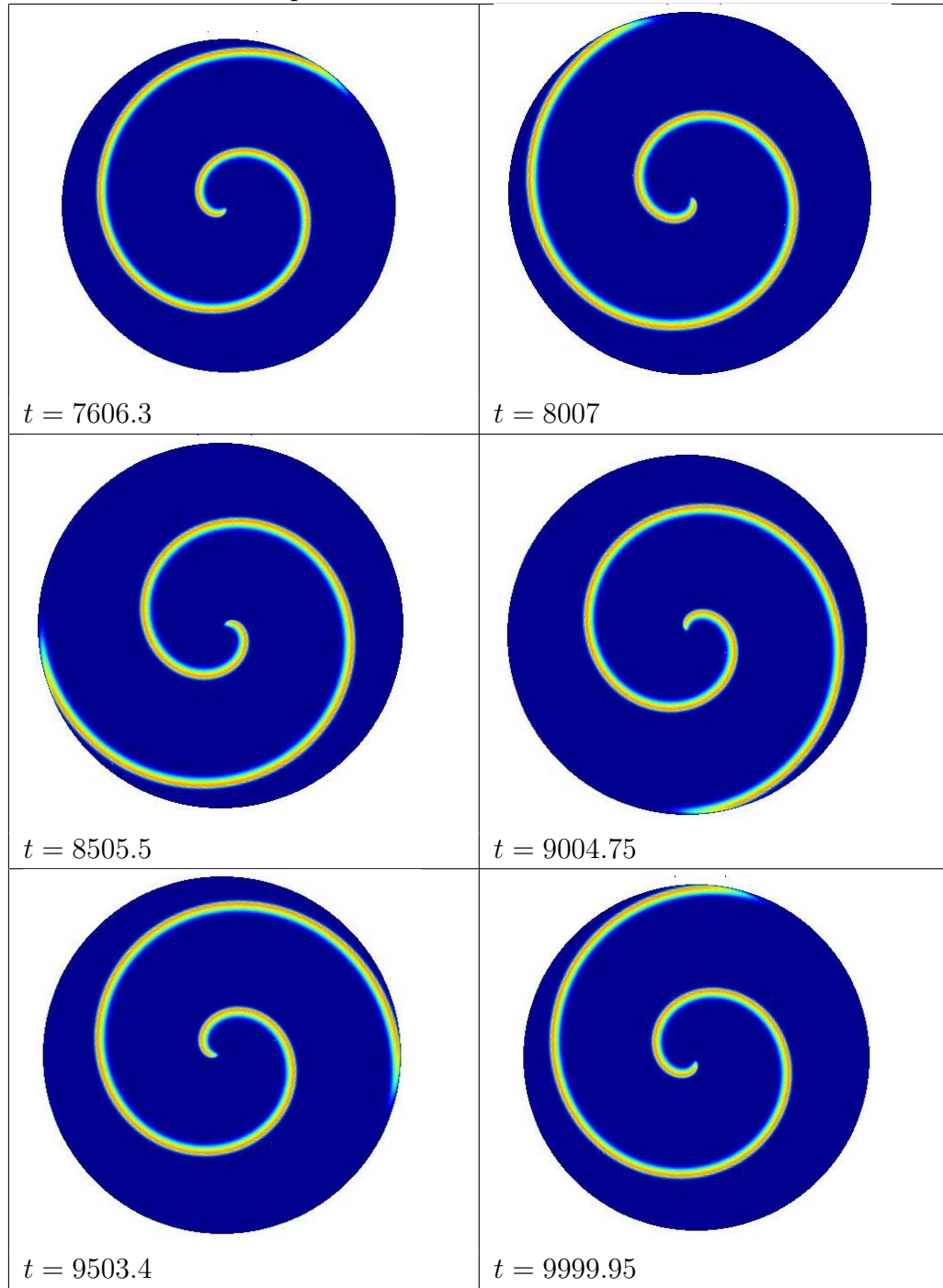


Table 13: Solving the FHN system Computationally in Polar Coordinates, with Randomized Initial Conditions and No External Stimulus Applied, Showing Counterclockwise Rotation of Spiral.



## 5.4 Results in Spherical Coordinates

The same process was followed for the results in spherical coordinates as in polar geometry, with a three-dimensional figure generated at different time steps rather than a simple disk or rectangle. If one wants to implement the code, one can actually rotate the figure to see how the system is behaving on different parts of the sphere and zoom in on certain areas to see greater detail. Early results were generated for zero initial conditions with stimulus and for random initial conditions with and without stimulus, as seen in Figures 14 - 16. Again, spirals were not observed in these simulations . One can see the diffusion across the sphere which would roughly simulate the movement of electrical current on the heart.

After determining appropriate diffusion constant ( $D = 1 \times 10^{-6}$ ) and time step ( $\Delta t = 0.1$ ) for generating spirals in polar coordinates, the same discovery was applied to spherical geometries. Tables 17 - 21 shows different views of the spherical figure at various times during the simulation. One can see early spiral formation at earlier time steps and then more pronounced spirals later, including multi-armed spirals. The top and bottom views show spirals at both poles of the sphere, which is called a source-sink pair. The singular spiral with the higher frequency will control the dynamics, i.e. the source. Röhlff, Glass, and Kapral described this behavior in detail, stating that singularities must occur in pairs of opposite topological charge (also known as index, winding number, or topological defect) so that the sum of the indices is zero [44]. They varied an excitability parameter, which they called  $\tau$ , as well as the radius of the sphere in order to study the dynamics of spiral waves on a sphere [44]. It is intriguing to be able to see some of the same behaviors they described in the results of the simulations carried out for this thesis. The images in Table 17 are viewing the sphere from the front with it tilted slightly forward so that one can see the top, or north pole, of the sphere. The figures in Tables 18 - 21 are

Table 14: Solving the FHN system Computationally in Spherical Coordinates, with  $u_0 = v_0 = 0$  and an External Stimulus Applied with Value  $I_{ex} = 30$ .

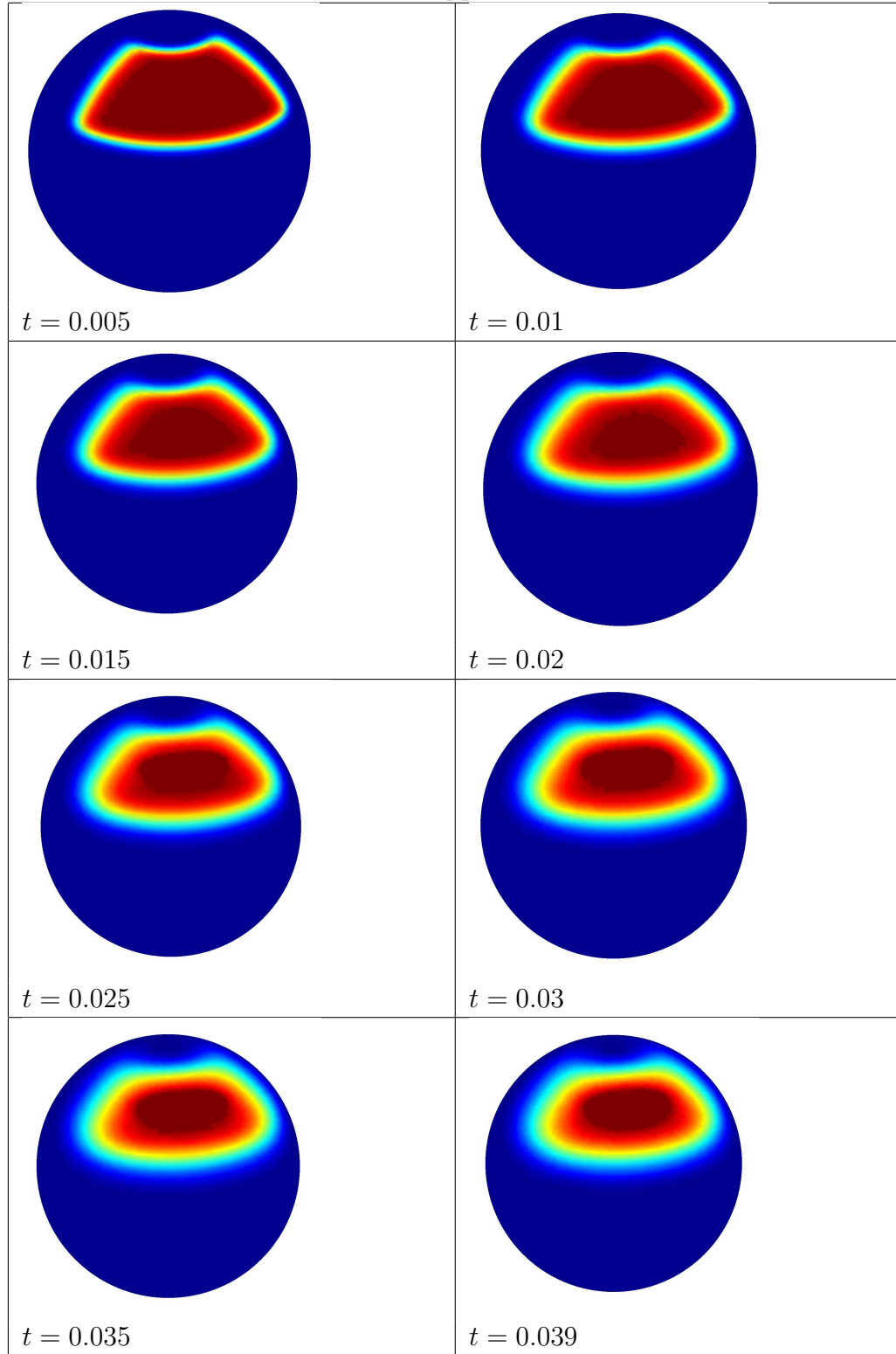


Table 15: Solving the FHN system Computationally in Spherical Coordinates, with Randomized Initial Conditions and No External Stimulus Applied.

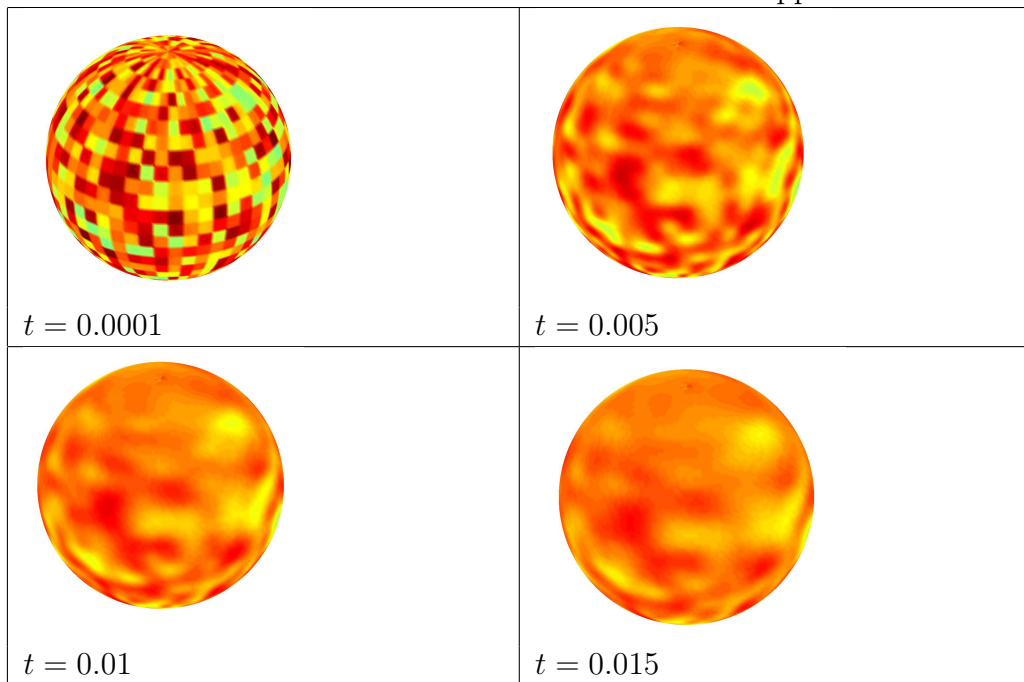
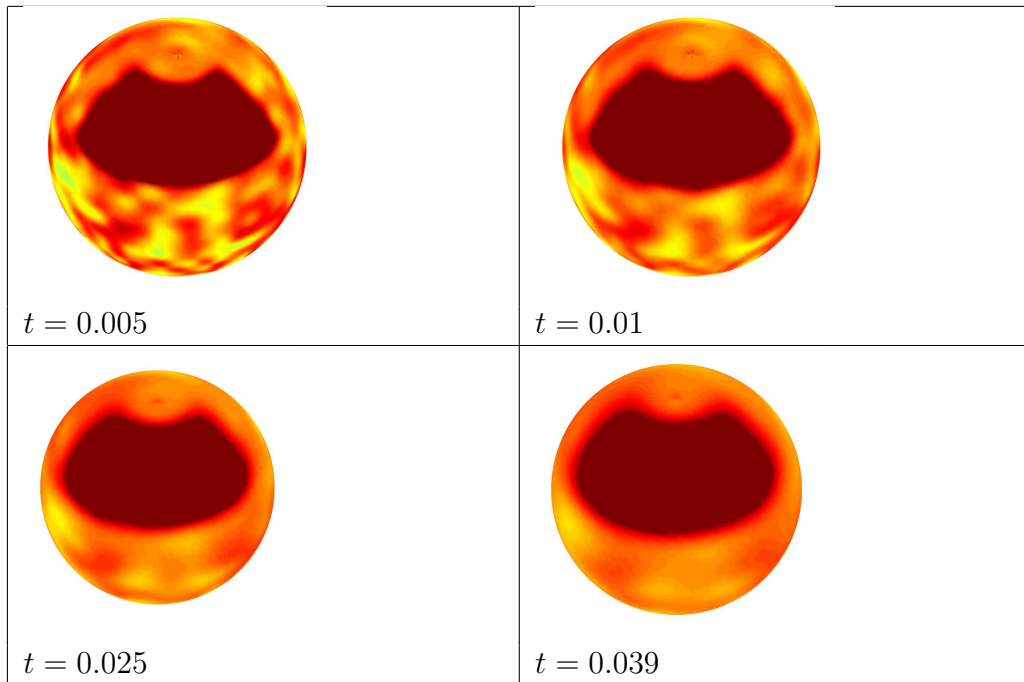


Table 16: Solving the FHN system Computationally in Spherical Coordinates, with Randomized Initial Conditions and an External Stimulus Applied with Value  $I_{ex} = 30$ .



labeled as to which side one is viewing, along with the time at which the image was captured.

Table 17: Solving the FHN system Computationally in Spherical Coordinates, with Randomized Initial Conditions and No External Stimulus Applied.

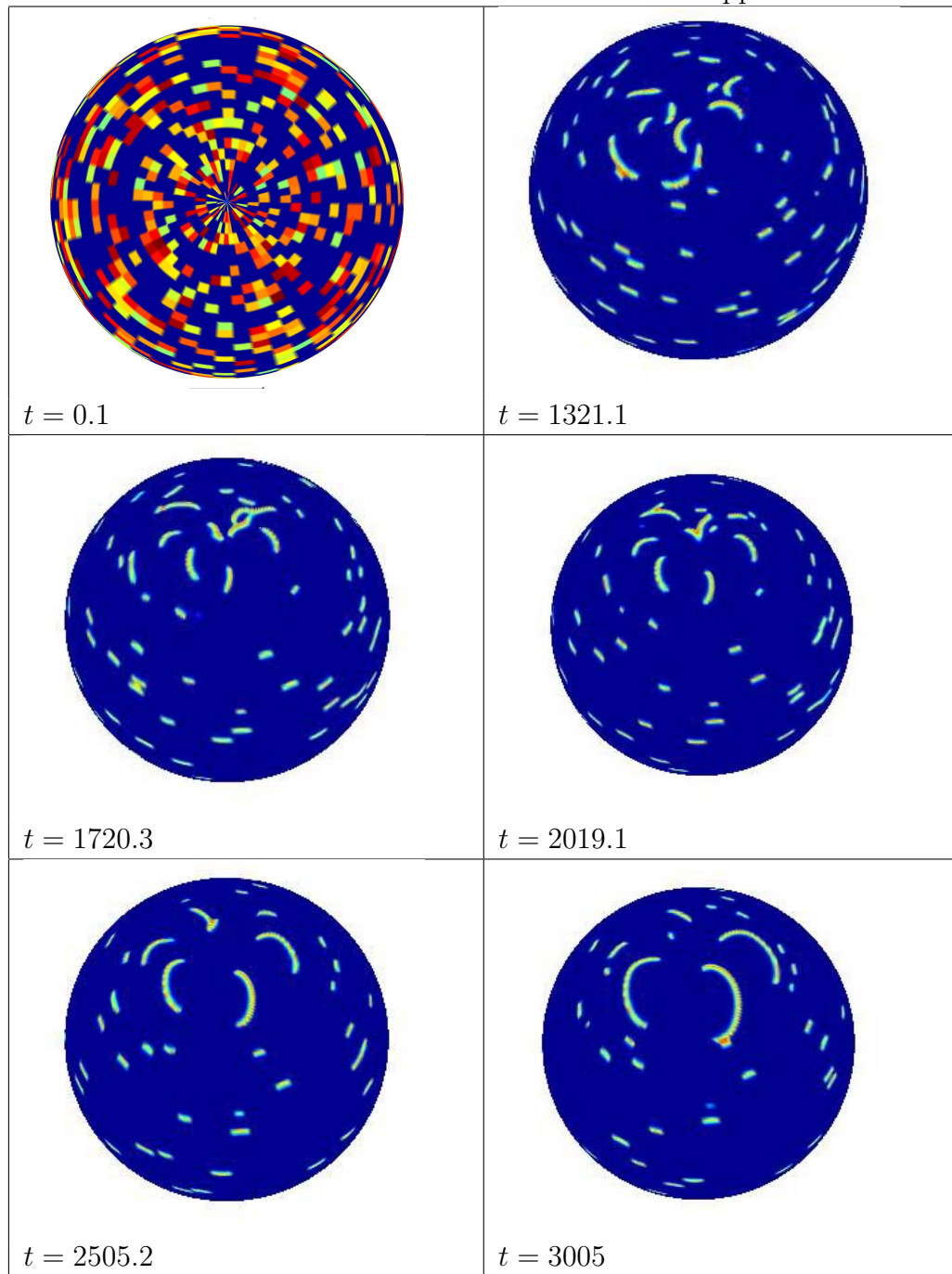


Table 18: Solving the FHN system Computationally in Spherical Coordinates, with Randomized Initial Conditions and No External Stimulus Applied.

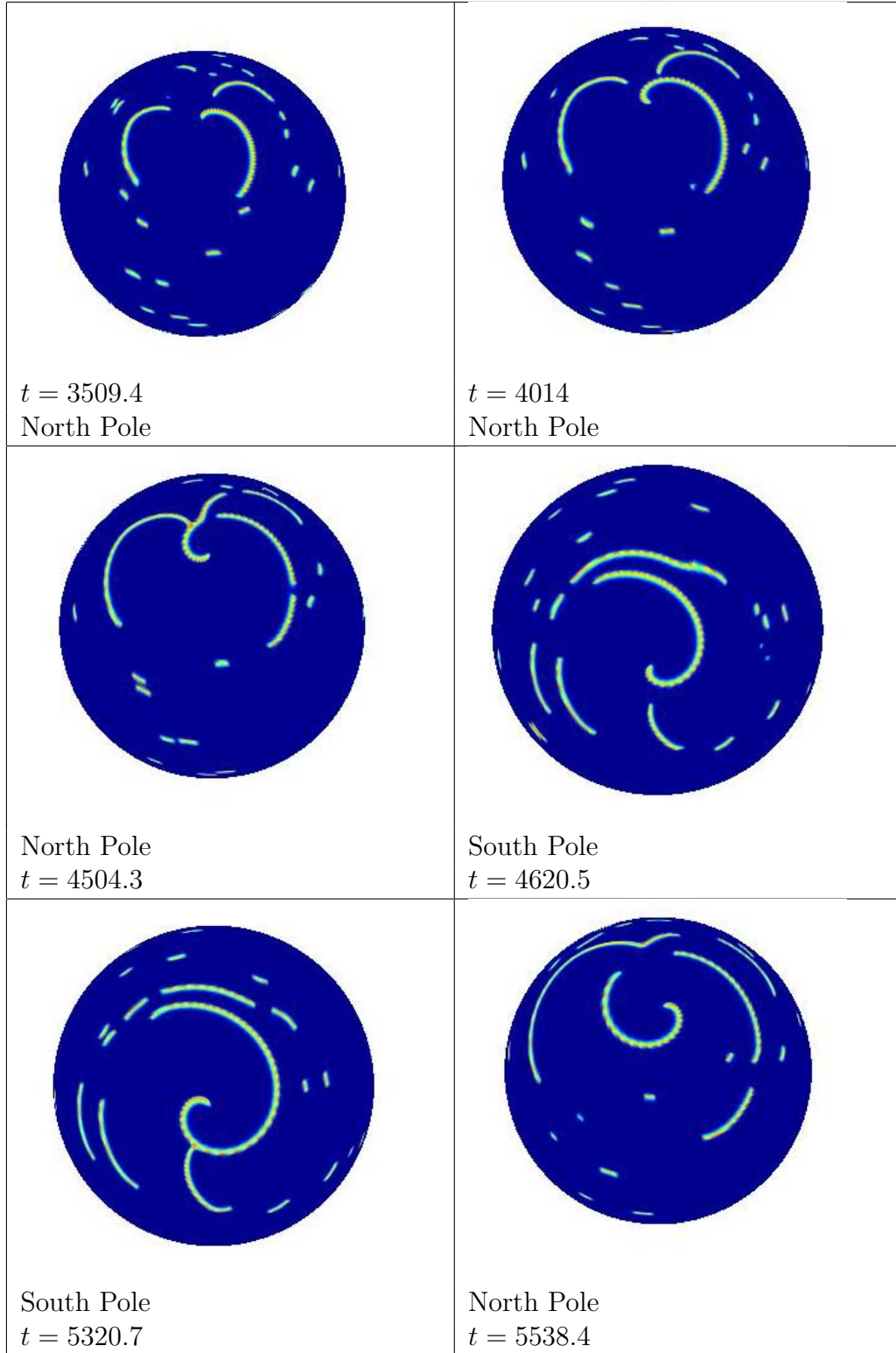


Table 19: Solving the FHN system Computationally in Spherical Coordinates, with Randomized Initial Conditions and No External Stimulus Applied.

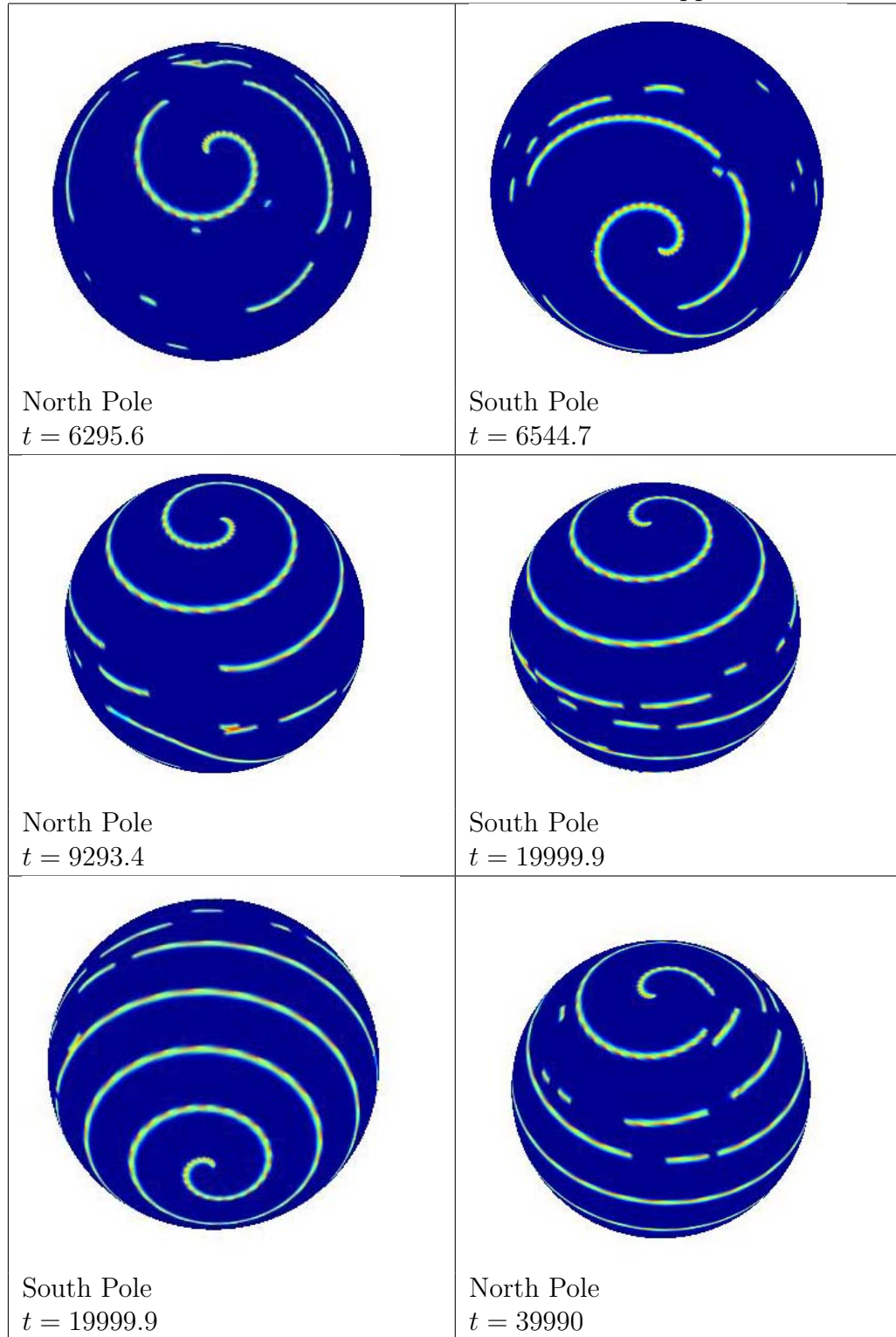


Table 20: Solving the FHN system Computationally in Spherical Coordinates, with Randomized Initial Conditions and No External Stimulus Applied.

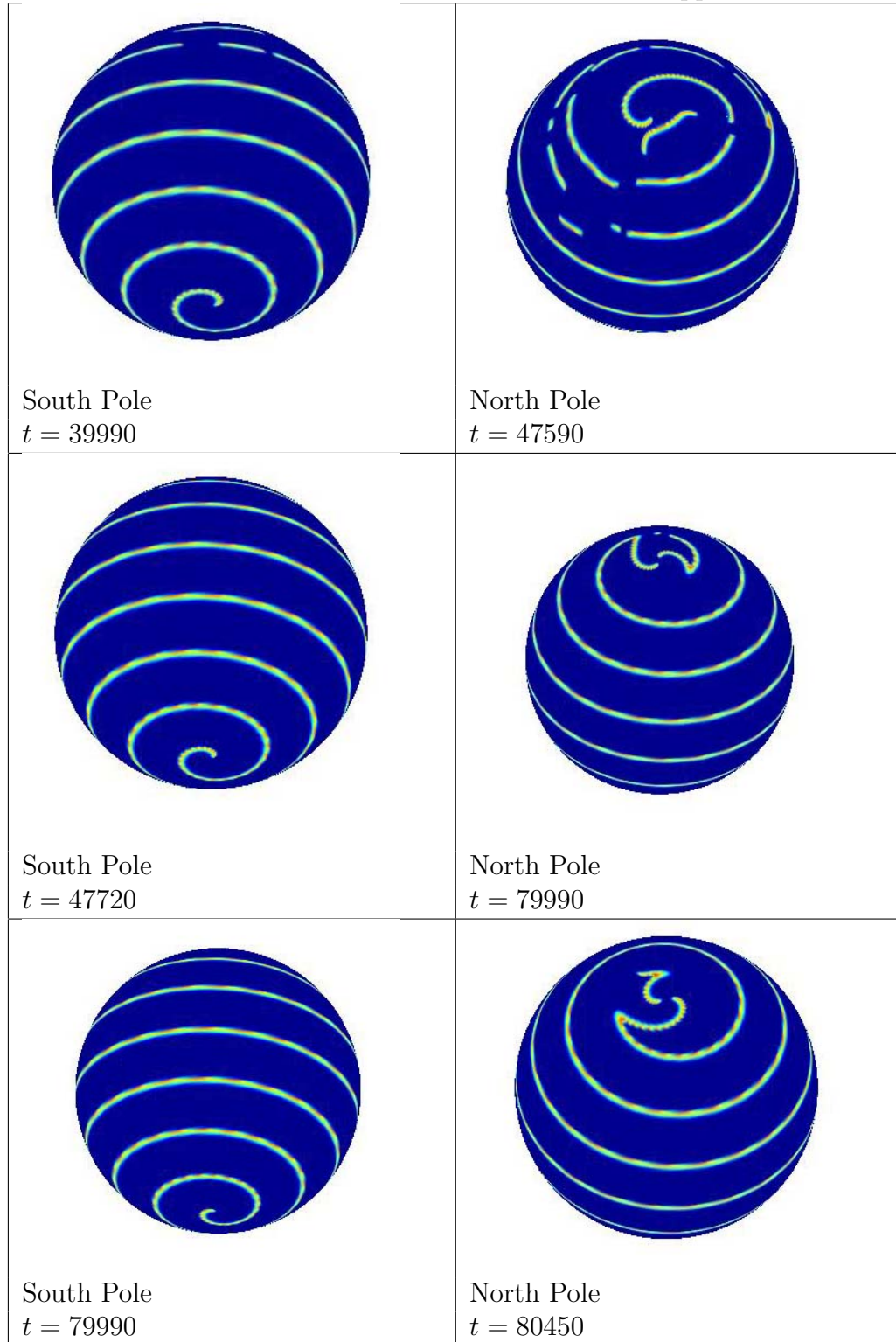
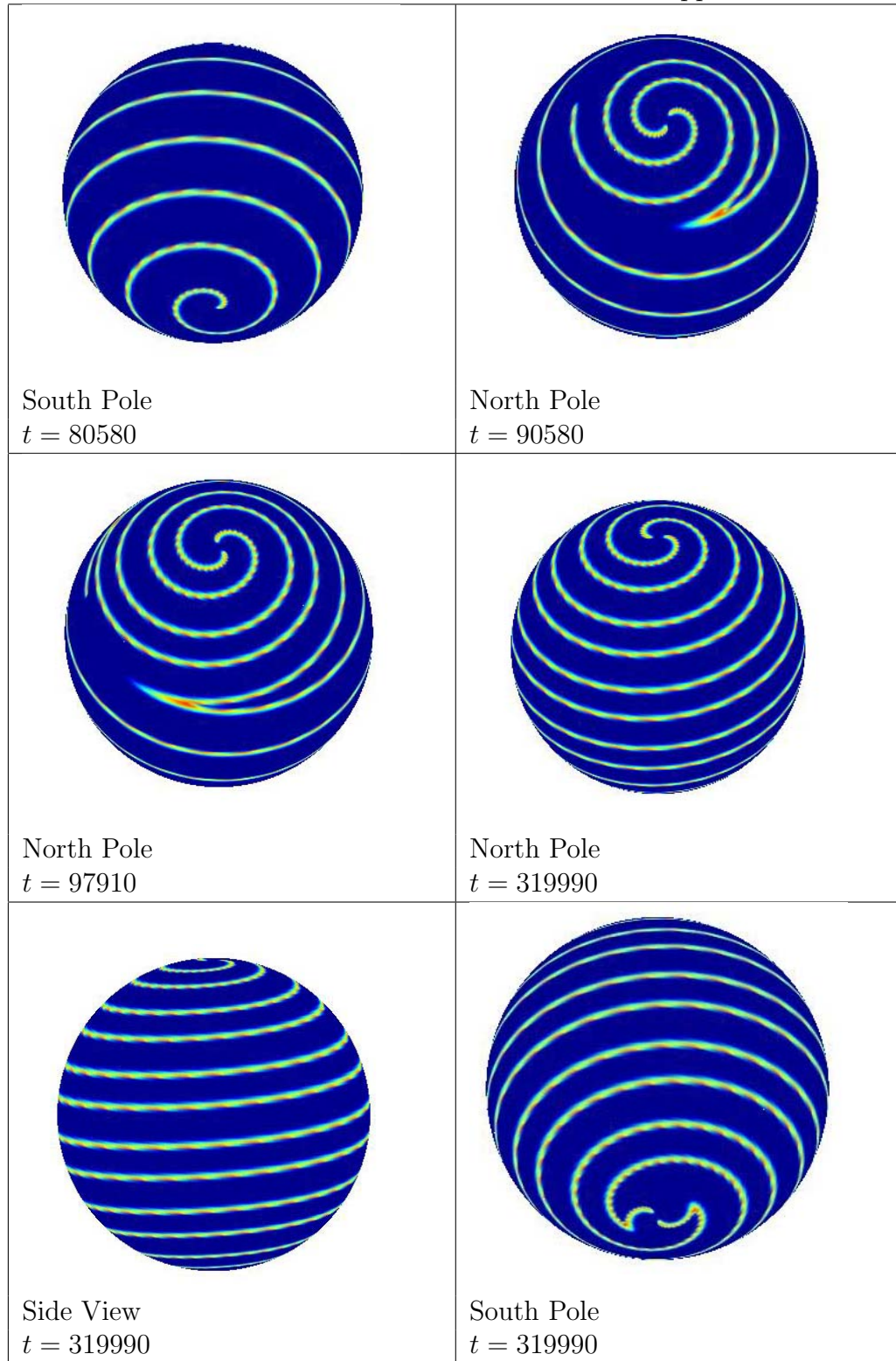


Table 21: Solving the FHN system Computationally in Spherical Coordinates, with Randomized Initial Conditions and No External Stimulus Applied.



## 6 CONCLUSIONS

The author's contributions to research in this field were to build on the ideas of Rogers, McCulloch, and Peter Hammer, namely the modified FitzHugh-Nagumo system used by Rogers and McCulloch [43] and the code developed by Hammer [22] to solve this system in Cartesian coordinates, by also solving the system in polar and spherical geometries and comparing the results to those of other models and numerical methods. MATLAB code was modified from Peter Hammer's code and developed with the assistance of Dr. Russell Herman to solve the system numerically using finite difference methods. This differs from the previous results of Rogers and McCulloch with this system, because they used their own specific modified finite element method, which they term a "collocation-Galerkin finite element method," which they believed to be more appropriate than existing methods to handle the complexities of simulating electric wave propagation in myocardial tissue [43].

The author chose this field because of a lifetime interest in the heart and a desire to perhaps make a small contribution to research in the mechanisms behind cardiac arrhythmias, in the hope that more and more insight into these mechanisms will aid in treatment of such conditions. Naturally, one hopes in undertaking thesis research to make a breakthrough in the field chosen, to win a Nobel prize, et cetera. Applied mathematics is like a haystack built one straw at a time, however, and one should not undervalue the significance of adding a straw to the pile.

Much time was spent looking to see if Hammer had published any results with his code, but no papers were found, so these results are believed to be the first published results implementing a Hammer-style code. In simulations done on a modified form of Hammer's code in Cartesian coordinates, parameter changes were investigated, and it was determined that spirals form with initial values of zero across the medium and an external stimulus applied. Amplitude of current seemed not to affect spiral

formation, as long as  $0 < I_{ex} \leq 30$ , but spirals seemed most likely to form for choosing  $a = 0.13$  as the value of the activation threshold. Spirals were not seen in the system with other constants besides zero used for the initial conditions, so one could build on this research by continuing to tweak parameter values to generate spirals with nonzero constant initial conditions in the Cartesian form of the code. Results of other models and a different form of the FHN model were compared by Rohlff et alia to their results with that form of the FHN model in spherical coordinates which do show spiral results for randomized initial conditions one could use for comparison [44]. Simple geometries like this allow for one to study certain aspects of larger problems, like the irregularity of the surface of the heart, with more computational efficiency. A run-through of the Cartesian code, for instance, takes under a minute, while a run-through of the spherical code takes hours. Although technology is improving, experimental scientists look at small rectangular slices of cardiac tissue taken from animals and shock the samples to look for spiral waves [40], so this model could be directly compared to such tissue samples.

The ultimate goal with this thesis was to find results on the surface of a sphere, but results were generated for a polar system as an intermediate step in the process. Behavior of the diffusion constant was compared to the results of a code written to solve the diffusion term analytically on a disk to check that the polar system was working before transforming into spherical coordinates. The main difference observed is due to the behavior of the Bessel functions in the analytical solutions but otherwise the diffusion pattern is consistent. In polar coordinates, spirals were observed in the system with no external stimulus applied and inhomogeneous randomized initial conditions after giving the simulation an ample duration time and making the diffusion constant small while maintaining stability through appropriate time step size. Eventually, a steady-state counterclockwise rotating spiral formed in the center of the medium. Spirals were not seen in zero or nonzero constant initial

conditions, but perhaps they would form at a later time step. A simple suggestion for further research in this area would be to try to modify the parameters for the system so that spirals could potentially be seen in zero and constant initial conditions on a disk. Truly, the heart is not a flat disk, but this model could possibly have practical value in other applications. A petri dish, for example, is a disk, so one might model certain chemical reactions or diffusion of a current across a disk-shaped cardiac tissue sample. The polar model does not compute as rapidly as the Cartesian model but is still faster than running the code in spherical coordinates. In these simulations, the radius of the disk was given the value  $R = 1$ , but one could alter the radius of the disk and look for spiral behavior.

The spherical model was developed in order to more closely mimic how spirals might travel on the surface of the heart. Simulations with stimulus added in both homogeneous and inhomogeneous media did not show spiral solutions, but this is potentially due to parameter choices. Spirals did form in system with inhomogeneous refractoriness after a sufficient duration. A source-sink pair develops in the solutions to the FHN system solved using finite difference methods, as seen in other papers describing spiral solutions to other models in spherical coordinates [44, 50, 52, 9]. Asymmetrical spiral formation is consistent with the results of Yagisita et alia [50]. One might further the research from here by transforming to yet another geometry, such as ellipsoid, or by changing the radius of the sphere (which in these results was  $R = 1$  as in the spiral results), the thickness of the spherical shell, or tweaking the code to look for spirals in the homogeneous system. If one were to thicken the shell, one could look for scroll waves, which are the three-dimensional version of spiral waves, and compare these results to experimental data for these phenomena.

## REFERENCES

- [1] Konstantin Agladze, James P. Keener, Stefan C. Müller, & Alexander Panfilov, “Rotating spiral waves created by geometry”, *Science*, V 264, June 1994, 1746-1748.
- [2] Anthony Atkielski, “Sinus rhythm labels”, accessed from <http://commons.wikimedia.org/wiki/File:ECG-PQRST2Bpopis.svg> on 25 August 2010.
- [3] Alberto Barbati, “An un-official 80cm FITA archery target”, accessed from [http://commons.wikimedia.org/wiki/File:Archery\\_Target\\_80cm.svg](http://commons.wikimedia.org/wiki/File:Archery_Target_80cm.svg) on 4 December 2010.
- [4] Dwight Barkley, Mark Kness, & Laurette S. Tuckerman, “Spiral-wave dynamics in a simple model of excitable media: The transition from simple to compound rotation”, *Physical Review A*, V 42, No. 4, 15 August 1990, 2489-2492.
- [5] William O. Bray, “Lecture 6: the FitzHugh-Nagumo model”, Part of lecture notes for his course on nonlinear dynamics & biological systems, 2002, accessed from [http://www.math.umaine.edu/~bray/Archive\\_res/Lecture6.PDF](http://www.math.umaine.edu/~bray/Archive_res/Lecture6.PDF) on 3 March 2010.
- [6] Donna A. Calhoun, Christiane Helzel, & Randall J. Leveque, “Logically rectangular grids and finite volume methods for PDEs in circular and spherical domains,” *SIAM Review*, V 50, No. 4, 2008, 723-752.
- [7] William F. Case, “Pink water, white salt crystals, black boulders, and the return of spiral jetty!”, accessed from <http://geology.utah.gov/surveynotes/geosights/spiraljetty.htm> on 25 August 2010.

- [8] The Cleveland Clinic Foundation, “The heart’s electrical system”, accessed from <https://www.clevelandclinic.org/heartcenter/pub/guide/disease/electric/nmlhrtbeat.htm> on 25 August 2010.
- [9] J’orn Davidsen, Leon Glass & Raymond Kapral, “Topological constraints on spiral wave dynamics in spherical geometries with inhomogeneous excitability”, *Physical Review E*, No. 70, 2004.
- [10] Irving R. Epstein, “Spiral waves in Chemistry and Biology”, *Science, New Series*, V 252, No. 252, 5 April 1991, 67, accessed from <http://www.jstor.org/stable/2875573> on 16 February 2010.
- [11] Steven J. Evans, Harold M. Hastings, Sachin Nangia, Joanne Chin, Michael Smolow, Obi Nwasokwa, & Alan Garfinkel, “Ventricular fibrillation: one spiral or many?”, *Proceedings of the Royal Society of London. Series B, Biological Sciences*, V 665, 1998, 2167-2170.
- [12] Vladimir G. Fast & André G. Kléber, “Role of wavefront curvature in propagation of cardiac impulse,” *Cardiovascular Research*, V 33, 1997, 258-271.
- [13] Richard Fitzhugh, “Impulses and physiological states in theoretical models of nerve membrane,” *Biophysical Journal*, V 1, 1961, 445-466.
- [14] R. Fitzhugh & H.A. Antosiewicz, “Automatic Computation of Nerve Excitation—Detailed Corrections and Additions,” *Journal of the Society for Industrial and Applied Mathematics*, V 7, No. 4, Decemeber 1959, 447-458.
- [15] Annovi Frizio, “Ionic Capital”, accessed from <http://www.clker.com/clipart-30033.html> on 25 August 2010.

- [16] C. Michael Gibson, “Diagram of the Human Heart.” accessed from [http://www.wikidoc.org/index.php/Image:Diagram\\_of\\_the\\_human\\_heart\\_28cropped29.svg](http://www.wikidoc.org/index.php/Image:Diagram_of_the_human_heart_28cropped29.svg) on 25 August 2010.
- [17] S. Girod & Anton Becker, “Glanzstreifen im Myokard”, accessed from <http://en.wikipedia.org/wiki/File:Glanzstreifen.jpg> on 4 December 2010.
- [18] Jagannathan Gomatam & Faridon Amdjadi, “Reaction-diffusion systems on a sphere: Meandering of spiral waves,” *Physical Review E*, V 56, No. 4, October 1997, 3913-3919.
- [19] Henry Gray, *Anatomy of the Human Body*. Philadelphia: Lea & Febiger, 1918, accessed from <http://www.bartleby.com/107/138.html> on 8 October 2010.
- [20] Richard A. Gray & Nipon Chattipakorn, “Termination of spiral waves during cardiac fibrillation via shock-induced phase resetting,” *Proceedings of the National Academy of Sciences*, V 102, No. 13, 2005, 4672-4677.
- [21] Richard Haberman, *Applied Partial Differential Equations with Fourier Series and Boundary Value Problems, Fourth Edition*. Upper Saddle River: Pearson Education, Inc., 2004.
- [22] Peter E. Hammer, “Spiral waves in monodomain reaction-diffusion model,” October 2006, accessed from <http://www.mathworks.cn/matlabcentral/fileexchange/22492-spiral-waves-in-monodomain-reaction-diffusion-model> on 1 October 2009.
- [23] S.P. Hastings, “Some mathematical problems from neurobiology,” *The American Mathematical Monthly*. V 82, No. 9, November 1975, 881-895.

- [24] Soren Hayward, “Spiral Jetty from atop Rozel Point, in mid-April 2005.” accessed from <http://en.wikipedia.org/wiki/File:Spiral-jetty-from-rozel-point.png> on 25 August 2010.
- [25] A. L. Hodgkin & A. F. Huxley, “Measurement of current-voltage relations in the membrane of the giant axon of *Loligo*,” *J. Physiol.* V 116, 1952, 424-448.
- [26] A. L. Hodgkin & A. F. Huxley, “Currents carried by sodium and potassium ions through the membrane of the giant axon of *Loligo*,” *J. Physiol.* V 116, 1952, 449-472.
- [27] A. L. Hodgkin & A. F. Huxley, “The components of membrane conductance in the giant axon of *Loligo*,” *J. Physiol.* V 116, 1952, 473-496.
- [28] A. L. Hodgkin & A. F. Huxley, “The dual effect of membrane potential on sodium conductance in the giant axon of *Loligo*,” *J. Physiol.* V 116, 1952, 497-506.
- [29] A. L. Hodgkin & A. F. Huxley, “Propagation of electrical signals along giant nerve fibres,” *Proceedings of the Royal Society of London. Series B, Biological Sciences*, V 140, No. 899, 16 October 1952, 177-183.
- [30] Lara Hopley & Jo van Schalkwyk, “The Cardiac Myocyte,” 2000, accessed from <http://www.anaesthetist.com/icu/organs/heart/Findex.htm#ion.htm> on 8 October 2010.
- [31] R. Hurt, “Milky Way 2005,” Nasa/JPL, 2008, accessed from [http://www.nasa.gov/mission\\_pages/spitzer/multimedia/20080603a.html](http://www.nasa.gov/mission_pages/spitzer/multimedia/20080603a.html) on 12 October 2010.
- [32] “Ionic capital, torus (foliated base), and parts of a fluted column shaft [Greek, Lydian] (26.59.1)”. In *Heilbrunn Timeline of Art History*. New York: The

Metropolitan Museum of Art, 2000. Accessed from <http://www.metmuseum.org/toah/works-of-art/26.59.1> (October 2006) on 25 August 2010.

- [33] Dana Mackenzie, “Making Sense of a Heart Gone Wild,” *Science*, V 303, 6 February 2004, 786-787.
- [34] David R. Neal, “Finite difference approximations of advection-diffusion equations for modeling shark populations”, MS Thesis. University of North Carolina, Wilmington, 2007. Electronic resource.
- [35] The National Institute of Standards and Technology (NIST), “A Walk Through Time: The Evolution of Time Measurement Through the Ages,” accessed from <http://physics.nist.gov/GenInt/Time/revol.html> on 25 August 2010.
- [36] The Nobel Foundation, “The Nobel Prize in Physiology or Medicine 1963,” accessed from [http://nobelprize.org/nobel\\_prizes/medicine/laureates/1963/](http://nobelprize.org/nobel_prizes/medicine/laureates/1963/) on 12 March 2010.
- [37] Denis Noble & Yoram Rudy, “Models of Cardiac Ventricular Action Potentials: Iterative Interaction between Experiment and Simulation”, *Philosophical Transactions: Mathematical, Physical and Engineering Sciences*, V 359, No. 1783, The Integrated Heart: Modeling Cardiac Structure and Function, 15 June 2001, 1127-1142.
- [38] JJ O’Connor & E F Robertson, “Christiaan Huygens” accessed from <http://www-history.mcs.st-and.ac.uk/Biographies/Huygens.html>, 1 April 2010.
- [39] Alexander Panfilov & Arkady Pertsov, “Ventricular fibrillation: evolution of the multiple wavelet hypothesis”, *Phil. Trans. R. Soc. Lond. A*, No. 359, 2001.

- [40] Arkady M. Pertsov, Jorge M. Davidenko, Remy Salomonsz, William T. Baxter, & José Jalife, “Spiral waves of excitation underlie reentrant activity in isolated cardiac muscle”, *Circulation Research*, V 72, No. 3, March 1993, 631-650.
- [41] Clifford Pickover, “Mathematics and Beauty: A Sampling of Spirals in Science, Nature, and Art”, *Leondardo*, V 21, No. 2, 1988, 173-181.
- [42] RnCeus Interactive, LLC, “EKG Strip Identification and Evaluation,” 1999, accessed from [http://www.rnceus.com/course\\_frame.asp?exam\\_id=16&directory=ekg](http://www.rnceus.com/course_frame.asp?exam_id=16&directory=ekg) on 12 March 2010.
- [43] Jack M. Rogers & Andrew D. McCulloch, “A Collocation-Galerkin Finite Element Model of Cardiac Action Potential Propogation”, *IEEE Transactions on Biomedical Engineering*, V 41, No. 8, 1994, 743-757.
- [44] Katrin Röhl, Leon Glass & Raymond Kapral, “Spiral wave dynamics in excitable media with spherical geometries”, *Chaos*, No. 16, 2006.
- [45] spiral. (2010). In *Merriam-Webster Online Dictionary*. Retrieved 26 March 2010, from <http://www.merriam-webster.com/dictionary/spiral>
- [46] spiral. (2010). In *Encyclopdia Britannica*. Retrieved 26 March 2010, from Encyclopdia Britannica Online: <http://www.britannica.com/EBchecked/topic/560299/spiral>
- [47] “Tridiag.m”, accessed from <http://www.cs.ucdavis.edu/~bai/ROMmatlab/tridiag.m> on 18 March 2010.
- [48] Vladimir K. Vanag & Irving R. Epstein, “Segmented spiral waves in a reaction-diffusion system,” *Proceedings of the National Academy of Sciences of the United States of America*, V 100, No. 25, 9 December 2003, 14635-14638.

- [49] Greg von Winckel, “Bessel Function Zeros,” January 2005, accessed from <http://www.mathworks.com/matlabcentral/fileexchange/6794> on 10 March 2010.
- [50] Hiroki Yagisita, Masayasu Mimura & Michio Yamada, “Spiral wave behaviors in an excitable reaction-diffusion system on a sphere”, *Physica D*, No. 124, 1998.
- [51] A.M. Zhabotinsky & A.N. Zaikin, “Development of spiral waves after hydrodynamic breaking of a concentric wave,” 1971, accessed from [http://www.scholarpedia.org/article/Image:BZ\\_Spiral\\_waves.jpg](http://www.scholarpedia.org/article/Image:BZ_Spiral_waves.jpg) on 8 October 2010.
- [52] V.S. Zykov & S.C. Müller, “Spiral waves on circular and spherical domains of excitable medium,” *Physica D*, V 97, 1996, 322-332.

## APPENDIX

### Peter Hammer’s MATLAB Code

Here is the original Peter Hammer code, called SpiralWaves.m [22]. It was our starting point, which we then tweaked.

```

ncols=128;                                % Number of columns in domain
nrows=128;                                % Number of rows in domain
dur=25000;                                 % Number of time steps
h=2.0;                                     % Grid size
h2=h^2;
dt=0.15;                                   % Time step
Iex=30;                                    % Amplitude of external current
mu=1.0;                                    % Anisotropy
Gx=1; Gy=Gx/mu;                           % Conductances
a=0.13; b=0.013; c1=0.26; c2=0.1; d=1.0; % FHN model parameters
v=zeros(nrows,ncols);                      % Initialize voltage array
r=v;                                       % Initialize refractoriness array

```

```

% Set initial stim current and pattern
iex=zeros(nrows,ncols);
if StimProtocol==1
    iex(62:67,62:67)=Iex;
else
    iex(:,1)=Iex;
end

% Setup image
ih=imagesc(v); set(ih,'cdatamapping','direct')
colormap(hot); axis image off; th=title('');
set(gcf,'position',[500 600 256 256],'color',[1 1 1],'menubar','none')

% Create 'Quit' pushbutton in figure window
uicontrol('units','normal','position',[.45 .02 .13 .07], ...
    'callback','set(gcf,''userdata'',1)',...
    'fontsize',10,'string','Quit');

n=0; % Counter for time loop
k=0; % Counter for movie frames
done=0; % Flag for while loop

n1e=20; % Step at which to end 1st stimulus
switch StimProtocol
    case 1 % Two-point stimulation
        n2b=3800; % Step at which to begin 2nd stimulus
        n2e=3900; % Step at which to end 2nd stimulus
    case 2 % Cross-field stimulation
        n2b=5400; % Step at which to begin 2nd stimulus
        n2e=5420; % Step at which to end 2nd stimulus
end

while ~done % Time loop

    if n == n1e % End 1st stimulus
        iex=zeros(nrows,ncols);
    end

    if n == n2b % Begin 2nd stimulus
        switch StimProtocol
            case 1

```

```

    iex(62:67,49:54)=Iex;
    case 2
        iex(end,:)=Iex;
    end
end

if n == n2e      % End 2nd stimulus
    iex=zeros(nrows,ncols);
end

% Create padded v matrix to incorporate Newman boundary conditions
vv=[[0 v(2,:) 0];[v(:,2) v v(:,end-1)];[0 v(end-1,: ) 0]];

% Update v
vxx=(vv(2:end-1,1:end-2) + vv(2:end-1,3:end) -2*v)/h2;
vyy=(vv(1:end-2,2:end-1) + vv(3:end,2:end-1) -2*v)/h2;
dvdt=c1*v.* (v-a).* (1-v)-c2*v.* r+iex+Gx*vxx+Gy*vyy;
v_new=v + dvdt*dt;

% Update r
drdt=b*(v-d*r);
r=r + drdt*dt;
v=v_new; clear v_new

% Map voltage to image grayscale value
m=1+round(63*v); m=max(m,1); m=min(m,64);

% Update image and text
set(ih,'cdata',m);
set(th,'string',sprintf('%d %0.2f %0.2f',n,v(1,1),r(1,1)));
drawnow

% Write every 500th frame to movie
if rem(n,500)==0
    k=k+1;
    mov(k)=getframe;
end

n=n+1;
done=(n > dur);
if max(v(:)) < 1.0e-4, done=1; end      % If activation extinguishes, quit early.

```

```

if ~isempty(get(gcf,'userdata')), done=1; end % Quit if user clicks on 'Quit' button.
end

% Write movie as AVI
if isunix, sep='/' ; else sep='\' ; end
[fn,pn]=uiputfile([pwd sep 'SpiralWaves.avi'],'Save movie as:');
if ischar(fn)
    movie2avi(mov,[pn fn],'quality',75)
else
    disp('User pressed cancel')
end

close(gcf)

```

## Testing Leveque's Mapping Function

This code, spiralw2.m, was testing solving the system and mapping onto a sphere using Leveque's mapping function, mapc2m [6]. The mapc2m function is also included in this subsection.

```

% Set initial stim current and pattern
iex=zeros(nrows,ncols);
if StimProtocol==1
    iex(iex2:iexb2,iexa:iexb)=Iex;
else
    iex(:,1)=Iex;
end

% Setup image
n=128;
[xc,yc] = meshgrid(linspace(-3,1,2*n), linspace(-1,1,n+1));
[xp,yp,zp] = mapc2m(xc,yc);
ih=surf(xp,yp,zp,v);
%shading interp
set(ih,'cdatamapping','direct','EdgeColor','none')
%colormap(hot);
axis image off; th=title('');
set(gcf,'position',[300 200 512 512],'color',[1 1 1])
% Create 'Quit' pushbutton in figure window
uicontrol('units','normal','position',[.45 .02 .13 .07], ...

```

```

'callback','set(gcf,'userdata',1)',...
'fontsize',10,'string','Quit');

n=0;                      % Counter for time loop
done=0;                     % Flag for while loop

n1e=20;                   % Step at which to end 1st stimulus
switch StimProtocol
    case 1                % Two-point stimulation
        n2b=3800;          % Step at which to begin 2nd stimulus
        n2e=3900;          % Step at which to end 2nd stimulus
    case 2                % Cross-field stimulation
        n2b=5400;          % Step at which to begin 2nd stimulus
        n2e=5420;          % Step at which to end 2nd stimulus
end

while ~done                 % Time loop

    if n == n1e            % End 1st stimulus
        iex=zeros(nrows,ncols);
    end

    if n == n2b            % Begin 2nd stimulus
        switch StimProtocol
            case 1
                iex(iexa2:iexb2,49:54)=Iex;
            case 2
                iex(end,:)=Iex;
        end
    end

    if n == n2e            % End 2nd stimulus
        iex=zeros(nrows,ncols);
    end

    % Create padded v matrix to incorporate Newman boundary conditions
    vv=[[0 v(2,:) 0];[v(:,2) v v(:,end-1)];[0 v(end-1,:) 0]];

    % Update v
    vxx=(vv(2:end-1,1:end-2) + vv(2:end-1,3:end) -2*v)/h2;
    vyy=(vv(1:end-2,2:end-1) + vv(3:end,2:end-1) -2*v)/h2;

```

```

dvdt=c1*v.*(v-a).*(1-v)-c2*v.*r+iex+Gx*vxx+Gy*vyy;
v_new=v + dvdt*dt;

% Update r
drdt=b*(v-d*r);
r=r + drdt*dt;
v=v_new; clear v_new

% Map voltage to image grayscale value
m=1+round(63*v); m=max(m,1); m=min(m,64);

% Update image and text for n divisible by 4
if mod(n,4) == 0
    set(ih,'CDATA',m);
    set(th,'String',sprintf('%d %0.2f %0.2f',n,v(1,1),r(1,1)));
    drawnow
end

n=n+1;
done=(n > dur);
if max(v(:)) < 1.0e-4, done=1; end      % If activation extinguishes, quit early.
if ~isempty(get(gcf,'userdata')), done=1; end % Quit if user clicks on 'Quit' button.
end

```

Leveque's Mapping Function:

```

function [xp,yp,zp] = mapc2m(xc,yc);
%
% Specifies the mapping from computational coordinates to a 2d manifold.
% Maps the rectangle [-3,1] x [-1,1] to the sphere of radius Rsphere.
% [-1,1]x[-1,1] is mapped to the upper hemisphere.
% [-3,-1]x[-1,1] is mapped to the lower hemisphere.
%
% Wave Propagation Software, Computational Science, and Reproducible Research
% by R. J. LeVeque, http://www.amath.washington.edu/~rjl/pubs/icm06

Rsphere = 1;
r1 = Rsphere;
sgnz = ones(size(xc));
ij = find(xc < -1);
xc(ij) = -2 - xc(ij);

```

```

sgnz(ij) = -1;
xc1 = abs(xc);
yc1 = abs(yc);
d = max(xc1,yc1);
d = max(d, 1e-10);
D = r1*d.*(2-d) / sqrt(2);
R = r1*ones(size(d));

center = D - sqrt(R.^2 - D.^2);
xp = D./d .* xc1;
yp = D./d .* yc1;

ij = find(yc1==d);
yp(ij) = center(ij) + sqrt(R(ij).^2 - xp(ij).^2);
ij = find(xc1==d);
xp(ij) = center(ij) + sqrt(R(ij).^2 - yp(ij).^2);

xp = sign(xc) .* xp;
yp = sign(yc) .* yp;
zp = sgnz .* sqrt(r1^2 - (xp.^2 + yp.^2));

```

### Code for Solving the System in Cartesian Coordinates

To make the code more consistent with the equations used in this paper, spiralwu.m has the v's replaced with u's and the r's with v's. It also does not generate an .avi file but one can easily capture images from the code. This code gives the extra option of having randomized initial conditions and calls in a separate function for the stimulus, stim.m, which is given afterwards:

```

clear

% Modification of function written by Peter E. Hammer (hammer@usa.com)
% for R. Herman and Kara Blalock Roberson

% System parameters
L=1/256; % Scale factors
T=1;

```

```

a=0.15; d=1.0;                                % FHN model parameters - scaled
b=0.013/T; c1=0.26/T; c2=0.1/T;

mu=1.0;                                         % Anisotropy
Gx=L^2/T; Gy=Gx/mu;                          % Conductances

% Domain Ly by Lx
Lx=256*L;
Ly=256*L;
ncols=128;                                     % Number of columns in domain
nrows=128;                                      % Number of rows in domain

hx=Lx/ncols;                                    % Grid sizes dx,dy
hy=Ly/nrows;
hx2=hx^2;                                       % dx^2, dy^2 for scheme
hy2=hy^2;
ts=hx2/4/Gx;
nstep=round(1/ts);

dt=0.15*ts;                                     % Time step
dur=round(25000/ts);                           % Number of time steps

% Stimulus - Turn off using Iex0=0, Turn on with Iex0=30
% Uses stim.m to create stimuli
Iex0=30;
Iex1=Iex0/T;                                    % Amplitude of external currents
Iex2=Iex0/T;
iex1=stim(Lx/20,Ly/20,Lx/2,Ly/2,hx,hy,nrows,ncols,Iex1);      % Stim 1
iex2=stim(Lx/20,Ly/20,Lx/2.5,Ly/2,hx,hy,nrows,ncols,Iex2);    % Stim 2
iex=iex1;

n1e=round(3.0/dt);                            % Step at which to end 1st stimulus
n2b=round(570/dt);                           % Step at which to begin 2nd stimulus
n2e=round(585/dt);                           % Step at which to end 2nd stimulus

% Initial conditions
ictype=0;
if ictype==0
    % Constant ICs - ictype=0 (with Iex=30 gives original)
    u0=0; v0=0;                               % Initial values for u and v
    u=u0*ones(nrows,ncols);                  % Initialize voltage array

```

```

v=v0*ones(nrows,ncols); % Initialize refractoriness array

else
    % Grid of random ICs - ictype>0
    for i=1:nrows/4
        i1=4*(i-1)+1;
        for j=1:ncols/4
            j1=4*(j-1)+1;
            u(i1:i1+3,j1:j1+3)=rand/2;
            v(i1:i1+3,j1:j1+3)=rand/2;
        end
    end
end

% Setup image
ih=imagesc(u); set(ih,'cdatamapping','direct')
colormap(hot); axis image off; th=title('');
set(gcf,'position',[300 200 512 512],'color',[1 1 1])

% Create 'Quit' pushbutton in figure window
uicontrol('units','normal','position',[.45 .02 .13 .07], ...
    'callback','set(gcf,''userdata'',1)',...
    'fontsize',10,'string','Quit');

n=0; % Counter for time loop
done=0; % Flag for while loop
t=0; % Initialize time
while ~done % Time loop

    t=t+dt;
    if n == n1e % End 1st stimulus
        iex=zeros(nrows,ncols);
    end

    if n == n2b % Begin 2nd stimulus
        iex=iex2;
    end

    if n == n2e % End 2nd stimulus
        iex=zeros(nrows,ncols);
    end

    % Create padded u matrix to incorporate Newman boundary conditions

```

```

uu=[[0 u(2,:) 0];[u(:,2) u u(:,end-1)];[0 u(end-1,: ) 0]];

% Update u
uxx=(uu(2:end-1,1:end-2) + uu(2:end-1,3:end) -2*u)/hx2;
uyy=(uu(1:end-2,2:end-1) + uu(3:end,2:end-1) -2*u)/hy2;
dudt=c1*u.* (u-a).* (1-u)-c2*u.* v+iex+Gx*uxx+Gy*uyy;
u_new=u + dudt*dt;

% Update v
dvdt=b*(u-d*v);
v=v + dvdt*dt;
u=u_new; clear u_new

% Map voltage to image grayscale value
m=1+round(63*u); m=max(m,1); m=min(m,64);

% Update image and text for n divisible by 4
if mod(n,nstep) == 0
    set(ih,'cdata',m);
    set(th,'string',sprintf('%s %0.1f %s %0.2f %s %0.2f',...
        't = ',t, ' , max u,v = ', max(u(:)), ' , ',max(v(:))))
    drawnow
end

n=n+1;
done=(n > dur);
if max(u(:)) < 1.0e-4, done=1; end      % If activation extinguishes,
                                            % quit early.
if ~isempty(get(gcf,'userdata')), done=1; end % User clicks 'Quit'.
end

```

Here is the stim.m code, which is used to pinpoint the stimulus regions:

```

function iex = stim(bx,by,cx,cy,hx,hy,nrows,ncols,Iex)

% Stim area center (cx,cy) widths bx by and value Iex

iex=zeros(nrows,ncols);
iexxa=round((cx-bx/2)/hx);           % Indices for stimulus area
iexxb=round((cx+bx/2)/hx);
iexya=round((cy-by/2)/hy);
iexyb=round((cy+by/2)/hy);

```

```
iex(iexya:iexyb,iexxa:iexxb)=Iex;      % Set initial stimulus
```

## MATLAB Code for Polar Coordinates

This subsection contains a code which solves the diffusion term analytically in polar coordinates as well as the code used to solve the entire system numerically. It also contains the besselzero.m code used in the analytical solution as well as the tridiag.m function used in the optimized codes for both polar and spherical geometries [49, 47].

This first code, DiffusionPolar.m, is the code that uses the exact solution to the diffusion term omits the rest of the FHN system. It calls up a function called besselzero.m, which is listed immediately after.

```
clear

a = 1.0;                                % Radius of disk
ncols=256/2;                             % Number of columns in domain
nrows=256;                               % Number of rows in domain
Nt=50;                                   % Number of time steps
dr=a/ncols;
dtheta=2*pi/nrows;
dt=0.01;                                 % Time step
beta=1;                                   % Strength of IC
D=0.1;                                   % Diffusion constant
c=2*beta/pi/a^2;                         % Fourier coefficients factor
u=zeros(nrows,ncols);                     % Initialize array u

%Initialize Figure
[xr,xtheta] = meshgrid(linspace(0,a,ncols), linspace(0,2*pi,nrows));
xp=xr.*cos(xtheta);
yp=xr.*sin(xtheta);
zp=ones(nrows,ncols);
ih=surf(xp,yp,zp,u);
view(2);
%shading interp
set(ih,'cdatamapping','direct','EdgeColor','none')
axis image off; th=title('');
```

```

set(gcf,'position',[300 200 512 512],'color',[1 1 1])
% Create 'Quit' pushbutton in figure window
%uicontrol('units','normal','position',[.45 .02 .13 .07], ...
%    'callback','set(gcf,''userdata'',1)',...
%    'fontsize',10,'string','Quit');

% Bessel Functions
M=5;                                % # orders of Bessel functions
N=3;                                % # zeros of Bessel functions
for m=1:M
    jmn(m,:)=besselzero(m,N,1);        % MxN matrix of Bessel zeros
    bess2(m,:)=bessel(m+1,besselzero(m,N,1)); % J(m+1,jmn), MxN matrix
end
j0n=besselzero(0,N,1);                % zeros of J0
bess20 = bessel(1,besselzero(0,N,1));   % J1(j0n)
kmn=(jmnm/a).^2;                      % k-values
k0n=(j0n/a).^2;
IntBess=zeros(M,N);
IntBess0=zeros(N,1);

% Initial condition u=beta for r1<r<r2, theta1<theta<theta2
r1=0.25;
r2=0.50;
theta1=pi/6;
theta2=pi/3;

% IntBess0 = integral(rJ0(j0n r/a),r=r1..r2)
F = @(s) besselj(0,j0n.*s/a).*s;
IntBess0=quadv(F,r1,r2);

% IntBess = integral(r Jm(jmn r/a),r=r1..r2)
for m=1:M
    F = @(s) besselj(m,jmn(m,:).*s/a).*s;
    IntBess(m,:)=quadv(F,r1,r2);
    SI(m)=(sin(m*theta2)-sin(m*theta1))/m;
    CI(m)=(cos(m*theta1)-cos(m*theta2))/m;
end
SS = repmat(SI,[N,1])';
CC = repmat(CI,[N,1])';
TT= repmat(theta2-theta1,[N,1]);

```

```

% Fourier Coeffcients, MxN
A=c./bess2.^2.*SS.*IntBess;
B=c./bess2.^2.*CC.*IntBess;
A0=c./bess20.^2.*TT.*IntBess0;

for k=1:Nt;
    t=k*dt;
    for n=1:N
        u= u + A0(n)*bessel(0,j0n(n)*xr/a)*exp(-D*k0n(n)*t);
    end
    for m=1:M
        C=cos(m*xtheta);
        S=sin(m*xtheta);
        for n=1:N
            J=besselj(m,jmn(m,n)*xr/a,1);
            E=exp(-D*kmn(m,n)*t);
            u=u+(A(m,n)*C+B(m,n)*S).*J*E;
        end
    end

    % Map voltage to image grayscale value
    im=1+round(63*u); im=max(im,1); im=min(im,64);

    % Update image and text for k divisible by stp
    stp=1;
    if mod(k,stp) == 0
        set(ih,'CDATA',im);
        drawnow
    end
end

```

The besselzero.m code:

```

function x=besselzero(n,k,kind)

%
% besselzero.m
%
% Find first k positive zeros of the Bessel function J(n,x) or Y(n,x)
% using Halley's method.

```

```

%
% Written by: Greg von Winckel - 01/25/05
% Contact: gregvw(at)chtm(dot)unm(dot)edu
%
%%%%%%%%%%%%%%%
k3=3*k;

x=zeros(k3,1);

for j=1:k3

    % Initial guess of zeros
    x0=1+sqrt(2)+(j-1)*pi+n+n^0.4;

    % Do Halley's method
    x(j)=findzero(n,x0,kind);

    if x(j)==inf
        error('Bad guess.');
    end

end

x=sort(x);
dx=[1;abs(diff(x))];
x=x(dx>1e-8);

x=x(1:k);

function x=findzero(n,x0,kind)

n1=n+1;      n2=n*n;

% Tolerance
tol=1e-12;

% Maximum number of times to iterate
MAXIT=100;

% Initial error

```

```

err=1;

iter=0;

while abs(err)>tol & iter<MAXIT

    switch kind
        case 1
            a=besselj(n,x0);
            b=besselj(n1,x0);
        case 2
            a=bessely(n,x0);
            b=bessely(n1,x0);
    end

    x02=x0*x0;

    err=2*a*x0*(n*a-b*x0)/(2*b*b*x02-a*b*x0*(4*n+1)+(n*n1+x02)*a*a);

    x=x0-err;
    x0=x;
    iter=iter+1;

end

if iter>MAXIT-1
    warning('Failed to converge to within tolerance. ',...
        'Try a different initial guess');
    x=inf;
end

```

This code is the code from which the pictures of spirals were generated, DiffusionFDcyl.m, which calls up the tridiag.m function:

```

% Numerical solution of diffusion equation on a disk using optimized code

clear

% Constants
R=1.0;                                % Radius of disk

```

```

N=64;                                % Number of columns in domain
M=100;                                 % Number of rows in domain
Nt=200000;                             % Number of time steps
dr=R/N;
dz=2*pi/(M+1);                         % dz = dtheta
dt=0.1;                                 % Time step
beta=0;                                  % Strength of IC
D=1.0e-6;                               % Diffusion constant
Tmax=Nt*dt;
Dt=D*dt;
a=0.13; b=0.013; c1=0.26; c2=0.1; d=1.0; % FHN model parameters

% Stimulus (Iex=0 or Iex=30)
Iex=0;
iex=zeros(N,M);
iexa1=round(1+0.30/dr);      iexb1=round(1+0.6/dr);
iexc1=round(1+60*pi/180/dz); iexd1=round(1+100*pi/180/dz);
iexa2=round(1+0.45/dr);      iexb2=round(1+0.55/dr);
iexc2=round(1+80*pi/180/dz); iexd2=round(1+90*pi/180/dz);
%iexa1=1; iexb1=20;
%iexc1=1; iexd1=100;
%iexa2=4; iexb2=7;
%iexc2=1; iexd2=60;

% Initial Conditions
ictype=1;
if ictype==0
    % Constant ICs - ictype=0
    % Initial condition u=beta for r1<r<r2, theta1<theta<theta2
    r1=0.25;
    r2=0.75;
    i1=floor(r1/dr);
    i2=ceil(r2/dr);
    theta1=0;
    theta2=2*pi/3;
    j1=floor(theta1/dz)+1;
    j2=ceil(theta2/dz);

    % Initialize matrices
    u0=zeros(N,M);                      % Initialize voltage array
    v0=zeros(N,M);                      % Initialize refractoriness array

```

```

u0(i1:i2,j1:j2) = beta;
v0(i1:i2,j1:j2) = beta;

else
    % Grid of random ICs - ictype>0
    for i=1:N/4
        i1=4*(i-1)+1;
        for j=1:M/4
            j1=4*(j-1)+1;
            u0(i1:i1+3,j1:j1+3)=0;
            v0(i1:i1+3,j1:j1+3)=0;
            if rand<.4
                u0(i1:i1+3,j1:j1+3)=rand;
                v0(i1:i1+3,j1:j1+3)=rand;
            end
        end
    end
    end

u1=zeros(N,M);
v1=zeros(N,M);
uu(1:N,1:M)=u0;
uu(:,M+1)=u0(:,1);
r=linspace(0, R, N);
r(1,1)=1;
rr=repmat(r',1,M);
rr2=rr.*rr;

% FD Matrices
Az=-tridiag(M)/dz^2;
Az(M,1)=1/dz^2;
Az(1,M)=1/dz^2;
s=r(1:N-1)+r(2:N);
Ar=tridiag(N,s,[0,-s(1:N-2)-s(2:N-1),0],s)/dr^2;
Ar(:,N)=0;
Ar(N,:)=0;
Ar(1,1)=-1/dr^2;
Ar(1,2)=1/dr^2;

%Initialize Figure
[xr,xtheta]=meshgrid(linspace(0,R,N), linspace(0,2*pi,M+1));
xp=xr.*cos(xtheta);

```

```

yp=xr.*sin(xtheta);
zp=ones(N,M+1);
ih=surf(xp,yp,zp',uu');
view(2);
shading interp
set(ih,'cdatamapping','direct','EdgeColor','none')
axis image off; th=title('');
set(gcf,'position',[300 200 512 512],'color',[1 1 1])

% Create 'Quit' pushbutton in figure window
uicontrol('units','normal','position',[.45 .02 .13 .07], ...
    'callback','set(gcf,'userdata',1)',...
    'fontsize',10,'string','Quit');

for n = 1:Nt-1
    t=n*dt;

    if n == 1 % Begin 1st stimulus
        iex(iexa1:iexb1,iexc1:iexd1)=Iex;
    end

    if n == 500 % End 1st stimulus
        iex=zeros(N,M);
    end

    if n == 3000 % Begin 2nd stimulus
        iex(iexa2:iexb2,iexc2:iexd2)=Iex;
    end

    if n == 3500 % End 2nd stimulus
        iex=zeros(N,M);
    end

    u1=u0+Dt*(Ar*u0./rr+u0*Az./rr2)...
        +(c1*u0.* (u0-a).*(1-u0)-c2*u0.*v0+iex)*dt;

    % Update v
    v1=v0 + dt*b*(u0-d*v0);

    % BCs
    u1(N,:)=0;

```

```

uu(1:N,1:M)=u1;
uu(:,M+1)=u1(:,1);

%figure
if mod(n,1) == 0
    im=1+(63*uu');
    set(ih,'cdata',im);
    set(th,'string',sprintf('%s %d %s %0.4f \n %s %0.2f %s %0.2f',...
        'n = ',n,', t = ',t, ' max u,v = ', max(u1(:)), ', ', ...
        ,max(v1(:))))
    %colorbar
    %set(gca, 'CLim', [0, beta]);
    drawnow
end
u0=u1; %update u0, v0 for next step
v0=v1;
if ~isempty(get(gcf,'userdata')), break; end % Quit if user clicks
    % on 'Quit' button.
end

```

This code generates a tridiagonal matrix with diagonal rows of  $-1$ ,  $2$ , and then  $-1$ . The `tridiag.m` function:

```

%T = b*diag(ones(n,1)) + c*diag(ones(n-1,1),1) + a*diag(ones(n-1,1),-1)
function T = tridiag(n, x, y, z)
%TRIDIAG Tridiagonal matrix (sparse).
%
% TRIDIAG(X, Y, Z) is the tridiagonal matrix with subdiagonal X,
% diagonal Y, and superdiagonal Z.
%
% X and Z must be vectors of dimension one less than Y.
%
% Alternatively TRIDIAG(N, C, D, E), where C, D, and E are all
% scalars, yields the Toeplitz tridiagonal matrix of order N
%
% with subdiagonal elements C, diagonal elements D, and superdiagonal
%
% elements E. This matrix has eigenvalues (Todd 1977)
%
% D + 2*SQRT(C*E)*COS(k*PI/(N+1)), k=1:N.
%
% TRIDIAG(N) is the same as TRIDIAG(N,-1,2,-1), which is
%
% a symmetric positive definite M-matrix (the negative of the
%
% second difference matrix).

%
% References:
%
% J. Todd, Basic Numerical Mathematics, Vol. 2: Numerical Algebra,

```

```

%
% Birkhauser, Basel, and Academic Press, New York, 1977, p. 155.
%
% D.E. Rutherford, Some continuant determinants arising in physics and
%
% chemistry---II, Proc. Royal Soc. Edin., 63, A (1952), pp. 232-241.

if nargin == 1, x = -1; y = 2; z = -1; end
if nargin == 3, z = y; y = x; x = n; end

x = x(:); y = y(:); z = z(:); % Force column vectors.

if max( [ size(x) size(y) size(z) ] ) == 1
    x = x*ones(n-1,1);
    z = z*ones(n-1,1);
    y = y*ones(n,1);
else
    [nx, m] = size(x);
    [ny, m] = size(y);
    [nz, m] = size(z);
    if (ny - nx - 1) | (ny - nz -1)
        error('Dimensions of vector arguments are incorrect.')
    end
end
end

% T = diag(x, -1) + diag(y) + diag(z, 1); % For non-sparse matrix.
n = max(size(y));
T = spdiags([ [x;0] y [0;z] ], -1:1, n, n);

```

MATLAB Code for Solving the Modified FHN system in Spherical Coordinates

The two code, DiffusionFDsphere.m, again uses finite difference methods to solve the entire FHN system on a sphere. It calls up the tridiag.m function as well.

DiffusionFDsphere.m:

```

% Numerical solution of diffusion equation on a sphere using optimized code

clear

% Constants
R=1.0; % Radius of sphere
N=200; % Number of columns in domain

```

```

M=200;                                     % Number of rows in domain
Nt=200000;                                    % Number of time steps
dr=pi/N;
dz=2*pi/(M+1);                                % dz = dtheta
dt=0.1;                                         % Time step
beta=0;                                         % Strength of IC
D=1.0e-6;                                       % Diffusion constant
Tmax=Nt*dt;
Dt=D*dt;
a=0.13; b=0.013; c1=0.26; c2=0.1; d=1.0; % FHN model parameters

% Stimulus (Iex=0 or Iex=30)
% set view(0, 90) below
Iex=0;
iex=zeros(N,M);
iexa1=round(1+20*pi/180/dr); iexb1=round(1+60*pi/180/dr);
iexc1=round(1+pi/180/dz);     iexd1=round(1+120*pi/180/dz);
iexa2=round(1+35*pi/180/dz); iexb2=round(1+40*pi/180/dz);
iexc2=round(1+40*pi/180/dz); iexd2=round(1+80*pi/180/dz);

% Initial Conditions
ictype=1;
if ictype==0

    % Constant ICs - ictype=0
    % Initial condition u=beta for r1<r<r2, theta1<theta<theta2
    % set view(0, 90) below
    theta1=20*pi/180;
    theta2=60*pi/180;
    i1=floor(theta1/dr)+1;
    i2=ceil(theta2/dr);
    phi1=20*pi/180;
    phi2=120*pi/180;
    j1=floor(phi1/dz)+1;
    j2=ceil(phi2/dz)

    % Initialize matrices
    u0=zeros(N,M);                         % Initialize voltage array
    v0=zeros(N,M);                         % Initialize refractoriness array
    u0(i1:i2,j1:j2) = beta;
    v0(i1:i2,j1:j2) = beta;

```

```

else
    % Grid of random ICs - ictype>0
    u0=zeros(N,M); % Initialize voltage array
    v0=zeros(N,M); % Initialize refractoriness array
    for i=1:N/4
        i1=4*(i-1)+1;
        for j=1:M/4
            j1=4*(j-1)+1;
            u0(i1:i1+3,j1:j1+3)=0;
            v0(i1:i1+3,j1:j1+3)=0;
            if rand<.4
                u0(i1:i1+3,j1:j1+3)=0.5+rand/2;
                v0(i1:i1+3,j1:j1+3)=rand;
            end
        end
    end
    end

    u1=zeros(N,M);
    v1=zeros(N,M);
    uu(1:N,1:M)=u0;
    uu(:,M+1)=u0(:,1);
    theta=linspace(0,pi,N);
    r=sin(theta);
    r(1,1)=1;
    rr=repmat(r',1,M);
    rr2=rr.*rr;

    % FD Matrices
    Az=-tridiag(M)/dz^2;
    Az(M,1)=1/dz^2;
    Az(1,M)=1/dz^2;
    s=r(1:N-1)+r(2:N);
    Ar=tridiag(N,s,[0,-s(1:N-2)-s(2:N-1),0],s)/dr^2;
    Ar(:,N)=0;
    Ar(N,:)=0;
    Ar(1,1)=-1/dr^2;
    Ar(1,2)=1/dr^2;

    %Initialize Figure
    [xtheta,xphi]=meshgrid(linspace(0,pi,N), linspace(0,2*pi,M+1));

```

```

xp=R*sin(xtheta).*cos(xphi);
yp=R*sin(xtheta).*sin(xphi);
zp=R*cos(xtheta);
ih=surf(xp,yp,zp,uu');
view(0,90);                                % View from pole
% view(10,30);
shading interp
set(ih,'cdatamapping','direct','EdgeColor','none')
axis image off; th=title('');
set(gcf,'position',[300 200 512 512],'color',[1 1 1])

% Create 'Quit' pushbutton in figure window
uicontrol('units','normal','position',[.45 .02 .13 .07], ...
    'callback','set(gcf,''userdata'',1)',...
    'fontsize',10,'string','Quit');

for n = 1:Nt-1
    t=n*dt;

    if n == 1                      % Begin 1st stimulus
        iex(iexa1:iexb1,iexc1:iexd1)=Iex;
    end

    if n == 500                     % End 1st stimulus
        iex=zeros(N,M);
    end

    if n == 3000                    % Begin 2nd stimulus
        iex(iexa2:iexb2,iexc2:iexd2)=Iex;
    end

    if n == 3500                    % End 2nd stimulus
        iex=zeros(N,M);
    end

    u1=u0+Dt*(Ar*u0./rr+u0*Az./rr2)...
        +(c1*u0.* (u0-a).*(1-u0)-c2*u0.*v0+iex)*dt;

    % Update v
    v1=v0 + dt*b*(u0-d*v0);

```

```

% BCs
u1(N,:)=mean(u1(N-1,:)); % poles
u1(1,:)=mean(u1(2,:));
uu(1:N,1:M)=u1;
uu(:,M+1)=u1(:,1); % periodic BC for phi

%figure
if mod(n,1) == 0
    im=1+(63*uu');
    set(ih,'cdata',im);
    set(th,'string',sprintf('%s %d %s %.4f \n %s %.2f %s %.2f',...
        'n = ',n,', t = ',t, ' max u,v = ', max(u1(:)), ',',...
        ,max(v1(:))))
    %colorbar
    %set(gca, 'CLim', [0, beta]);
    drawnow
end
u0=u1; %update u0, v0 for next step
v0=v1;
if ~isempty(get(gcf,'userdata')), break; end % Quit if user clicks
    % on 'Quit' button.
end

```

## Generating Phase Fields

If one wants to further investigate the phase fields for the system, one can use this code, spiralfield.m to do so. It also calls in a function called spiralf.m, listed immediately following spiralfield.m.

```

% Generates field plot for system
% du/dt = c1*u.* (u-a).* (1-u)-c2*u.*v;
% dv/dt = b*(u-d*v);
% and plots zero isoclines for du/dt =0, dv/dt=0:
% c2*v=c1*(u-a)*(1-u)
% v=u/d;
% Phase portrait can be drawn with graphical input of initial conditions
% Needs spiralf.m

clear
global a b c1 c2 d

```

```

% System parameters
a=0.13; b=0.013; c1=0.26; c2=0.1; d=1.0; % FHN model parameters
beta=c1/c2*d;
full=1;           % full = 0 for [0,1]x[0,1] view, full = 1 for zoomed view

% Intersection of y=x and y=beta*(1-x)(x-a)
D=sqrt(1-2*beta-2*beta*a+beta^2-2*beta^2*a+beta^2*a^2);
x2=(-1+beta+beta*a+D)/2/beta+.01;
x1=(-1+beta+beta*a-D)/2/beta;
sc=5;             % sc = scale for arrows
dx=0.01;          % sets mesh resolution
if (imag(x1)~=0 || full==0)           % checks for non-intersection
    x1=0;
    x2=1;
    sc=3;
    dx=0.05;
end
y1=x1;
y2=x2;

% Independent variables for plotting
[u, v] = meshgrid(x1:dx:x2, y1:dx:y2);
x=x1:dx:x2;

% Field plot using quiver
udot = c1*u.* (u-a).*(1-u)-c2*u.*v;
vdot = b*(u-d*v);
quiver(u,v,udot, vdot,sc)
axis([x1,x2,y1,y2])
axis square
hold on

% Plot curves y=x/d and y=c1/c2*(x-a)*(1-x)
plot(x,c1/c2.* (1-x).*(x-a), 'k')
plot(x,x/d, 'k')

% Solution of system for IC (0.3,0.4) - t=0 to 100
[t y] = ode45('spiralf',[0 100],[0.3 0.4]);
plot(y(:,1),y(:,2), 'r')

```

```

% Graphical input of ICs
% bt = button - right click to end (bt^=3 depends on mouse)
% Click on plot to generate phase portrait
bt=0;

while bt^=3
    [xx,yy,bt]=ginput(1);
    if bt==1
        [t y] = ode45('spiralf',[0 100],[xx yy]);
        plot(y(:,1),y(:,2),'r')
    end
end
hold off

```

Here is spiralf.m:

```

function [xprime] = spiralf(t,x)
global a b c1 c2 d
xprime(1,1)=c1*x(1)*(x(1)-a)*(1-x(1))-c2*x(1).*x(2);
xprime(2,1)=b*(x(1)-d*x(2));

```

### Recommended Website

The Virtual Heart is a webpage that houses interactive Java applets, pictures, and 2D and 3D animations of the heart and its electrical system. One can see a single, real cardiac cell contracting or a computer simulation of the whole heart beating both with normal sinus rhythm and with customizable irregularities, along with numerous other applets and videos.

<http://thevirtualheart.org/>